Charles University
Faculty of Science

Study Programme: Animal Physiology

MSc. Dmitry Manakov

Protein profiling, metabolic enzymes and transmembrane signaling in the heart of spontaneously hypertensive SHR-Tg19 rat

Proteinový profil, metabolické enzymy a transmembránová signalizace v myokardu spontánně hypertenzního potkana kmene SHR-Tg19

Doctoral Thesis

Supervisor: doc. RNDr. Jiří Novotný, DSc.

Prague 2018

Declaration

I hereby declare that this PhD thesis is exclusively my own work, and that it has not been submitted (or any of its part) in order to obtain any academic degree earlier or at another institution. My contribution to the research presented in the thesis is reflected by the order of authors of the included publications. All publications and other sources used in the thesis have been properly cited.

Prague, 11.10.2018

…….

Dmitry Manakov

ACKNOWLEDGEMENT

I would like to express my deep gratitude to Assoc. Prof. Jiří Novotný for years of his professional assistance, dedicated time and guidance during the course of this work. This thesis would not be possible without the support of Lucie Hejnová, Ph.D. I want to acknowledge the valuable help of Jitka Škrabalová, Ph.D., Mgr. Klara Hahnova, Mgr. Barbora Melkes and all my colleagues at Faculty of Science, Charles University who helped me with this research and created intellectually stimulating and warm environment at the workplace.

I owe my sincere thanks to Hana Ujčíková, PhD. at the Czech Academy of Sciences, Prague who shared her knowledge of proteomics and David Kolář, Ph.D. whose energetic personality helped catalyze the respirometric experiments. It is my pleasure to thank Jitka Žurmanová, Ph.D. and Barbara Elsnicová, Ph.D. for their time and valuable advice.

Warm thanks to my wife and family for their support and inspiration.

ABSTRACT

Cardiovascular diseases account for the majority of deaths both worldwide and in the Czech Republic. Main factors contributing heart disease development, aside age and sex, are obesity, high blood pressure and high blood cholesterol and triglyceride levels. Spontaneously hypertensive rat (SHR) was developed and used for search of genetic determinants of these traits. This commonly used rat model develops hypertension, dyslipidemia, and insulin resistance naturally which is caused by aberrant Cd36 fatty acid translocase gene. Previous studies have shown that rescue of Cd36 performed in the transgenic SHR-Tg19 strain enhances cardiac beta-adrenergic system, slightly increases heart mass and leads to higher susceptibility to arrhythmias.

The present thesis had two main aims:

1) To investigate whether and how a transgenic rescue of Cd36 in SHR affects protein composition, mitochondrial function and activity of selected metabolic enzymes of the heart.

2) To study the expression and distribution of selected components of beta-adrenergic signaling system in lipid raft isolated form membranes using the TX-100 detergent.

We set to compare two commonly used proteomic approaches, 2D electrophoresis with MALDI-TOF mass spectrometry and label-free LC-MS. The results did not reveal any overlap between differently expressed proteins identified by these two methods. We also compared samples from both ventricles and found that both MALDI and LC-MS identified more changes in the RV of SHR-Tg19 than in the LV. These changes included several energy metabolism enzymes and cytoskeletal, structural and regulatory proteins. Changes in the LV included metabolic enzymes and, interestingly, translated products of pseudogenes similar to some OXPHOS enzymes, implicating their regulatory role.

Malate dehydrogenase, the enzyme that according to MALDI-TOF MS underwent a 6-fold downregulation in the LV of SHR-Tg19, had significantly lower activity in both cytoplasm and mitochondria samples of the LV from SHR-Tg19, as determined using an enzymatic assay. Activity of cytoplasmic hexokinase was also lower in the LV of SHR-Tg19. We also detected downregulated expression of the succinate dehydrogenase subunit SdhB (complex II) and 70 kDa peroxisomal membrane protein in the LV of SHR-Tg19. Although respirometric measurements did not reveal significant differences between the strains, our data demonstrated higher respiration rate of mitochondria isolated from the LV compared to RV.

We also adopted and elaborated a simplified method for lipid raft isolation from cardiac tissue. Feasibility of this methodology was tested by using a proteomic approach. The obtained results indicated that the method led to successful separation of typical raft and non-raft proteins. We used this method to analyze the distribution of several key components of beta-adrenergic signaling system in the LV of both rat strains. Expression of G protein beta subunit was lower in the raft fraction which could be linked to the enhanced cAMP signaling. Additionally, we found higher expression of connexin 43, which could be linked to increased arrhythmogenesis seen in SHR-Tg19, and higher expression of ERK1 and phosphorylation of RhoA, which may lead to an increase of heart mass observed in older SHR-Tg19. Connexin 43, ERK1 and RhoA are considered effectors of cAMP signaling network, thus showing its broad impact on heart function.

ABSTRAKT

Kardiovaskulární nemoci jsou nejčastější příčinou smrti jak na celém světě, tak v České republice. Hlavní faktory přispívající k rozvoji srdečních onemocnění, kromě věku a pohlaví, jsou obezita, vysoký krevní tlak a vysoká hladina cholesterolu a triglyceridů v krvi. Spontánně hypertenzní potkan (SHR) byl vyvinut a používán k vyhledávání genetických determinant těchto projevů. Tento běžně používaný potkaní model rozvíjí hypertenzi, dyslipidemii a inzulínovou rezistenci díky abnormálnímu genu translokázy mastných kyselin Cd36. Předchozí studie ukázaly, že transgenní oprava Cd36 u kmene SHR-Tg19 zlepšuje činnost beta-adrenergního systému v srdci, mírně zvyšuje srdeční hmotnost a vede ke zvýšení náchylnosti k arytmiím.

Tato práce měla dva hlavní cíle:

1) Zjistit, zda a jak transgenní náhrada Cd36 v SHR ovlivňuje proteinové složení, mitochondriální funkci a aktivitu vybraných metabolických enzymů srdce.

2) Studovat expresi a distribuci vybraných složek beta-adrenergního signálního systému v lipidových raftech izolovaných pomocí solubilizace membrán detergentem TX-100.

Rozhodli jsme se porovnat dva běžně používané proteomické přístupů, 2D elektroforézu spojenou s MALDI-TOF hmotnostní spektrometrií a tzv. label-free LC-MS. Výsledky neukázaly překryv mezi odlišně exprimovanými proteiny identifikovanými těmito dvěma metodami. Porovnávali jsme vzorky z obou komor a zjistili, že obě metody identifikovaly více změn v pravých než v levých komorách SHR-Tg19. Tyto změny se týkají několika enzymů energetického metabolismu a strukturních a regulačních proteinů cytoskeletu. Změny v levých komorách byly pozorovány u metabolických enzymů a také u proteinových produktů pseudogenů, podobných některým OXPHOS enzymům, což může poukazovat na jejich možnou regulační roli.

Malát dehydrogenáza je enzymem, který podle MALDI-TOF MS měl 6 krát nižší expresi v LV u SHR-Tg19. Tento enzym měl také významně nižší aktivitu ve vzorcích cytoplazmy a v mitochondriích izolovaných z levých komor SHR-Tg19. Aktivita cytoplazmatické hexokinázy byla také nižší v z levých komorách SHR-Tg19. Rovněž jsme zjistili sníženou hladinu exprese podjednotky sukcinát dehydrogenázy SdhB (součást komplexu II) a 70 kDa peroxisomálního membránového proteinu v levých komorách SHR-Tg19. Ačkoli respirometrická měření neodhalila významné rozdíly mezi kmeny, získané výsledky demonstrovaly vyšší míru respirace u mitochondrií izolovaných z levých než z pravých komor.

Nakonec jsme převzali a rozpracovali zjednodušený postup pro izolaci lipidových raftů ze srdeční tkáně. Použitelnost této metodologie byla testována pomocí proteomického přístupů. Získané výsledky ukázaly, že tato metoda vedla k úspěšné separaci typických raftových a neraftových proteinů. Použili jsme tuto metodu pro analýzu distribuce několika klíčových komponent beta-adrenergního signálního systému v levé komoře srdeční u obou potkaních kmenů. Raftová lokalizace G beta podjednotky byla významně snížena u SHR-Tg19, což by mohlo být spojeno se zvýšením signalizace cAMP. Celková exprese konexinu 43 byla vyšší v levých komorách SHR-Tg19, což je možnou příčinou zvýšené arytmogeneze pozorované u těchto zvířat. Také jsme nalezli zvýšenou expresi ERK1 a fosforylací RhoA, jejichž funkce může být spojena s hypertrofickými projevy v srdci u starších SHR-Tg19. Konexin 43, ERK1 a RhoA jsou považovány za efektory signalizační sítě cAMP, což poukazuje na její široky vliv na funkci srdce.

LIST OF ABBREVIATIONS

2DE	2-dimensional electrophoresis
ABC	ammonium bicarbonate
AC	adenylyl cyclase
ACN	acetonitrile
AMPK	5' AMP-activated protein kinase
AR	adrenergic receptors
ATP	adenosine triphosphate
AU	arbitrary units
BP	blood pressure
BSA	bovine serum albumin
BW	body weight
C/EBP	CCAAT-enhancer-binding protein
CAMKK	calcium/calmodulin-dependent protein kinase kinase
cAMP	cyclic adenosine monophosphate
Cav	caveolin
Cd36	cluster of differentiation 36
CHO	Chinese hamster ovary
CREB	cAMP response element-binding protein
CS	citrate synthase
CVD	cardiovascular disease
Cx43	connexin 43
DAPI	4′,6-diamidino-2-phenylindole
DHPR	dihydropyridine receptor
DOCA	deoxycorticosterone acetate
DRM	detergent-resistant membranes
DSM	detergent-soluble membranes
DTT	dithiothreitol
ECG	electrocardiography
ECM	extracellular matrix

EDTA	ethylenediaminetetraacetic acid
EndoG	endonuclease G
ER	endoplasmic reticulum
ERK	extracellular signal-regulated kinases
FA	fatty acids
FABP	fatty acid binding protein
FATP	fatty acid transport protein
GLUT	glucose transporter
GPCR	G protein-coupled receptor
HDL	high-density lipoprotein
HEK	human embryonic kidney
HEPES	4-(2-hydroxyethyl)-1-piperazineethanesulfonic acid
HK	hexokinase
HW	heart weight
LC	liquid chromatography
LCFA	long-chain fatty acids
LDL	low-density lipoprotein
L-NAME	N(ω)-nitro-L-arginine methyl ester
LV	left ventricle
MALDI	matrix-assisted laser desorption/ionization
MAPK	mitogen-activated protein kinase
MCFA	medium-chain fatty acids
MCT	medium chain triglycerides
MDH	malate dehydrogenase
MDH	malate dehydronegase
MetS	metabolic syndrome
MS	mass spectrometry
MT	mitochondria
NAD	nicotinamide adenine dinucleotide
NCOR	NADH:cytochrome c oxidoreductase
NIH	National institutes of health
NOS	nitric oxide synthase
PBS	phosphate-buffered saline

PDK	phosphoinositide-dependent kinase
PGC1α	PPARγ coactivator 1-α
PKA/PKC	protein kinase A / protein kinase C
PM	plasma membrane
PMP70	70-kDa peroxisomal membrane protein
PNS	post-nuclear supernatant
PPAR	peroxisome proliferator-activated receptor
RV	right ventricle
SCARB	scavenger receptor class B
SCOR	succinate:cytochrome c oxidoreductase
SDH(A/B/C/D)	succinate dehydrogenase (subunit A / B / C/ D)
SDS-PAGE	sodium dodecyl sulfate polyacrylamide gel electrophoresis
SHR	spontaneously hypertensive rat
SIRT	sirtuin
SR	sarcoplasmic reticulum
SSO	sulfo-N-succinimidyl oleate
TCA	trichloroacetic acid
TFA	trifluoroacetic acid
TG	triglyceride
TGF	tumor growth factor
TNF	tumor necrosis factor
TOF	time-of-flight
TSP	thrombospondin
VLDL	very low-density lipoprotein
WKY	Wistar Kyoto

TABLE OF CONTENTS

1. INTRODUCTION

According to World Health Organization, 17 million deaths a year (one third of the total) are accounted to cardiovascular disease, around 50% of these are the result of complications of hypertension (WHO, 2013). Hypertension is denoted primary or essential if no clear underlying condition can be identified. Primary hypertension is the most frequently encountered type in humans, contributing to 95% of incidences. It is a complex multifactorial disease influenced by genetic and environmental factors. It is estimated to affects one-third of the world population, both in developed and developing countries (Mills et al., 2016). Individuals with the blood pressure ≥140/90 mmHg are considered hypertensive. Not only it is a powerful underlying factor for CVD events, risk of which doubles for each 20/10 mmHg increment of blood pressure (BP), but also for chronic renal diseases (Monhart, 2013). Hypertension, together with such risk factors as central obesity, insulin resistance and dyslipidemia, is clustered into the metabolic syndrome (MetS). MetS is estimated to affect 17% of European population (van Vliet-Ostaptchouk et al., 2014). In the Czech Republic, however, this number is reported to be as high as 45.8% among adults aged 45-69 years (Huangfu et al., 2014). Cardiovascular mortality is increased three-fold in subjects with MetS (Isomaa et al., 2001).

Various animal models of experimental hypertension and MetS have been developed to obtain information on disease pathophysiology and etiology. These models are used to study the disease in both its early and progressive stages, they produce predictable symptoms, allowing to mimic responses observed in humans (Leong et al., 2015). However, some limitations of such studies should be taken into consideration, for example, primary causes of hypertension in rat models is different from what is typically observed in humans. Several rat models of systemic hypertension exist. Such strains as spontaneously hypertensive rat (SHR) and Prague hereditary hypertriglyceridemic (HTG) rat develop the condition without any intervention due to hereditary defects (Stolba et al., 1992). So do transgenic rat models, for example, TGR(mREN2)27 that was engineered to express murine renin (*Ren-2*) gene (Lee et al., 1996, p. 27). On the other hand, Dahl salt-sensitive rats (derived from

uninephrectomised Sprague-Dawley rats) require weekly subcutaneous injections of deoxycorticosterone acetate (DOCA) and oral NaCl loading. L-NAME administration can be used to inhibit NO synthase in Wistar rats and streptozotocin to induce diabetes and concomitant hypertension in Zucker rats (Doggrell and Brown, 1998). Detailed review of different hypertension models is beyond the scope of the present study, which will focus on the SHR strain hereafter.

1.1. Spontaneously hypertensive rat model

1.1.1. SHR development and characteristics

Spontaneous hypertensive rat model is a widely studied phenotype-driven genetic model suitable for the research of polygenic hypertension. It was developed by the selective breeding of WKY rats (Okamoto and Aoki, 1963). Male with high blood pressure (150-175 mmHg) and female with above average BP (130-140 mmHg) were used as the progenitors. The offspring was brother-sister mated for multiple generations to achieve relative genetic homogeneity.

By 15 week of age the blood pressure in SHR reliably reaches 250 mmHg in males and 180 mmHg in females. Besides hypertension SHR exhibits significantly increased ventricular weight (Sen et al., 1974) and elevated levels of cholesterol, triglycerides (TG) and fatty acids (FA) in plasma (Iritani et al., 1977). The ratio of glucose to FA oxidation is four times higher in SHR compared to normotensive rats regardless of workload (Christe and Rodgers, 1994). Along with elevated glucose uptake SHR shows increased hexokinase activity and decreased expression of insulin-dependent glucose transporter GLUT4 while the expression of insulin-independent GLUT1 remains unchanged, indicating the presence of insulin resistance in SHR (Giannocco et al., 2013; Paternostro et al., 1995). Indeed, systemic glucose disposal in response to insulin is slower in SHR compared with WKY (Rao, 1993) as well as glucose disposal in the heart alone (Zhang et al., 2008). Response to insulin of several of insulin signaling pathway effectors (such as IRS-1, phosphorylated Akt, phosphorylated eNOS) was shown to be blunted in SHR compared to WKY (Zecchin et al., 2003). Increasing insulin concentrations have less effect on the rate of isoproterenol-stimulated lipolysis in SHR adipocytes compared to WKY showing that the former strain possess a defective catecholamine action (Reaven et al., 1989).

Despite having high blood pressure and insulin resistance SHR is not an accurate model of MetS as it is not obese. However, SHR can mimic the situation observed in MetS patients when put on a high-calorie diet to induce obesity (Miesel et al., 2010).

Earlier studies of the strain also observed disturbances in calcium metabolism and lowered heart ADP phosphorylation potential (McCarron et al., 1981; Shimamoto et al., 1982). Intracellular concentration of Ca^{2+} ions was shown to be the same in WKY and SHR. The differences however lie in $[Ca^{2+}]_i$ transients (i.e. brief releases of Ca^{2+} ions by the sarcoplasmic reticulum (SR) that activate myofilament shortening) which have higher amplitude in SHR due to a higher calcium content in the SR (Brooksby et al., 1993). In addition, isolated SHR cardiomyocytes exhibit higher susceptibility to producing "calcium waves", a spontaneous and propagating increases in intracellular calcium (Failli et al., 1997). Higher density of L-type Ca^{2+} channels was observed in the hearts of SHR in relation to age indicating that calcium perturbations may be secondary to the onset of hypertension (Ebata et al., 1991; Galletti et al., 1991).

Rate of anaerobic glycolysis is accelerated in the LV of SHR heart (Raizada et al., 1993). Proteomic comparison of SHR and WKY revealed downregulation of beta-oxidation and upregulation of glycolytic enzymes in the heart of the former (Zamorano-León et al., 2010). Similar results were obtained by direct measurements of activities of beta-oxidation and glycolysis in isolated perfused hearts of SHR (Christe and Rodgers, 1994).

Hearts of SHR exhibit marked hypertrophy, however it not clear whether the increase in cardiac mass is a consequence of hypertension or a result of other deficiency (Bélichard et al., 1988). In favor of the first assumption speaks the fact that early in development of hypertension there is a period of stable compensatory hyperfunction, which is however limited and eventually heart becomes impaired. During that compensatory period SHR heart shows decreased β-adrenergic inotropic responsiveness which becomes more pronounced with the progression of hypertrophy (Keller et al., 1997). However, treatment with resveratrol ameliorates hypertrophy without lowering the blood pressure in SHR, questioning their connection (Thandapilly et al., 2010). This may indicate involvement of energy metabolism disturbances, as mechanisms of resveratrol action include oxidative stress reduction and activation of SIRT1 (Borra et al., 2005; Salminen et al., 2013). SHR indeed show elevated markers of oxidative damage, especially at an older age (Alvarez et al., 2008) as well as lowered expressions

and activities of mitochondrial complexes I and II associated with a decrease in mitochondrial biogenesis pathway elements SIRT1, AMPK and PGC-1α (Tang et al., 2014). Also, lipid-lowering agent atorvastatin lowered the extent of hypertrophy in SHR without affecting blood pressure (Chen et al., 2018). This change was also associated with PGC-1α.

Other possible determinants of hypertrophy in SHR were identified using recombinant inbred strains. They include mutant osteoglycin, an ECM protein that is linked to hypertrophic response via transforming growth factor beta (TGF-β) signaling (Petretto et al., 2008) and mitochondria-localized endonuclease G (EndoG), which was originally implicated in chromatin degradation after its translocation into the nucleoplasm during caspase-independent apoptosis (Vařecha et al., 2012). Research presented by McDermott-Roe et al. (2011) connects lack of mitochondrial EndoG activity with cardiac hypertrophy in SHR as well as isolated cardiomyocytes. They have also shown a link between central mitochondria biogenesis inducer PGC1α and EndoG activity. Indeed, as recent study has demonstrated, EndoG regulates ROS-induced depletion and subsequent compensatory replication of mtDNA (Wiehe et al., 2018). Independent of the underlying cause, loss of mtDNA integrity and altered mitochondrial biogenesis is characteristic of hypertrophied and failing heart. It is present in the earliest phases of cardiac remodeling, paving the way for cellular structural heterogeneity and fibrosis observed in a failing heart (Torrealba et al., 2017).

During the last quarter of SHR lifespan their heart progresses to failure (Mitchell et al., 1997) which is characterized by increase in collagen content and reduction in maximum myofibrillar force and cardiomyocyte mass due to apoptotic processes in these cells (Conrad et al., 1995; Li et al., 1997). This results in a sudden death unless treated with antihypertensive drugs, in which case SHR lifespan is significantly prolonged to similar length as that observed in normal albino rat (Freis and Ragan, 1975). Caloric restriction was also shown to enhance SHR survival (Lloyd, 1984). Same study demonstrated that neither decrease or increase in salt intake affected survival of SHR.

1.1.2. Genetic variations responsible for SHR pathology

Genome-wide investigation of multiple human ancestries showed 66 significant loci for higher BP that account only for ~3.5% of the hypertensive phenotype (Ehret et

al., 2016). However, a study of twins showed heritability to be in range of 25% to 64% (Kupper et al., 2006) leaving open the question of linking multiple known genetic variations and pathogenesis of hypertension in human individuals. Phenotype-driven models of hypertension have the potential to elucidate genetic mechanisms responsible for the disease development in humans. Quantitative trait locus mapping in inbred WKY\SHR cross helped identify regions on chromosomes 4 and 12 responsible for defective insulin and catecholamine action in SHR (Aitman et al., 1997). After refining these results using a combination of genetic approaches a mutated *Cd36* gene was discovered in the region of Chr.4 at the peak of linkage for defects in glucose and fatty acid (FA) metabolism in SHR (Aitman et al., 1999).

Cd36 is a multifunctional transmembrane glycoprotein that binds a variety of ligands including fatty acids (see chapter 1.2). In Wistar rats *Cd36* gene sequence is followed by two inactive homologous pseudogenes (PS1 and PS2). An unequal recombination event resulted in conjoining a part of *Cd36* wild-type sequence with a part of *Cd36-PS2* replacing all exons downstream of exon 4 with corresponding pseudogene sequences (Fig. 1).

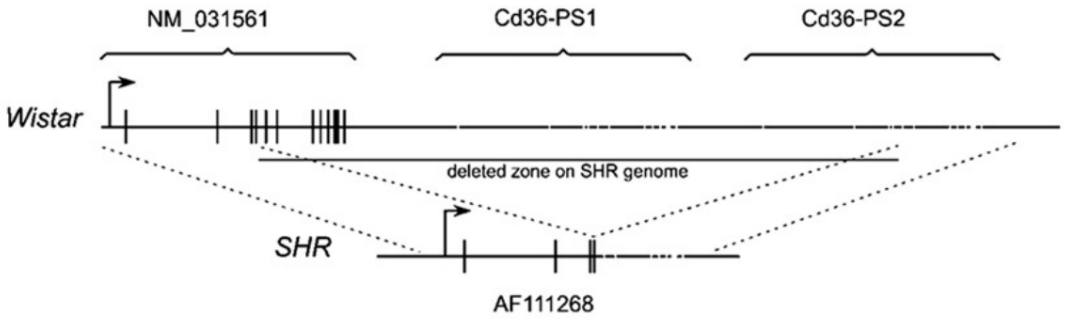

Fig. 1. Schematic representation of the *Cd36* gene in SHR and Wistar rats. In wild-type *Cd36* the expressed region is followed by 2 silent *Cd36* pseudogenes (PS1 and PS2). In SHR/NIH strains a recombination event between wild-type *Cd36* and *Cd36-PS2* occurred resulting in changes in Cd36 protein (reproduced from Lauzier et al., 2011).

However, only those rats that were sent to the National Institutes of Health (SHR/NIH strain) at generation F_{13} have shown the changes in *Cd36*. Rats from the original colony in Japan (SHR/Izm strain) express insulin-resistant and dyslipidemic phenotype despite having wild-type *Cd36* (Gotoda et al., 1999). This is because the separation occurred long before SHR was fully inbred which implies that pathologies in SHR/Izm are attributed to other mutations than in SHR/NIH. Indeed, genetic comparison of SHR/Izm and WKY revealed a different set of candidate genes for hypertension, such as *Bcl6* and *Sox2* (Watanabe et al., 2015). The present work is focused on SHR/Ola, a substrain of SHR/NIH which bears the *Cd36* mutation.

1.2. Cd36 - scavenger receptor and a fatty acid translocase

1.2.1. Discovery of Cd36

The multifunctional nature of Cd36 (cluster of differentiation 36) is reflected by its many names such as FAT (fatty acid translocase), platelet glycoprotein IIIb and IV, thrombospondin receptor, and SCARB3. Current classification puts it into a group of proteins called scavenger receptors for their role in recognition and removal of different particles from circulation by immune cells. There have been described 11 classes of these receptors ranging A to L and Cd36 was assigned into SR-B class together with lysosome membrane protein 2 (LIMP-2, also known as SCARB2). Despite propositions to name it SR-B2 as implied by the classification, in most of the literature it is still referred to as Cd36 (PrabhuDas et al., 2017).

First report of Cd36 described it as a 88-kDa glycoprotein IV on platelet membranes (Clemetson et al., 1977). During the efforts to catalogue and define antigens on the surface of human leukocytes (Franklin et al., 1987) an OKM-5 antibody was raised against adherent monocytes that was blocked by glycoprotein IV thus identifying it as a Cd36 molecule present on those cells (Talle et al., 1983). One decade after its initial discovery Cd36 was shown to mediate thrombospondin-1 antiangiogenic function in endothelial cells (Asch et al., 1987) as well as cytoadherence of erythrocytes infected with *Plasmodium falciparum* (Oquendo et al., 1989). It was also implicated in platelet aggregation during thrombus formation, further broadening its physiological importance (Tandon et al., 1989).

As a scavenger receptor it has a central role in the uptake of oxidized LDL (OxLDL) by macrophages which leads to foam cell formation and atherosclerosis (Endemann et al., 1993). Cd36 is also able to recognize and bind oxidized phospholipids, apoptotic cells, amyloid proteins and pathogens such as *Staphylococcus aureus* and *Cryptococcus neoformans* (Means et al., 2009). The proinflammatory signaling of Cd36 is mediated by heterodimerization with Toll-like receptors 4 and 6 (Stewart et al., 2010).

Cd36 also acts as a receptor for long-chain fatty acids on lingual gustatory cells, enabling the orosensory detection of dietary lipids and preparing gut for their digestion (Laugerette et al., 2005), and in proximal intestine where it aids in uptake of fatty acids and cholesterol (Nassir et al., 2007). The present thesis is focused on the ability of Cd36 to facilitate free fatty acid transport into the insulin-responsive cells: adipocytes, cardiac and skeletal myocytes (Abumrad et al., 1993).

1.2.2. Structure of Cd36

The crystal structure of Cd36 has been partially elucidated (Hsieh et al., 2016). Known structural features are depicted in Fig. 2. Cd36 has a hairpin-like architecture with two transmembrane regions near both its ends which themselves are located inside the cell. Inside the extracellular portion runs a tunnel that serves as a passage for long-chained fatty acids. It is laced with electron-dense sequences of hydrophobic amino acids allowing FA to pass through. When passing this tunnel, the FA are oriented with their acyl chain pointing towards from the membrane by the interaction with hydrophobic K164 residue and polar T195 residue with a bound water molecule. Two entrances to the tunnel have been identified and one exit that positions the FA to enter the outer leaflet of the membrane. From there the FA “flip-flops” into the inner leaflet independently of Cd36 (Jay and Hamilton, 2016) and gets transported into the cytoplasm with the help of fatty acid binding proteins (FABP).

The structure of FA binding site in Cd36 have been identified using sulfo-N-succinimidyl derivatives in a combination of mutagenic and proteomic approaches (Baillie et al., 1996; Kuda et al., 2013). Incubating adipocytes with sulfo-N-succinimidyl derivatives hampers the intracellular transport of long-chain fatty acids by 70%. Among those derivatives sulfo-N-succinimidyl oleate (SSO) was shown to block Cd36 by covalently binding lysine 164 in the FA binding pocket and restricting

permeability with its negatively charged sulfonate group (Harmon et al., 1991). Because of this sulfo-N-succinimidyl oleate is widely used to inhibit both Cd36-mediated FA uptake and intracellular FA signaling (e.g. via peroxisome proliferator-activated receptor pathway). SSO also inhibits oxLDL uptake by macrophages, indicating that FA and oxLDL compete for the same binding pocket on Cd36 (Kuda et al., 2013). Recently there have been identified a second binding site for FA on Cd36, however, this discovery was made *in silico* and no specific amino acid is associated with the second binding site (Hsieh et al., 2016).

An important role in Cd36 appearance and functions is played by its many post-translational modifications (PTMs). Firstly, the protein retains its structure due to three disulfide bridges (Rasmussen et al., 1998). The single chain of the protein consists of 472 amino acids with a predicted mass of 55 kDa, the difference between this and its observed molecular mass of 88 kDa is given mainly by its glycosylation. Cd36 has 10 sites within its large extracellular loop which undergo N-linked glycosylation at asparagine residues during protein maturation in the endoplasmic reticulum and the Golgi apparatus. Although only three glycosylated residues located at the core of the protein have been shown to be necessary for the correct folding and trafficking, the extent of glycosylation affects Cd36 expression (Hoosdally et al., 2009).

Cd36 has two known phosphorylation sites, both on its extracellular loop: T92, which is recognized by protein kinase C (PKC) and S237, by protein kinase A (PKA). Phosphorylation by PKC negatively regulates TSP-1 binding (Asch et al., 1993). The other site can undergo extracellular phosphorylation which inhibits FA uptake by platelets (Guthmann et al., 2002) but whether this is relevant in cardiomyocytes is presently unknown.

Ubiquitination by E3 ligases have been observed for Cd36, affecting its expression in insulin and FA dependent manner (Smith et al., 2008). However, this study was done using Chinese hamster ovary (CHO) and HEK 293 cells lines with artificially expressed Cd36, so the role of its ubiquitination in the heart cells is a subject for future research.

Cd36 has four lysine acetylation sites conserved in both rat and human (Lundby et al., 2012) which have been suspected to regulate FA transport (Khan and Kowluru, 2018), however more conclusive evidence is needed to ascertain that.

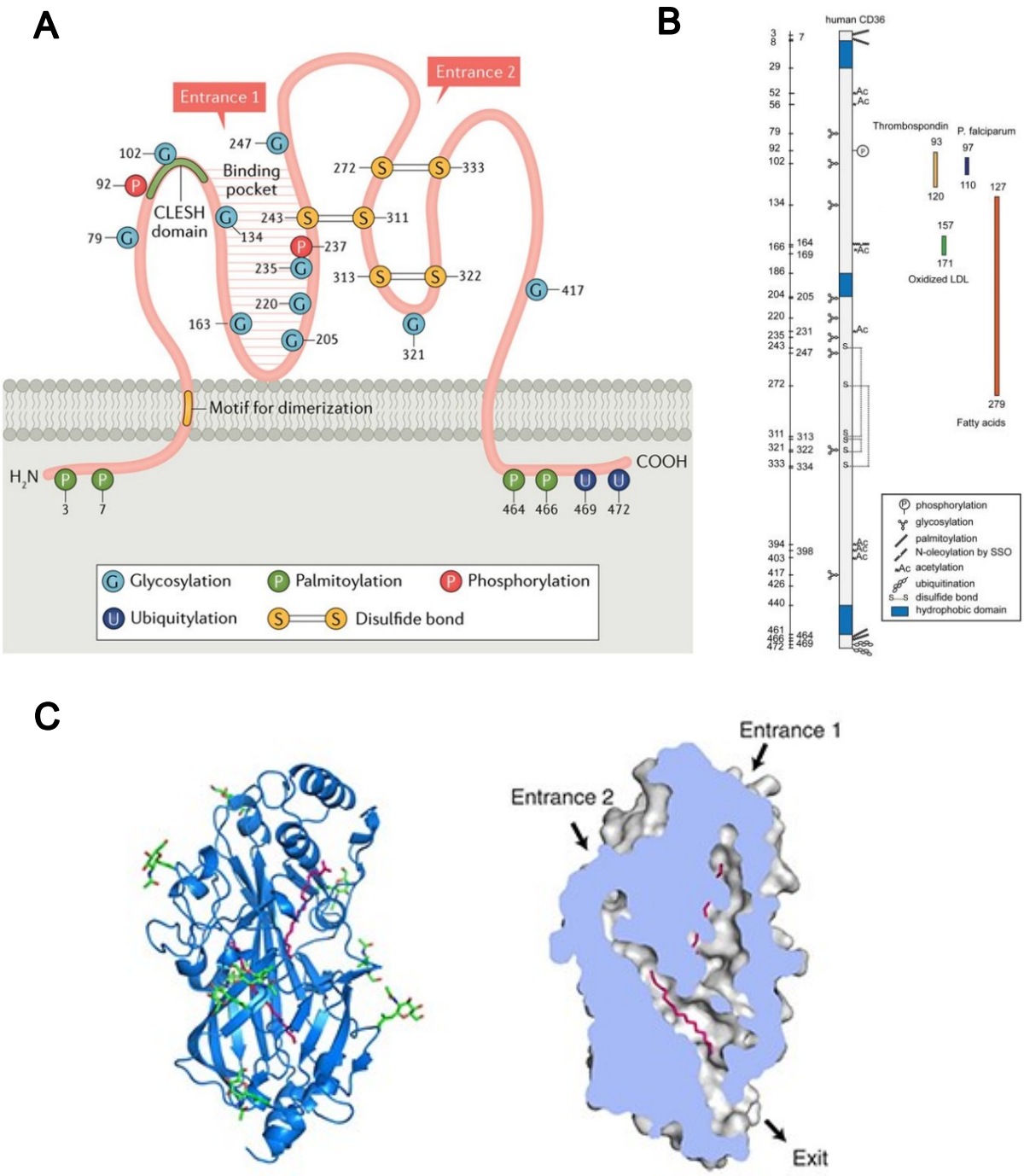

Fig. 2. A. Schematic representation of Cd36 structure highlighting the significance of post-translational modifications in its functioning (from Yang et al., 2017). **B.** Structural diagram representing the position of Cd36 binding sites for P. falciparum, TSP-1, OxLDL and fatty acids (adapted from Pepino et al., 2014). **C.** 3D model of Cd36. *Left:* ribbon model of the protein (blue) with two palmitic acids bound in the central cavity shown in pink and glycosylation sites with associated sugars in green. *Right:* Cross-section through the space-filling model showing the cavity and locations of its putative exit and two entrances. Two palmitic acid molecules (magenta) are rendered inside (adapted from Hsieh et al., 2016).

Palmitoylation, a reversible modification of a cysteine amino acid by a lipid moiety, was observed on four sites in Cd36, two on each of its intracellular tails (Jochen and Hays, 1993). All of these cysteine sites are essential for processing and translocation of the receptor (van Oort et al., 2014). Furthermore, lack of palmitoylation affects the ability to associate with lipid microdomains (Resh, 1999). Although direct impact of this on Cd36 membrane distribution have not been described, disruption of lipid raft partitioning by C terminus truncation negatively affects FA transport by Cd36 (Eyre et al., 2007).

1.1.1. Transcriptional regulation of Cd36

Experiments with adipocytes identified CCAAT/enhancer-binding protein α (C/EBPα) as a protomer of *Cd36* gene expression (Qiao et al., 2008). Mechanism of C/EBPα activation have been elucidated recently by Zaini et al. (2018), involving acetylation by p300 and deacetylation by SIRT1. Deacetylated C/EBPα becomes active, thus adding control of *Cd36* expression under already wide portfolio of effects SIRT1 has on energy metabolism.

Proteins of the Peroxisome Proliferator-Activated Receptor (PPAR) family bind FA while being localized in the nucleus where they exert transcriptional control over lipid metabolism genes including *Cd36*. Their isoforms include ubiquitously expressed PPARβ/δ, heart-specific PPARα and predominantly adipose-expressed PPARγ (Lamichane et al., 2018). In rat heart however, only PPARβ/δ activation induced significant elevation in Cd36 mRNA content and protein expression (Kalinowska et al., 2009). Same experiments also show increased Cd36 membrane translocation after chronic PPARβ/δ stimulation.

There is a report indicating involvement of cAMP response element-binding protein (CREB) in promoting *Cd36* expression (Zingg et al., 2017). Authors of this paper observed an increase in luciferase reporter signal coupled with human *Cd36* promoter in HEK293 cells stimulated with forskolin, a potent adenylyl cyclase agonist.

1.1.2. Cd36 membrane distribution and trafficking

Cd36 populations have been observed in both bulk membranes and lipid rafts (this membrane fraction is introduced in chapter 1.3), and its localization in the latter fraction was shown to be necessary for FA transport (Ehehalt et al., 2008) and signaling

(Githaka et al., 2016). Crosslinking of Cd36 using antibodies increased its distribution in lipid rafts and consequently its participation in the rate of FA transport and vice versa. Disruption of lipid rafts by cholesterol/sphingolipid depletion abolished FA transport (Ehehalt et al., 2008). The blocking of FA transport by lipid raft disruption could not be further strengthened using SSO thus confirming the role of lipid raft partitioning in Cd36 function (Pohl et al., 2005).

Initial studies concerned with involvement of Cd36 in caveolae showed no overlap of caveolin-1 and Cd36 membrane distribution and no impediment in Cd36-mediated oxLDL transport in the absence of caveolin-1 (Zeng et al., 2003). Several subsequent reports however challenged these findings. For example immunopurification and electron microscopy confirmed colocalization of Cd36 and caveolin-1 in adipocytes (Souto et al., 2003). Caveolae were also shown to be necessary for Cd36 raft localization in mouse embryonic fibroblasts (MEFs) (Ring et al., 2006).

Unlike its structurally similar family member LIMP-2, which adopts an "opened" conformation at pH 5.5 and "closed" at pH 7.5 (Zhao et al., 2014), Cd36 is regarded to be constitutively active. Its FA transport activity is regulated by vesicular trafficking of the receptor between the plasma membrane and the endosomal compartment in similar manner as GLUT4-mediated glucose uptake (van Oort et al., 2008). Specifically, upon stimulation with insulin or decline in ATP concentration associated with increased workload, vesicles containing Cd36 translocate to the plasma membrane to facilitate FA transport (Fig. 3).

The first regulatory mechanism relies upon insulin receptor pathway, which includes phosphorylation of insulin receptor substrate 1 (IRS-1), phosphoinositide 3-kinase (PI3K) and rise in the concentration of phosphatidylinositol-3,4,5-trisphosphate (PIP_3), a membrane phospholipid that is able to bind and activate phosphoinositide-dependent kinase (PDK). Eventually, cytosolic Akt (also known as protein kinase B, PKB) binds to PIP_3 on the membrane and gets phosphorylated by PDK thus becoming active (Miao et al., 2010; Vanhaesebroeck and Alessi, 2000).

Vesicle trafficking itself is controlled by Rab GTPases, a family of proteins that are regulated by binding and hydrolysis of guanosine triphosphate (GTP). Isoforms Rab8a, Rab13, and Rab14 were shown to be necessary for vesicle transport in C_2C_{12} myotubes (Li et al., 2018). They are subject to regulation by Rab-GTPase-activating protein TBC1D4, known as Akt substrate 160 kDa (AS160), which is an Akt direct

effector (Cartee and Wojtaszewski, 2007) although AMPK was also shown to play a role in its activation (Yuasa et al., 2009). Trafficking of Cd36 was shown to involve both AS160 and Rab8a (Samovski et al., 2012).

AMPK serves as cellular primary energy sensor, responding to changes in the [ATP]/[ADP] ratio (Hardie et al., 2012). Its activity regulates another Rab-GTPase-activating protein, TBC1D1, as was shown for GLUT4 vesicles (Taylor et al., 2008). Although knowledge of Cd36 trafficking mechanisms derives from that of GLUT4 due to an overwhelming similarity, there are some differences in their regulation. Müller et al. (2002) proposed that Cd36 and GLUT4 are transported in separate populations of vesicles. Additionally, a protein thiol-modifying agent arsenite is able to recruit GLUT4 containing vesicles to plasma membrane without relocating Cd36 (Luiken et al., 2006).

Among three Akt isoforms only Akt-2 (which is most abundant in the heart) appears to be essential for both insulin- and contraction-induced Cd36 translocation (Jain et al., 2015). PDK also phosphorylates atypical PKC-ζ (protein kinase C zeta) (Liu et al., 2007). Combined activity of both Akt and PKC-ζ is required for the translocation of GLUT4 and Cd36 containing vesicles although there is evidence that PKC-ζ remains constitutively active suggesting it acts as a negative switch of this process (Luiken et al., 2009). Notably, the effects of increased contraction and of insulin are additive for both Cd36 and GLUT4 recruitment (Jain et al., 2009).

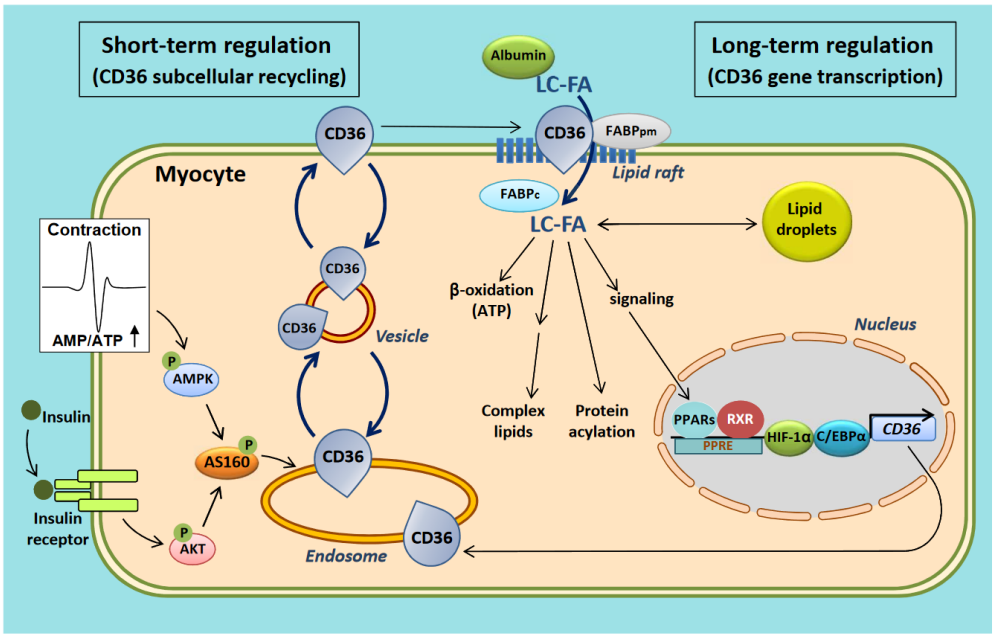

Fig. 3. Schematic overview of pathways regulating FA uptake by Cd36 and cellular effects of LCFA facilitated by Cd36-mediated uptake (reproduced from Glatz and Luiken, 2017).

1.1.3. Cd36 intracellular signaling

Cd36 possesses intracellular signaling capabilities mediated by its association with members of the Src protein-tyrosine kinase family: Fyn, Lyn, and Yes kinases (Huang et al., 1991). For example, TSP-1 or anti-Cd36 antibody induced Cd36 clustering in lipid microdomains on the surface of the endothelial cells which then led to Fyn phosphorylation and activation (Githaka et al., 2016). A downstream effector of this signaling event in endothelial cells is the mitogen-activated protein (MAP) kinase pathway (Yipp et al., 2003). Similar signaling mechanism was observed in macrophages where the binding of oxLDL to Cd36 starts an intracellular signaling cascade involving Fyn/Lyn kinases, MAP kinases and the guanine nucleotide exchange factor Vav and leads to foam cell formation and atherogenesis (Silverstein et al., 2010). Pathogenic Fyn/Lyn signaling was also observed in microglia where Cd36 reacts to β-amyloid leading to pro-inflammatory response via activation of Erk1/2 MAP kinase (Moore et al., 2002). Moreover, knockdown of Fyn in red blood cells protected the cells from malaria-induced endothelial leak (Anidi et al., 2013).

Cd36 association with Fyn allows it to regulate the activity of AMPK, as was shown in myotubes by Samovski et al. (2015). Fyn remained active and bound to Cd36 under low extracellular FA concentration, phosphorylating liver kinase B1 (LKB1) thus abolishing its activity in the cytoplasm by promoting its nuclear translocation. When extracellular FA binds to Cd36, Fyn is released which allows the raising of membrane-bound LKB1. The latter is homologous to CAMKK and has been proven to phosphorylate AMPK and activate its kinase activity (Shaw et al., 2004).

1.1.4. Role of Cd36 in cardiovascular metabolism

Increased workload and subsequent cardiac hypertrophy results in cardiomyocyte remodeling that seems to be instrumental in the development of heart failure although the specific mechanism of this progression remains elusive (Heinzel et al., 2015). A major part in the development of this disorder is attributed to energy metabolism disruption and mitochondria. These organelles occupy 25% of cardiomyocyte volume in humans and 32% in rats (Barth et al., 1992) and are responsible for 93% of the total ATP produced by the heart cell, the rest being provided by glycolysis (Allard et al., 1994). During high-intensity training the heart can utilize 80-90% of the aerobically

produced ATP, which is highly effective but leaves it vulnerable to bioenergetic deficiencies that accompany the hypertrophic heart failure (Mootha et al., 1997).

Fatty acids (FA) are a major energy substrate for cardiac muscle. Given that heart tissue is predominantly aerobic and contracts constantly, a stable supply of FA is crucial for its function. In blood FA are either bound to albumin or contained in the form of triacylglycerol (TG) in very low density lipoproteins (VLDL) and intestinally derived chylomicrons. FA are released from TG via lipoprotein lipase (LpL)-mediated enzymatic cleavage on the surface of endothelial cells through which they get transported to cardiomyocytes (Augustus et al., 2003). Although long chained FA (LCFA) are able to pass cardiomyocyte membranes passively, the speed of this process is insufficient for heart metabolic needs and would require unphysiologically high concentrations of unesterified LCFA. Instead, LCFA uptake is mediated by proteins in a highly effective manner as evident in experiments with blocking agents. For example, digestion of cardiomyocyte surface proteins with trypsin inhibits both uptake and esterification of palmitate by about 80%. Alternatively, incubation of cardiomyocytes with Cd36 blocking agent SSO (see chapter 1.4) inhibited the same processes by 50% (Luiken et al., 1997) and knockdown of Cd36 in mice resulted in 50-80% decrease of labeled LCFA analogs uptake into heart cells (Coburn et al., 2000). There are other proteins that facilitate cardiomyocytic LCFA uptake alongside with Cd36, namely heart-type FA binding protein (H-FABP) and FA transport protein (FATP, 70 kDa). Two types of FABP are distinguished based on their localization – FABPpm is 43 kDa plasma membrane- and mitochondria-associated protein and FABPc is a cytosolic 15 kDa protein. Inhibitory effects of anti-FABPpm antibody and SSO on LCFA transport were not additive indicating that FABPpm works independently from Cd36 (Luiken et al., 1999). FABPc, on the other hand, aids in desorption of FA from the membrane into the aqueous cytoplasm by non-covalently binding them with 1:1 molecular affinity (Glatz et al., 2003). Finally, FATP possesses a very long chain acyl-CoA synthase activity which “traps” LCFA inside the cell and also possibly a LCFA membrane transport mechanism, nature of which is poorly understood (Zou et al., 2002). Both Cd36 and FATP have been observed to localize in clusters adjacent to microvasculature surrounding the heart cells (Gimeno et al., 2003).

Cd36 functioning seems to be decisive in insulin-mediated regulation of LCFA uptake as stimulation with insulin induces Cd36 membrane translocation, but has little

effect on FABPpm and FATP localization (Chabowski et al., 2005). However, FABPpm may be required for proper Cd36 function as transfection of Cd36 into cells devoid of FABPpm does not result in FA uptake increase (Van Nieuwenhoven et al., 1998).

Tight physiological regulation of Cd36 level appears to be important for metabolic fuel selection. This is evident in obese Zucker rats, where increased FA uptake due to Cd36 overexpression leads to cardiac lipotoxicity and insulin insensitivity (Coort et al., 2004). On the other hand, *Cd36* knockout in mice enhanced blood glucose disposal and induce 5-fold faster cardiac glucose uptake as a compensatory response to reduced FA intracellular transport (Hajri et al., 2002). Hearts of Cd36KO mice exhibit downregulated expression of several FA oxidation enzymes and upregulated expression of hexokinase and ketone body metabolic enzymes plus only a modest increase in ADP concentration without significant changes in intracellular ATP (Nakatani et al., 2015). Heart function in Cd36KO mice is normal under baseline conditions and seems to be protected against age-associated cardiac dysfunction as shown by Koonen et al. (2007). This study also highlights lowered glucose oxidation in aged heart of WT but not Cd36KO mice, in which glucose oxidation levels remain high with age. This is commonly attributed to lower oxygen requirements of glucose metabolism, although other regulatory factors may come in play, such as lipotoxicity induced by Cd36 overexpression that was observed in aged WT mice (Koonen et al., 2007).

Increase in myocardial glucose metabolism is also evident in human patients with Cd36 deficiency (Fukuchi et al., 1999). Additionally, individuals with *rs1049673* SNP in *Cd36* gene are at risk of having impaired glucose tolerance and type 2 diabetes (Wang et al., 2012). Another study in humans with no Cd36 expression showed normal palmitate uptake only under elevated extracellular concentration, but not normal or lower, underscoring Cd36 importance for LCFA uptake by the heart (Hames et al., 2014). Same involvement of Cd36 in saturable high-affinity free FA transport is also evident in experiments with Cd36KO mice where the decrease in uptake of ^{3}H-labeled oleate was observed only for low concentrations of this FA (Febbraio et al., 1999).

However, the lack of myocardial metabolic versatility and increased reliance on glucose can be deleterious. High fructose diet caused profound insulin resistance in Cd36KO but not WT mice, characterized by increased insulin concentration and slower glucose clearance (Hajri et al., 2002). Interestingly, knockdown of liver and adipose

lipogenic regulator PGC-1β attenuated insulin resistance induced by high-fructose diet in Sprague-Dawley rats (Nagai et al., 2009).

When subjected to pressure overload induced by transverse aortic constriction, Cd36KO mice exhibited AMPK activation and reduced levels of energy metabolism intermediates (TCA cycle and ATP) despite an increase in glycolytic flux. Cardiac function of these mice was rescued by administration of medium chain FA (MCFA) for which transport through the membrane can be achieved without Cd36 (Sung et al., 2017; Umbarawan et al., 2018). Therefore, although glycolytic compensatory increase helps the heart to stay functional in the absence of normal FA metabolic flux, its protective effect is limited and prone to disruption.

The effect of MCFA-rich diet was also observed in both young and old SHR where it ameliorated hypertrophy and improves cardiac function, enhanced the activity of PPARα and consequentially FA-oxidation enzymes expression (Iemitsu et al., 2008). This was true even for the older animals with well-established LV hypertrophy and signs of fibrosis (Saifudeen et al., 2017). Moreover, high-carbohydrate low-fat diet increased LV mass in hypertensive salt-sensitive Dahl rats, unlike high-fat diet that induced protection from hypertrophy after salt loading (Okere et al., 2006). Similarly, cardiac hypertrophy was observed in Sprague-Dawley rats treated with sulfo-N-succinimidyl derivate of palmitate and in Cd36KO mice (Kusaka et al., 1995; Umbarawan et al., 2018). Results of both pharmacological inhibition and Cd36 knockout experiments indicate that cardiac FA uptake deficiency is linked to hypertrophy and progression to heart failure.

1.2. Study of Cd36 mutation effects in SHR

Unlike Cd36-null mouse, SHR/NIH is not a true knockout model as it is still expressing Cd36 albeit an aberrant form and at lower levels than WKY (Bonen et al., 2009). This mutant protein was undetectable using anti-Cd36 antibody in other studies, however (Hajri et al., 2001). Bonen et al. also reported in the same study that rate of cardiac palmitate absorption was the same in WKY and SHR. This was however determined using isolated giant vesicles and thus may not reflect physiological conditions. Hajri et al. (2001) showed on isolated whole cardiomyocytes that SHR that FA uptake was 50% lower compared to SH.chr4 rats that expressed wild-type Cd36.

SH.chr4 rats (or SHR.4) is a congenic strain that was used in first experiments aimed to evaluate the involvement of *Cd36*-containing genome locus in SHR pathologies by Aitman and colleagues (1999). It carries a region of chromosome 4 of Brown Norway rat in SHR genome. While adipocytes of SHR showed defective glucose uptake in response to insulin and catecholamines, in SHR.4 these values were restored to levels comparable with those in WKY. Compared to SHR, the congenic strain showed lower blood insulin, TG and free FA levels as well as lower blood pressure and faster blood glucose clearance (Pravenec et al., 1999).

To study the consequences of Cd36 dysfunction in SHR a transgenic rescue model SHR-Tg19 was developed by Pravenec et al. (2001). Recipient strain SHR/Ola is a direct descendant of SHR/NIH and therefore bears aberrant *Cd36*. The restoration of a wild-type protein variant improved insulin action and lowered plasma FA levels, but did not reliably lowered blood pressure in these rats (Pravenec et al., 2001). The authors reported several transgenic lines being created (abbreviated Tg-10, Tg-19, Tg-93 and Tg-106) but only one of them, Tg-19 (SHR/Ola-TgN(EF1aCd36)19Ipcv), enjoyed a significantly reduced blood pressure. This is due to the transgenic expression of wild-type Cd36 in the kidney, which has occurred only in Tg-19. This was proven in experiments involving kidney transplantation from SHR-Tg19 to SHR, in which Cd36-expressing kidney was able to lower the blood pressure (Pravenec et al., 2008). The line Tg-93, however, had blood pressure comparable to SHR and close to undetectable renal Cd36 mRNA. Despite this it showed improved glucose tolerance and lower circulation levels of free FA (Pravenec et al., 2003). Lack of effect on hypertension was also observed in MCFA-supplemented SHR despite that this diet improved cardiac function and prevented hypertrophy development (Sung et al., 2017). This may point to importance of scavenger function of Cd36 in renal regulation of blood pressure evident in SHR-Tg19.

Therefore, further research performed in the Institute of Physiology (Czech Academy of Sciences) and in our facility utilized the line Tg-19. Comparison of this strain to SHR by Neckář et al. (2012) revealed lower serum free FA and TG as well as cardiac TG levels and a significant decrease in infarct sizes was observed in isolated hearts of SHR-Tg19. On the other hand, transgenic strain exhibited marked increase in ventricular arrhythmias frequency and incidences of premature ventricular contractions.

This is an aggravation of arrhythmia susceptibility already present in SHR compared to WKY (Choisy et al., 2007).

Mitochondrial energy provision measured as respiration of heart homogenate was improved in SHR-Tg19 and expressions of mitochondrial genes involved in oxidative phosphorylation was increased compared to SHR. Interestingly, there was observed any decrease in reactive oxygen species (ROS) markers in SHR-Tg19 (Neckář et al., 2012). Neither there was a decrease in ventricular wall thickness or heart to body weight ratio. Despite the aforementioned antihypertrophic effect of such agents as resveratrol and statins or MCT supplementation, it appears that rescue of Cd36 alone is not sufficient to prevent hypertrophy progression, in fact the study by Klevstig et al. (2003) revealed a small but statistically significant increase in heart to body weight ratio of SHR-Tg19.

In the same study dobutamine stress ECG test showed higher maximal fractional shortening in SHR-Tg19 suggesting changes in β-adrenergic responsiveness. Experiments by our group showed that β-adrenergic signaling system elements are indeed upregulated in SHR-Tg19. This includes increase in total number of β-adrenergic membrane binding sites and an increase in the ratio of β1 to β2 binding sites. Expression of adenylyl cyclase isoform 5 (AC5) was increased in SHR-Tg19 as well as stimulated AC activity. Expression and phosphorylation of PKA were also elevated in the transgenic strain (Klevstig et al., 2013).

1.3. Beta-adrenergic signaling system in cardiomyocytes

One of the currently most used treatments for patients with primary hypertension are β-adrenergic receptor blockers which act by prohibiting the interaction of endogenous catecholamines with β-adrenergic receptors (βAR) (Frishman, 2016). Together with αAR they belong to the superfamily of G-protein-coupled receptors (GPCRs). These receptors have common structure that consists of 7 hydrophobic transmembrane α-helices connected by three extracellular and three intracellular loops, extracellular amino terminus and intracellular carboxyl terminus (Trzaskowski et al., 2012). GPCRs are present only in eukaryotes where they perform in a vast number of signaling events. Their ligands include hormones, neurotransmitters, odor and light-sensitive molecules (King et al., 2003).

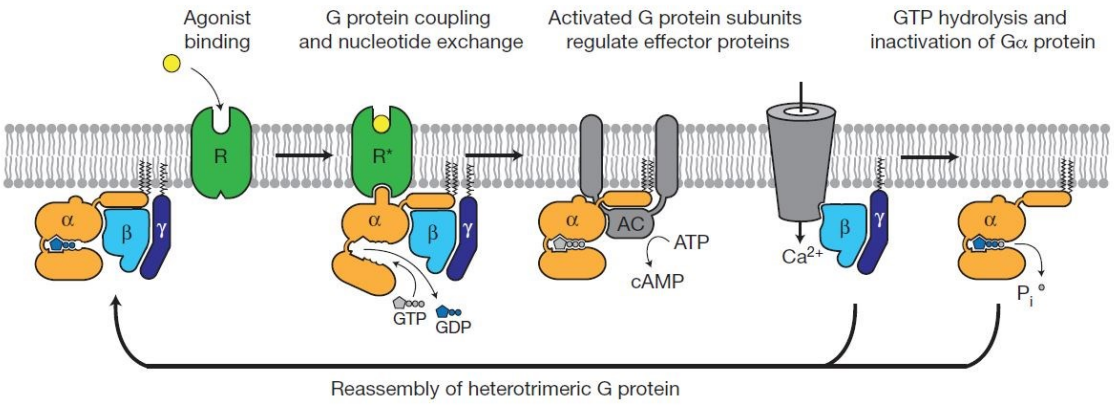

Fig. 4. Schematic illustration of GPCR-mediated G-protein activation cycle. Upon transition to ligand-bound active state R* the receptor binds trimeric G-protein complex. Subsequent activation and separation of α- and β/γ-subunits allow them to affect downstream targets. Reproduced from Rasmussen et al. (2011).

Three types of βAR are identified – β1, β2 and β3. They are 70% homological and differ in tissue expression, membrane distribution and downstream signaling. β1-AR is the predominant subtype in the heart whereas β2 is most expressed in the lung smooth muscle cells and β3 in brown adipocytes. Nevertheless, they are also expressed in cardiomyocytes, although in lesser proportions than β1. Sympathetic stimulation of β1-AR is a very effective mechanism of increasing cardiac output. It results in positive inotropic and chronotropic effects which are utilized during the "fight-or-flight" response.

Upon agonist binding the GPCR molecule changes its conformation by adjusting the position of its transmembrane helices. For β2-AR at least three conformational states are known: inactive, intermediate and active (Dror et al., 2011). The latter state allows for guanosine nucleotide-binding protein (G-protein) complex to bind to a specific domain on GPCR and become activated (Fig. 4). This complex consists of Gα- and Gβ/γ-subunits that exist as a heterotrimer but dissociate upon activation during which Gα-subunit exchange bound GDP to GTP. This allows it to convey its effects to downstream targets at the cost of bound GTP hydrolysis. Afterwards, GDP-bound α-subunit associates with Gβ/γ-subunit and restores complex's inactive conformation (Taylor, 1990).

There are three main types of Gα proteins: $G\alpha_s$ and $G\alpha_i$ exhibit stimulatory and inhibitory effect respectively on adenylyl cyclase (AC) activity, while $G\alpha_q$ activates

phospholipase Cβ thus resulting in IP_3 second messenger production. $G\alpha_s$ couples to all three β-AR subtypes whereas $G\alpha_i$ only to β2- and β3-AR (Birnbaumer, 2007). Active AC catalyzes the formation of cyclic adenosine monophosphate (cAMP) which serves as a second messenger and amplifier of intracellular β-AR signaling.

Canonical downstream cAMP pathway involves activation of PKA, phosphorylation of targets that include phospholamban (PLB), troponin and cAMP response element-binding protein (CREB). Phosphorylated PLB relaxes its inhibition of sarcoplasmic reticulum calcium pump (SERCA) which results in an increase of intracellular Ca^{2+} concentration. Phosphorylated troponin enhances myofilament relaxation kinetics during diastole (Frank and Kranias, 2000; Rao et al., 2014). CREB is a transcription factor that binds to cAMP response element (CRE) DNA sequences using leucine zipper motif (Shaywitz and Greenberg, 1999).

Noncanonical mediators of cAMP effects are termed exchange proteins activated by cAMP (Epac). There are two isoforms of Epac. These proteins regulate many physiological processes either independently or in combination with PKA. Epac1 controls cardiac hypertrophy during neonatal development overriding PKA effects by inhibiting ERK5 (Bos, 2006). Expression of both Epac1 and 2 is subject to change depending on the developmental stage (Grandoch et al., 2010). Epac proteins are implicated in gap junction formation by enhancing connexin 43 expression (for detailed Cx43 description see 1.5) whereas PKA potentiates gap junctional gating function (Somekawa et al., 2005).

Continuous β1-AR stimulation is considered detrimental as it is one of the determinants of pathologic cardiac hypertrophy that precedes heart failure. Healthy cells possess a mechanism of GPCR downregulation which includes G protein-coupled receptor kinase (GRK) and β-arrestin mediated signaling a result of which is GPCR internalization. This signaling appears deficient in hypertrophied myocardium. On the other hand, PKA signaling is increased under these conditions (Grisanti et al., 2018). Unlike β1, β2-AR signaling may be cardioprotective as indicated by some studies (Talan et al., 2011; Woo et al., 2015). This may be due to β2-AR coupling with $G\alpha_i$ and to the spatial differences in β1 and β2 signal propagation. Under physiological conditions β2-AR are localized to caveolae and the t-tubules whereas β1-AR are distributed between bulk sarcolemma and caveolae (Rybin et al., 2000). Another degree of signal spatial resolution is achieved by association of cAMP producers and effectors

with membrane-bound A-kinase anchoring proteins (AKAPs). These proteins create specific signaling hubs that cluster together PKA as well as different isoforms of AC and phosphodiesterases (PDEs). The latter convert cAMP to AMP thus spatially confining the signal propagation (Boularan and Gales, 2015).

During the onset of heart failure the β-AR signaling pathway becomes chronically overstimulated leading to apoptotic response and loss of pumping function. The ratio of β2 to β1 AR dramatically increases, although this is considered cardioprotective due to $G\alpha_i$ restrictive action on AC. Nevertheless, chronically stimulated β2-AR activity was shown to lead to hypertrophic response involving CaMKII activation (Anderson et al., 2011). In heart failure cardiomyocytes show loss of their normal morphology including t-tubule disruption. Compartmentalization of cAMP signaling becomes impaired as β2-AR are losing their caveolar association and instead signal outside their usual membrane domain confinement (Nikolaev et al., 2010). Notably, overexpression of Cav-3 restores the disrupted localization of signaling of β2-AR (Wright et al., 2014).

1.4. Lipid microdomains and caveolae in cardiomyocytes

Lipid bilayer can be seen as a two-dimensional fluid that has regions of increased or decreased molecular mobility. Two distinct membrane phases can exist in the living cell: L_d (liquid disordered) characterized by irregular orientation of the fatty acid tails and L_o (liquid ordered) regions that are enriched in cholesterol, sphingolipids in their outer leaflet and GPI-linked proteins. These membrane regions are termed lipid rafts due to their relative stability compared to the "sea" of surrounding L_d membrane. Lipid rafts measure 25-200 nm in diameter and can serve as a scaffolding platforms for many membrane proteins thus influencing their distribution and signaling (Lingwood and Simons, 2010). One of the commonly used methods for study of lipid microdomains is based on their insolubility in non-ionic aqueous detergents, allowing researches to isolate so called detergent-resistant membranes (DRM) (Brown and Rose, 1992). DRMs are generally considered to represent naturally occurring membrane microdomains although the extent of their similarity have been questioned (Sonnino and Prinetti, 2013). These are also different imaging techniques available to study lipid domains such as FRET (Förster resonance energy transfer) (Castro et al., 2013).

Caveolae are a subtype of lipid rafts 50-100 nm in diameter. They are characterized by flask-like invaginated shape and include such proteins as caveolins and

cavins (Parton and Collins, 2016). Caveolins have a high affinity to cholesterol and are able to bind numerous proteins due to their intracellular scaffolding domain (Lisanti et al., 1994). There are three subtypes of caveolin proteins found in vertebrates, denoted 1 to 3. Caveolin-1 (Cav-1) is ubiquitously expressed with highest levels found in adipocytes and endothelial cells, Cav-2 is co-expressed and co-localizes with Cav-1, forming a heterodimer together (Williams and Lisanti, 2004).

Immunodetection of caveolin isoforms initially performed by Song et al. (1996), showed that the only isoform in mouse heart tissue is Cav-3. This, however, was challenged later by Volonte et al. (2008), who detected Cav-1 expression in mice atria in form of heterodimers with Cav-3. They however did not observe presence of Cav-1 in ventricles. Later, studies by Patel et al. showed that all caveolin isoforms are expressed in rat and mouse cardiomyocytes isolated by collagenase perfusion and that Cav-1 and 3 are expressed in similar levels (Head et al., 2006; Patel et al., 2007). Loss of Cav-1 in mice results in a progressive cardiomyopathy and hypertrophy via a mechanism that involves p44/42 MAP kinases hyperactivation (Cohen et al., 2003). Same effects were observed in the hearts of Cav-3 KO mice (Woodman et al., 2002). Further studies on rodent KO models revealed that Cav-3 is muscle cell specific while Cav-1 is localized in cardiac fibroblasts and endothelial cells (Razani and Lisanti, 2001). Cav-3 is indeed crucial for caveolae formation in the sarcolemma, as Cav-1 KO mice still form observable caveolae in their cardiomyocytes (Tsutsumi et al., 2010). Heart of SHR expresses both caveolins 1 and 3, which are colocalized with α1-AR in the heart (Fujita et al., 2001).

Scaffolding domain of caveolins allows them to act as a platform for signaling proteins such as ERK1/2, eNOS and adenylyl cyclase. Cav-1 expression is negatively regulated by tumor necrosis factor α (TNF-α) in both isolated adipocytes (Palacios-Ortega et al., 2015) and heart cells. In the latter cells the activity of TNF-α was induced using ozone administration in experiments which have demonstrated differential regulation of Cav-3. Unlike Cav-1, its expression levels were elevated in rats after a month of O_3 exposure, but at the end of second month both Cav-1 and Cav-3 were downregulated (Sethi et al., 2012).

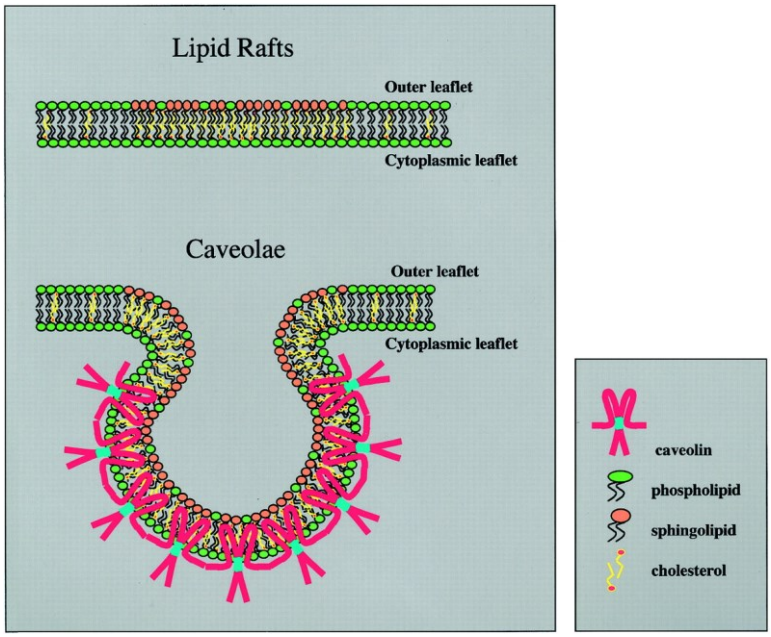

Fig. 5. Schematic representation of lipid raft and caveolae membrane microdomains molecular organization (reproduced from Razani et al., 2002).

One of the functions of caveolae in the heart is signaling induced by cell stretching. Mechanical stretching of the cells forces caveolar membranes to unfold which influence signaling by caveolae-associated proteins such as kinases Src, RhoA and ERK (Gervásio et al., 2011). This leads to changes in cell proliferation and hypertrophic growth. Small GTPase RhoA is particularly known for its regulation of cytoskeletal dynamics (Shimokawa et al., 2016). GTPase RhoA is activated by guanine nucleotide exchange factors (GEFs) and regulated by phosphorylation on Ser188 by PKA and PKG. The phosphorylation leads to translocation of RhoA from the membrane to cytosol (Sawada et al., 2001) while protecting it from proteasomal degradation (Rolli-Derkinderen et al., 2005). Ser188 phosphorylation of RhoA does not affect GTP binding, on the contrary, it promotes formation of a complex with Rho-GDP dissociation inhibitor (Lang et al., 1996). RhoA in its GTP-bound form binds to a Rho-kinase and activates it. By troponin phosphorylation Rho-kinase inhibits tension generation in the cardiomyocyte and promotes cardiac hypertrophy (Fukui et al., 2008).

While all caveolins are expressed on the surface of cells, Cav-3 additionally associates with the t-tubule network and is implicated in their formation, as determined using immunoelectron microscopy (Parton et al., 1997). Additionally, experiments were

done with Amphotericin B, a cholesterol depleting agent, to disrupt Cav-3 membrane localization in C_2C_{12} myotubes. Cav-3 normal co-localization with t-tubular protein α1-DHPR was ablated after t cholesterol depletion (Carozzi et al., 2000). Similar t-tubular localization was shown for Cav-3 in isolated skeletal muscle fibers (Ralston and Ploug, 1999). Moreover, ultrastructural study of Cav-3 null mice showed abnormally organized t-tubule system in skeletal muscle (Galbiati et al., 2001). Therefore, it appears that the t-tubular system, which is essentially a deep and branched sarcolemma invagination, is stabilized by raft-associated Cav-3. Mutations of this protein lead to the development of limb-girdle muscular dystrophy is which a severe impairment of muscular caveolae formation and t-tubular disorganization is observed (Minetti et al., 2002).

Co-localization with caveolae was observed for β1 and β2 AR as well as their cognate trimeric G-protein subunits (Schwencke et al., 1999). Interestingly, there is a difference between basal and apical ventricular cardiomyocytes in caveolae content. In the basal cells there were more caveolae associated with β2-AR signaling hubs whereas the signaling machinery of apical cells was more broadly distributed to the crest area of cardiomyocytic sarcolemma which results in less confined cAMP signal and increased contractility (Wright et al., 2018).

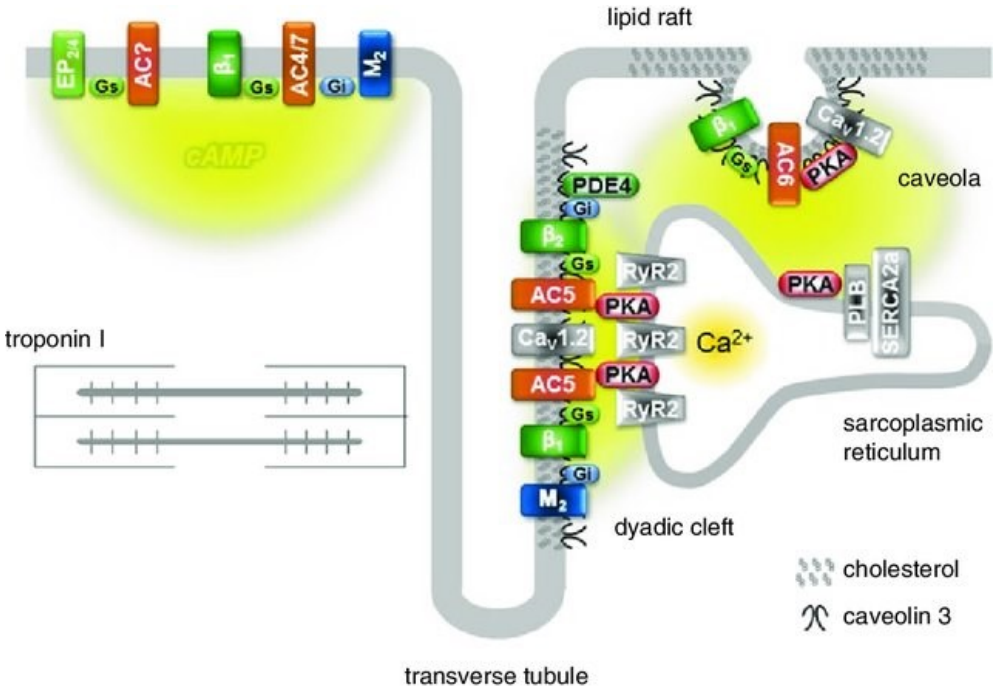

Fig. 6. Spatial separation of cAMP signal (yellow) originating from different membrane signaling domains. Reproduced from Agarwal et al. (2012).

1.5. Connexin 43 function and role in heart disease

Synchronous heart contractility requires the propagation of action potentials between the neighboring cells. This is achieved due to gap junctions located at the intercalated disc membrane. Gap junctions become functional when two protein complexes termed connexon hemichannels dock to each other thus connecting adjacent membranes. Resultant pores allow rapid exchange of metabolites up to ~1 kD in size.

Each hemichannel consists of 6 protein subunits of the connexin family, in which there are 21 known members named after their theoretical molecular mass (Esseltine and Laird, 2016). The most abundant and well-studied member of this family in cardiac myocytes is connexin 43. It passes the membrane four times with its alpha-helices and has one intracellular loop and two extracellular loops with which it docks to the opposing hemichannel. Both N- and C-tails are located in the cytoplasmic side of the membrane (Bai et al., 2018).

Phosphorylation of the C-terminal region regulates the open/closed state of gap junctions and turnover of its connexin subunits by inducing conformational changes in the protein. PKA was shown to be a positive regulator of connexin 43 assembly into hemichannels and their trafficking to the plasma membrane (Atkinson et al., 1995; Paulson et al., 2000; TenBroek et al., 2001). Casein kinase 1 (CK1) inhibition led to an increase of non-junctional connexin 43 and decrease of Cx43 associated with DRM fraction (Cooper and Lampe, 2002). Connexin 43 was shown to be targeted to lipid rafts where it was co-localized with caveolin-1 (Schubert et al., 2002). This co-localization was shown to be induced by interaction of both cav-1 and Cx43 with PKCγ (Lin et al., 2003)

Connexin is essential for heart development as Cx43-knockout mice die prenatally. Partial knockout experiments showed that low levels of connexin 43 expression led to slowed ventricular conduction and increased arrhythmias susceptibility (Jansen et al., 2010).

2. AIMS OF THE THESIS

Cd36 is a multifunctional protein which along with facilitating LCFA uptake possesses signaling capabilities. We wondered what changes could bring the restoration of expression of this protein to the protein makeup of cardiac ventricles, to metabolic activity and distribution of some signaling proteins.

AIM I – Investigation of the effect of Cd36 expression in SHR on a broader protein composition of left and right ventricles using a combination of top-down and bottom-up proteomic approaches.

AIM II – Assessment of activity and expression of metabolic enzymes in mitochondria isolated from the left and right ventricles of SHR and SHR-Tg19.

AIM III – Characterization of expression and membrane fraction distribution of connexin 43 as well as selected components of β-adrenergic signaling system.

3. MATERIALS AND METHODS

3.1. Animals

All procedures were performed in conformity with the Animal Protection and Welfare Law of the Czech Republic (311/1997) and were approved by the Ethics Committee of the Institute of Physiology, Academy of Sciences of the Czech Republic. Two groups of animals were used to conduct the experiments: SHR/Ola (referred to as SHR) and transgenic SHR/Ola-TgN(EF1aCd36)19Ipcv line (SHR-Tg19). Second group harbors the wild type of Cd36 transgene (Pravenec et al., 2001). Rats were kept at a 12 h : 12 h light/dark period with free access to standard laboratory chow and water. Adult males around the age of 4 month and weighting 250-270 g were sacrificed by cervical dislocation and used for tissue procurement. For biochemical experiments, the hearts were quickly excised, placed into an ice-cold PBS solution and disserted into the right ventricle, septum and left ventricle. Each part was snap-frozen in liquid nitrogen and stored at –80 °C until use. Left and right ventricles were used immediately in case of respiratory measurements.

3.2. Chemicals and reagents

All chemicals, unless stated otherwise, were obtained from Sigma Aldritch (St. Louis, MO, USA) in the highest purity available. Sucrose, HEPES, acrylamide and bis-acrylamide were purchased from SERVA (Heidelberg, Germany). Pyruvate, ADP, ATP, NADH, acetyl-CoA, 5,5-dithio-bis-(2-nitrobenzoic acid) and cytochrome c were purchased from Boehringer Ingelheim (Ingelheim, Germany). SuperSignal West Dura chemiluminescent substrate was from Pierce Biotechnology (Rockford, IL, USA). Antibodies that were used in experiments are listed in Table 1.

Table 1. List of primary antibodies used in the study

Antibody	Producer	Cat. number	Dilution
Catalase	SCBT*	sc-50508	1:2000
Caveolin-1	SCBT	sc-894	1:10000
Caveolin-3	SCBT	sc-5310	1:5000
Cd36	SCBT	sc-9154	1:1000
Connexin 43	SCBT	sc-9059	1:8000
ERK1/2	SCBT	sc-292838	1:10000
p-ERK1/2	SCBT	sc-101761	1:2000
Flotilin-1	SCBT	sc-25506	1:5000
Gαi2	SCBT	sc-7276	1:1000
Gβ	SCBT	sc-378	1:10000
Pmp70	SCBT	sc-514728	1:1000
Prohibitin	SCBT	sc-28259	1:2000
RhoA	SCBT	sc-418	1:5000
p-RhoA	SCBT	sc-32954	1:5000
SDHA	Thermo	#459200	1:40000
Total OXPHOS	Abcam	ab110413	1:10000
β1-AR	Alomone labs	AAR-023	1:2000
β2-AR	Alomone labs	AAR-016	1:2000

* - Santa Cruz Biotechnology

3.3. Sample preparation

The postnuclear supernatant (PNS) was obtained from left and right ventricular tissue samples. All steps were performed either on ice or at 4°C. Samples were allowed to thaw on ice, weighted and placed in 4 ml per 1 g of tissue of buffer TMES (20 mM Tris, 3 mM $MgCl_2$, 1 mM EDTA, 250 mM sucrose; pH 7.4) containing cOmplete protease inhibitor cocktail and phosStop phosphatase inhibitor cocktail diluted according to manufacturer's instructions (Roche). Tissue was finely cut with scissors

and processed using Ultra-Turrax T25B tissue disperser 2 times ×15 s at 24000 rpm (IKA Works, Inc., Wilmington, NC, USA) and then passed through the motorized Potter-Elvehjem Teflon-glass homogenizer (1200 rpm, 10 strokes). The resulting homogenate was centrifuged at 720 ×g for 10 min (Hettich Universal 320R centrifuge). The supernatant was collected and the pellet was resuspended in the initial volume of the buffer TMES and then homogenized with a Teflon-glass homogenizer and centrifuged under the same conditions as before. Two supernatants were pooled, resulting in the PNS which was aliquoted, frozen in liquid nitrogen and stored at –70°C for further use.

Plasma membrane-enriched fraction (PM) was isolated from PNS. 4 ml of PNS was gently pipetted on top of 20 ml of 18% Percoll gradient centrifugation medium in buffer TME (20 mM Tris, 3 mM $MgCl_2$, 1 mM EDTA; pH 7.4) in Beckman tubes which were subsequently centrifuged using Beckman Coulter Optima L-90K centrifuge (Beckman Coulter Inc., Brea, CA, USA) in a Type Ti 50.2 Beckman rotor at 26000 rpm for 15 min with maximal acceleration and "slow" deceleration at 4°C. Two light-scattering areas were observed in the middle of the tubes. Higher one was carefully collected using a 1000 µl pipette and mixed with 20 ml of buffer TME in a new set of Beckman tubes. Afterwards the tubes were centrifuged in Type Ti 50.2 Beckman rotor at 40000 rpm for 1 h with maximal acceleration and deceleration at 4°C. Pellet was resuspended in a small amount of buffer TME, aliquoted, frozen in liquid nitrogen and stored at –70°C.

For high-resolution respirometry and enzyme activity assays samples of subsarcolemmal mitochondrial population were isolated. After rapid excision, rat hearts were put in an ice-cold phosphate-buffered saline (137 mM NaCl, 2.7 mM KCl, 10 mM Na_2HPO_4, 1.8 mM KH_2PO_4; pH 7.4). The left and right ventricles were separated and finely minced on an ice-cold Petri dish covered with parafilm. The sliced tissue was suspended in 20 volumes of buffer A (250 mM sucrose, 10 mM Tris, 2 mM EDTA, 2 mM EGTA, 0.5 mg/ml BSA; pH 7.2) and homogenized with a Teflon-glass homogenizer (600 rpm, 1 min.). The homogenate was centrifuged (800 ×g, 10 min) and the resulting supernatant was filtered through a 56 µm nylon mesh and then centrifuged again (8000 ×g, 10 min). The obtained pellet was resuspended in buffer B (250 mM sucrose, 10 mM Tris; pH 7.2) and kept on ice for high-resolution respirometry

measurements that were performed on the day of sample preparation. The leftover samples (to be used in enzyme assays) were stored at −20°C.

3.4. One-step separation of detergent-resistant membranes (DRM)

This method was adapted with modifications from Rubin and Ismail-Beigi (2003). Samples of PM were treated with 1% Triton X-100 in a buffer containing 20 mM Tris HCl, 3 mM $MgCl_2$, 2 mM $CaCl_2$, 1 mM EDTA (pH 7,4). Samples were diluted with the buffer to 1 µg of protein per 1 µl. After 1 h on ice the samples were centrifuged (128000 × g, 1h, 4 °C) in Beckman tabletop ultracentrifuge. After the supernatant (soluble fraction) was collected the pellet (insoluble fraction) was resuspended in the same volume of buffer TME. Both were snap-frozen and stored at –70 °C for further analysis.

3.5. Protein concentration assay

Concentration of the total protein in the samples was determined using the Smith assay (Smith et al., 1985). Samples were pipetted on a microtiter plate in triplicates, covered and incubated for 30 min at 60 °C. The plate was read at 562 nm on Synergy™ HT microplate reader (BioTek Instruments, Inc., Winooski, VT, USA) and analyzed using Gen5 application.

3.6. SDS electrophoresis and western immunoblot analysis

Expression of selected proteins was assessed using SDS polyacrylamide gel electroseparation (SDS-PAGE) and western immunoblotting. SDS-PAGE was conducting using Bio-Rad Mini-PROTEAN® Tetra Handcast System. Separating gel solution (10% bis-acrylamide, 375 mM Tris, 2,5% ammonium persulfate, 0,1% SDS, 0,04% TEMED) was cast into a 1,5 mm-wide glass chamber under a layer of butanol, which was washed out after gel stiffening and replaced with focusing gel solution (4% bis-acrylamide, 125 mM Tris, 0.09% ammonium persulfate, 0,1% SDS, 0,08% TEMED) covered with 10- or 15-welled comb. PNS and membrane samples were diluted with H_2O and Laemmli buffer to obtain 2 mg/ml protein concentration and incubated for 2 min at 95 °C. 10 µg of thusly prepared sample solution was carefully pipetted into each well. The system was run at 200 V for 1 h. After the electroseparation

the proteins were transferred onto 0,45 nm nitrocellulose membranes using Bio-Rad Mini Trans-Blot® cells (100 V, 1 h) filled with 25 mM Tris, 190 mM glycine, 20% methanol blotting buffer.

To quantify total protein signal, membranes were stained with Ponceau S. Then, to wash out the stain and block the membranes 5% skimmed milk in TWEEN-Tris buffered saline (TTBS) was used (20 mM Tris, 150 mM NaCl, 0,1% TWEEN 20, pH 7,4). Primary antibodies were diluted in 1% skimmed milk TTBS. Membranes were incubated in blocking solution for 30 minutes at RT and then overnight in the solution with primary antibodies at +4 °C on the rocking platform. Next day the membranes were washed 3 ×10 min with washing buffer (TBS, 0,3% TWEEN 20) and incubated with secondary antibodies diluted in 1% skimmed milk TTBS for 1 h at RT. Afterwards the membranes were washed 3 ×10 min again and treated with SuperSignal™ West Dura substrate (Thermo Fisher Scientific, Rockford, IL, USA) for 1 minute. X-ray medical films were used to capture the signal.

Densitometric analysis of the bands was conducted using FIJI software (Schindelin et al., 2012). Immunoblot assays were performed at least three times on each type of sample.

3.7. Dot blot technique

Nitrocellulose membrane was soaked in the blotting buffer described above. Drops of PM samples (1 µl) were placed on the membrane. Subsequent procedure is similar to immunoblotting. The membrane was incubated in the blocking buffer for 30 min at RT. Afterwards it was placed in a TTBS containing 1% skimmed milk and 5 ng/ml cholera toxin subunit B HRP conjugate (Thermo Fisher Scientific) for 1 h at RT. The membranes were washed 3 x 10 min and signal was captured on film using the same reagents and equipment as in Western blotting.

3.8. α-Adrenoceptor saturation binding

Myocardial α-AR density and affinity were determined by specific binding of the α-AR antagonist [^{3}H]Prazosin (Amersham Biosciences, Buckinghamshire, UK). Samples of myocardial crude membranes (100 µg protein) were incubated in buffer A (50 mM tris–HCl, 10 mM MgCl2, 1 mM ascorbic acid; pH 7.4) containing increasing concentrations of [^{3}H]Prazosin (0.0625–2 nM) for 1 h at 37 °C in a total volume of 0.5

ml. The binding reaction was terminated by addition of 3 ml ice-cold buffer B (50 mM Tris–HCl, 10 mM MgCl2; pH 7.4) and subsequent filtration through GF/C filters (Whatman Ltd., Oxford, UK) presoaked for 1 h with 0,3% polyethylenimine. The filters were washed twice with 3 ml of ice-cold buffer B. Radioactivity retained on the filters were determined by liquid scintillation counting using Cytoscint cocktail (ICN Biomedicals, Irvine, CA, USA). Nonspecific binding was defined as that not displaceable by 10 μM phentolamine, and it represented <25 % of total binding.

3.9. Two-dimensional electrophoresis

Samples of PNS prepared as described before and diluted to protein concentration of 1 mg/ml were precipitated with ice-cold acetone overnight at −20 °C. Next day the samples were centrifuged at 9000 ×g for 20 min at 4 °C, the supernatant was discarded and the pellet was precipitated by the addition of ice-cold 6% trichloroacetic acid (TCA). After 1.5 h samples were centrifuged at 9000 ×g for 10 min at 4 °C, the supernatant was again discarded. The pellet was resuspended in 600 μl of ice-cold 96% ethanol. After 1 h at room temperature the mixture was centrifuged again at 9000 ×g for 10 min at 4 °C, supernatant was discarded and the pellet was resolubilized in 250 μl isoelectric focusing (IEF) sample buffer (7 M urea, 2 M thiourea, 4% CHAPS, 1% DTT, 1% ampholines pH 3–10, 0.01% bromphenol blue). Samples were left for 3 h at room temperature, and then transferred into a groove of the Immobiline DryStrip reswelling tray (GE Healthcare). In the reswelling tray grooves the protein samples were covered with Immobiline DryStrips (linear pH gradient 3-11 NL, 13 cm) and left overnight.

We performed isoelectric focusing using the Multiphor II system (GE Healthcare). The system was programmed to sustain several voltages during run: 150 V for 5 h, 500 V for 1 h, 3500 V for 12 h and 500 V for 3 h. The cooling was set at 14 °C. After the IEF the strips were either stored at −20 °C or used immediately. Strips were rinsed thoroughly with ultrapure water then dried quickly on filter paper, and placed into 5 ml of equilibration buffer 1 (50 mM Tris– HCl pH 6.8, 6 M urea, 0.1 mM EDTA, 2% SDS, 30% glycerol and 0.01% bromophenol blue) with 1% DTT for 10 min. The purpose of this solution is to reduce disulfide bridges and other oxidized groups. Then the strips were alkylated for 10 min in equilibration buffer 2 containing 2.5% iodoacetamide instead of 1% DTT. Finally, the strips were placed on top of an SDS-

polyacrylamide gel. Molecular weight (Mw) markers were absorbed into a piece of filter paper and placed near the alkaline side of the strips. Then the strip and paper containing the Mw markers were covered with 0.5% agarose. Gels were run vertically at a constant current of 20 mA for 20 min and then at 90 mA for 4 h untill the bromophenol blue dye reached the bottom of the gel. During run the apparatus was cooled to 15 °C using the Hoefer SE 600 unit (GE Healthcare).

For mass spectrometric (MS) analysis, the gels were stained by colloidal Coomassie Brilliant Blue G-250 (CBB). The gels were fixed in 50% methanol / 7% acetic acid for 1 h and incubated with CBB (17% ammonium sulfate, 34% methanol, 3% orthophosphoric acid and 0.1% Coomassie G-250) overnight. After staining, the gels were washed three times in ultrapure sterile water and stored in 1% acetic acid at 4 °C. The stained 2D gels were scanned with an imaging densitometer ScanJett 5370C (HP) and quantified by PDQuest software (Bio-Rad, version 7.3.1). The process included spot detection, gel matching and spot quantification. Master gel was constructed as a synthetic image that contains the spot data from all the gels in the MatchSet. At least four replicates were performed for each sample. All matched and unmatched spots were then checked in a manual manner. Protein levels showing significant quantitative differences at least two-fold were selected to mass spectrometric analysis. Protein levels showing significant quantitative differences at least two-fold (Student's t-test, $p \geq 0.05$) were selected for mass spectrometric analysis.

3.10. MALDI-TOF MS/MS

For the matrix-assisted laser desorption/ionization – time of flight tandem mass spectrometry (MALDI-TOF MS/MS) analysis we excised individual CBB-stained spots from 2D gel, then sliced them into 1 mm^3 pieces and placed into microtubes which were then covered with 100 µl of 50 mM ammonium bicarbonate (ABC) buffer in 50% acetonitrile (ACN) with 50 mM DTT. The samples were sonicated in an ultrasonic bath for 5 min. After 15 min the supernatant was discarded and the gel covered with 100 µl of 50 mM ABC/50% ACN with 50 mM iodoacetamide and sonicated for 5 min. After 25 min, the supernatant was removed and exchanged for 100 µl 50 mM ABC/50% ACN with 50 mM DTT and sonicated for 5 min again. Supernatant was discarded and samples were sonicated for 5 min in 100 µl of ultra-pure water. The water was then discarded and samples sonicated for another 5 min in 100 µl of ACN. ACN was

discarded and microtubes with samples were left open for a few minutes to allow the rest of ACN to evaporate. Five nanograms of trypsin in 10 µl of 50 mM ABC were added to the gel. Samples were incubated at 37 °C overnight. Trifluoroacetic acid (TFA) and ACN were added to the final concentration of 1% TFA and 30% ACN. Samples were sonicated for 10 min and 0.5 ml aliquot of trypsin digest was transferred onto MALDI target and let to dry. The area covered by dried trypsin digest was covered with 0.5 ml drop of alpha-cyano-hydroxycinnamic acid solution (2 mg/ml in 80% ACN) and let to dry again. Samples were measured using a 4800 Plus MALDI TOF/TOF analyzer (Applied Biosystems/MDS Sciex) equipped with a Nd:YAG laser (355 nm, firing rate 200 Hz). The data were analyzed using in-house running Mascot server 2.2.07 and matched against comprehensive SwissProt 20140303 database of protein sequences (542,503 sequences; 192,888,369 residues). Database search criteria were as follows: enzyme = trypsin; taxonomy =Rattus norvegicus. Cysteine carbamidomethylation was set as fixed modification. Methionine oxidation and deamidation (NQ) were set as variable modifications. One missed cleaving site was allowed. Precursor accuracy was set at 50 ppm and the accuracy for MS/MS spectra at 0.25 Da. Only hits that were scored as significant (MASCOT score ≥ 51, p b 0.05) were accepted. Protein scores were derived from ions scores at a non-probabilistic basis for ranking protein hits.

3.11. Label-free quantification, MaxLFQ

Samples containing 200 µg of total protein were dissolved in 2% sodium deoxycholate/200 mM tetraethylammonium bicarbonate buffer (pH 8.0) and reduced with 5 mM tris-(2-carboxyethyl)-phosphine. After 60 min at 60 °C, the free cysteine residues were blocked by 10 mM methyl methanethiosulfonate in isopropanol and incubation at room temperature for 10 min. Digestion was carried out by addition of 4 µg of trypsin to each sample and incubation for 12 h at 37 °C. Trypsin cleavage was terminated by acidification of reaction mix with trifluoroacetic acid (TFA) to a final concentration of 0.1%. Removal of sodium deoxycholate was performed five times by extraction with two volumes of ethyl acetate (8000 ×g, 30 s). The aqueous phase containing the peptide mixture was placed into SpeedVac for 20 min and samples were desalted with MacroTrap C18 cartridge (MICHROM Bioresources, Inc., USA). Finally, the 2 µg of the peptide mixture were loaded on trap column PepMap 300C 18 column, 5 mm × 300 µm ID, 5 µm particles, 300 Å pore size (163589, Thermo Scientific).

Individual peptides were separated by HPLC using EASY-Spray column, 50 cm × 75 μm ID, PepMap C18, 2 μm particles, 100 Å pore size (ES 803, Thermo Scientific). The separation of peptides was achieved via a linear gradient for 2 h between mobile phase A (2% acetonitrile, 0.1% formic acid) and B (80% acetonitrile, 0.1% formic acid). Separation was started by running the system with 2% mobile phase B, followed by gradient elution to 40% B. Eluting peptide cations were converted to gas-phase ions by electrospray ionization and analyzed on a Thermo Orbitrap Fusion mass spectrometer (Q-OT-qIT, Thermo Fisher Scientific, Rockford, IL, USA). Survey scans of peptide precursors from 400 to 1600 m/z were performed at 120K resolution (at 200 m/z) with a 5 × 105 ion count target. Tandem MS was performed by isolation at 1.5 Th with quadrupole, HCD fragmentation with normalized collision energy of 30, and rapid scan MS analysis in the ion trap. The MS2 ion count target was set to 104 and the max injection time was 35 ms. Only those precursors with charge state 2–6 were sampled for MS2. The dynamic exclusion duration was set to 45 s with a 10 ppm tolerance around the selected precursor and its isotope. Monoisotopic precursor selection was turned on. The instrument was run in top speed mode with 2 s cycles. All data were analyzed and quantified with MaxQuant software (version 1.5.2.4.). The false discovery rate (FDR) was set to 1% for both proteins and peptides and a minimum length of seven amino acids was specified. The Andromeda search engine was used for the MS/MS spectra search against the UniProt Rattus norvegicus database of protein sequences. Enzyme specificity was set as C-terminal to Arg and Lys, also allowing cleavage at proline bonds and a maximum of two missed cleavages. Dithiomethylation of cysteine was selected as fixed modification and N-terminal protein acetylation and methionine oxidation as variable modifications. The “match between runs” feature of MaxQuant was used to transfer identifications to other LC–MS/MS runs based on their masses and retention time (maximum deviation 0.7 min) and this was also used in quantification experiments. Quantifications were performed with the label-free algorithms (Rabilloud and Lescuyer, 2014). Binary logarithms of intensity ratios were then median calculated for each group and the difference between control and sample was determined. Only at least 2-fold differences calculated for at least 2 measured values from 3 replicates were taken into consideration.

3.12. High-resolution respirometry

Mitochondrial respiration was analyzed using high-resolution polarographic respirometry in a two-channel titration injection respirometer Oxygraph-2k (Oroboros Instruments, Innsbruck, Austria) at 25 °C (Gnaiger et al., 2000). Isolated mitochondria were loaded into a chamber filled with a mitochondrial respiration medium MiR05 (110 mM sucrose, 0.5 mM EGTA, 3.0 mM MgCl2, 80 mM KCl, 60 mM K-lactobionate, 10 mM KH2PO4, 20 mM taurine, 20 mM HEPES, 1.0 g/l BSA; pH 7.1). The order and concentrations of substrates injected into the chambers are presented in figure 7. Polarographic signal was recorded and processed using DatLab 5 software (Oroboros Instruments).

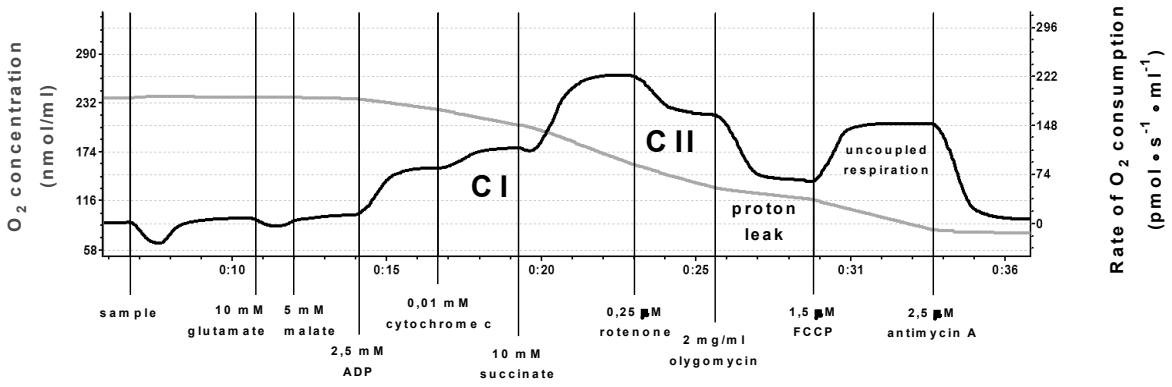

Fig. 7. Representative plots of oxygen concentration (grey line; left y-axis [nmol/ml]) and oxygen flux rate (black line; right y-axis [pmol·s^{-1}·ml^{-1}]) during a stepwise protocol designed for functional assessment of mitochondria. The sequence of successive additions of substrates, uncouplers and inhibitors is defined below the x-axis. Respiratory complexes (CI and CII) activated and the induced respiratory states (proton leak and uncoupled respiration) are indicated inside the figure. Oxidative phosphorylation was stimulated by subsequent addition of CI substrates glutamate and malate followed by addition of ADP. Addition of the CII-linked substrate succinate enabled convergent electron input via both CI and CII. Inhibition of CI by rotenone revealed CII-supported respiration. The respiration rate in the presence of oligomycin, an inhibitor of ATP synthase, reflected the proton leak rate across the mitochondrial membrane. Maximal respiratory capacity of the electron transfer system was induced by titration of FCCP. The CIII inhibitor antimycin A left residual, primarily non-mitochondrial oxygen consumption.

3.13. Enzyme activity assays

Activities of malate dehydrogenase (MDH), citrate synthase, NADH:cytochrome c and succinate:cytochrome c oxidoreductase complexes were measured spectrophotometrically in the samples of isolated mitochondria. All measurements were carried out in triplicate at room temperature.

Activity of malate dehydrogenase (MDH) was assayed in a solution consisting of 100 mM potassium phosphate and 15 mM NADH (pH 7.4). The reaction was started by addition of 150 mM oxaloacetate. The absorbance changes at 340 nm reflected altered activity of MDH.

Activity of citrate synthase was determined in a solution containing 100 mM Tris-HCl, 12 mM acetyl-CoA and 10 mM 5,5-dithio-bis-(2-nitrobenzoic acid). The shift in absorbance at 412 nm after addition of 10 mM oxaloacetate (pH 8.1) represented change in the activity of citrate synthase (Srere, 1969).

Enzyme activities of NADH:cytochrome c and succinate:cytochrome c oxidoreductase complexes were measured in a solution containing 100 mM potassium phosphate, 8 mM cytochrome c and 5 mM NaCN (pH 7.4). Absorbance shift at 550 nm after addition of 15 mM NADH represented activity of NADH:cytochrome c oxidoreductase complex. Absorbance shift at the same wavelength after addition of 500 mM succinate represented activity of succinate:cytochrome c oxidoreductase complex.

Hexokinase activity was assayed according to a modified Worthington protocol (Worthington Biochemical Corp., Lakewood, CO, USA). Phosphorylation reaction was coupled with the reduction of NAD^+ by glucose-6-phosphate dehydrogenase. Subsequently, the activity of hexokinase was determined as a shift in absorbance at 340 nm. Modified assay buffer consisted of 0.05 M TRIS, 13.3 mM $MgCl_2$, 0.8 mM NAD, 0.8 mM ATP, 0.5% Triton X-100, and 1 U/ml G-6-P dehydrogenase (pH 8.0). Samples (final concentration of protein 0.3 µg/µl) of either isolated mitochondria or PNS were pipetted into 96-well plates containing the assay buffer. After 2 min the starting solution (1.5 M glucose in TRIS-$MgCl_2$ buffer, pH 8.0) was added to a total volume of 200 µl and the plate was incubated at 30 °C for 15 min (Waskova-Arnostova et al., 2014).

3.14. Immunofluorescence imaging

Five rats from each group were used for immunofluorescence imaging experiments. To prepare left ventricular sections the hearts were excised from sacrificed rats with aorta intact and quickly connected to the tube for Langendorff perfusion with ice-cold Tyrode buffer. After initial perfusion the hearts were the tube was gently moved upwards, so the buffer would flow into the coronary arteries while the ventricles remained filled with liquid and the perfusion solution was switched to 4% paraformaldehyde (PFA). After being fixated for five minutes, the hearts were placed into PFA for 3 h and then into 20% sucrose solution in PBS overnight. After 24 h they were frozen in liquid nitrogen until later use.

12 μm thick longitudinal sections of LV were prepared in Leica CM1850 cryostat. Sections had to be treated with SDS solution (1% in PBS) to allow antigen retrieval and facilitate Ig binding. Sliced were then washed with PBS 2 times for 5 min. Non-specific sites were blocked using 2 step approach: first, a solution containing 10% donkey serum, 1% BSA, 0.3 M glycine and 0,3% TX-100 in PBS buffer was applied for 30 min. Then, after one 5 min washing with PBS, a 30 min incubation in a mix of anti-rabbit and anti-mouse unconjugated secondary antibodies took place. The absence of non-specific binding was later confirmed using negative (no antibody) and positive (only secondary conjugated antibody) controls. To stain the slices, we used caveolin-1 (rabbit, 1:500) and caveolin-3 (mouse, 1:500) primary antibodies separately and caveolin-3 in combination with either β2-AR (rabbit, 1:100) or connexin 43 (rabbit, 1:100) antibody (see Table 1 for specifications). Primary antibody incubation lasted 1 h. After 3 x 15 min PBS washing secondary antibodies were applied. Donkey anti-mouse antibody was conjugated with Alexa Fluor 488 (green, 1:200), donkey anti-rabbit with Alexa Fluor 546 (red, 1:200) both are from Thermo Scientific. All antibodies used in this experiment were diluted using 1% BSA solution in PBS. After final washing (same as above) a ProLong mountant containing DAPI (Thermo Scientific) was applied on slices which were then topped with the cover glass. After a 30 min drying period the glasses were sealed with nail polish and stored at −20 °C.

Microscopy was performed in the Laboratory of Confocal and Fluorescence Microscopy co-financed by the European Regional Development Fund and the state budget of the Czech Republic, projects no. CZ.1.05/4.1.00/16.0347 and CZ.2.16/3.1.00/21515 and supported by the Czech-BioImaging large RI project

LM2015062. The images were acquired using Olympus Cell^R system which is based around broad-band fluorescence inverted microscope equipped with a CCD camera.

Subsequent processing of the images included deconvolution by Classic Maximum Likelihood Estimation algorithm using Huygens Software and background subtraction (sliding paraboloid, 50 px radius) in FIJI. Co-localization analysis was performed in FIJI using colocalization threshold plugin (Schindelin et al., 2012).

4. RESULTS

4.1. Body weight, heart weight and heart-to-body weight ratio

Body and heart weights of the animals in each experimental group were determined on the day of experiment. The average body and heart weights did not significantly differ between SHR and SHR-Tg19 (table 2).

Table 2. Body and heart weight parameters of SHR-Tg19 and corresponding SHR. Data are mean ± SEM.

	Body weight, g	Heart weight, g	HW/BW, mg/g	LV weight, g	RV weight, g
SHR	293.75 ± 5.64	0.96 ± 0.0425	3.52 ± 0.122	0.57 ± 0.012	0.17 ± 0.01
SHR-Tg19	261.63 ± 9.182	0.87 ± 0.0337	3.57 ± 0.236	0.53 ± 0.021	0.17 ± 0.009

4.2. Expression of Cd36 in cardiac tissue of SHR and SHR-Tg19

To test whether the membrane population of Cd36 is rescued in the SHR transgenic animals, we compared the distribution of Cd36 in the PM and cytoplasmic preparations enriched in mitochondria isolated from the LV of SHR and SHR-Tg19. An antibody was directed against an epitope of the Cd36 that includes the aberrant site in SHR. The results indicated that optic density of Cd36 signal was dramatically higher in the PM of SHR-Tg19. Similar amount of the protein was detected in the mitochondrial fraction of both strains (Fig. 8).

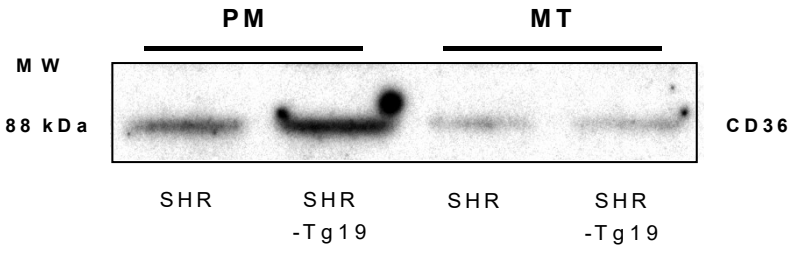

Fig. 8. A representative immunoblot showing the effect of transgenic expression of Cd36 in SHR on the distribution of its protein product in the PM- and mitochondria-enriched samples of LV tissue.

4.3. α-Adrenoceptor binding experiments

Saturation binding experiments were used to determine the total expression of α-adrenergic receptors. Specific binding of [^{3}H]-prazosin ligand was compared between SHR and SHR-Tg19 in plasma membrane samples of left and right ventricles (Fig 9). The results have shown no statistical significance in either quantity or binding affinity of α-adrenergic receptors (LV: 127.3 ± 6.343 vs. 118 ± 3.027 fmol/mg protein, kD: 0.07596 ± 0.004484 vs. 0.0893 ± 0.007716 nM. RV: 139.5 ± 3.65 vs. 131.8 ± 5.629, kD: 0.2005 5 ± 0.01505 vs. 0.1904 ± 0.03122 nM).

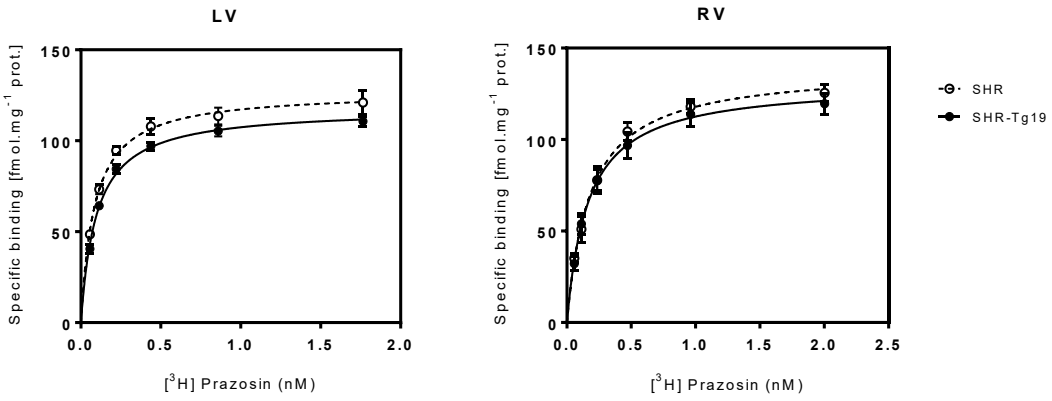

Fig. 9. Saturation binding curves showing the specific binding of [^{3}H]-prazosin to α-adrenergic receptors on plasma membranes isolated from the left and right ventricles of SHR and SHR-Tg19.

4.4. 2DE and MALDI-TOF MS/MS analysis

In the first part of our work we used 2D gel-based analysis followed by MALDI-TOF MS/MS in order to identify quantitative changes in protein composition of the postnuclear supernatant isolated from the left and right ventricles of SHR and SHR-Tg19 rats. Samples of PNS (1 mg) were extracted in ice-cold acetone/TCA/96% ethanol, separated in the first dimension on pH 3-11 IPG strips and then by SDS-PAGE on 10% acrylamide gels. Whereas the total number of CBB-stained protein spots in SHR and SHR-Tg19 samples isolated from the left ventricles was 411, there were 357 protein spots detected in PNS prepared from the right ventricles. The stained 2D gels were scanned with an imaging densitometer and the differences between the SHR and SHR-Tg19 samples were analyzed by PDQuest software. Protein levels altered at least

two-fold were taken into consideration and selected for mass spectrometric analysis. The functional significance and subcellular localization of identified proteins was determined according to the current annotations in the UniProt database. In the left ventricles of SHR-Tg19, only 3 altered proteins were recognized compared to SHR that are involved in *the tricarboxylic acid cycle* and *immunity* (Fig. 10A and 11A, Table 3 and 4): malate dehydrogenase (spot **1**, fraction, ↓6.2-fold), proteasome subunit alpha type-1 (spot **2**, ↑2.4-fold), and aconitate hydratase (spot **3**, ↑2.2-fold).

Table 3: **MALDI-TOF MS/MS** analysis of altered CBB-stained spots in PNS prepared from the **left ventricles**; difference of protein composition in PNS samples isolated from SHR and SHR-Tg19 rats. Please refer to **supplementary Table 2** for a complete list of peptides.

Spot	Accession number	Protein name	Mascot score	Matched peptides	SC[a] [%]	MW[b] (kDa)	pI[c]	Change (fold)
1	MDHC_RAT	Malate dehydrogenase, cytoplasmic (fraction)	376	23	48	36.6	6.16	↓ 6.2
2	PSA1_RAT	Proteasome subunit alpha type-1	266	17	42	29.8	6.15	↑ 2.4
3	ACON_RAT	Aconitate hydratase, mitochondrial	846	47	53	86.1	7.87	↑ 2.2

[a] sequence coverage, [b] theoretical molecular weight, [c] theoretical isoelectric point

Table 4: Subcellular localization and biological processes of altered proteins in the **left ventricle** PNS samples of SHR and SHR-Tg19 rats identified by **MALDI-TOF MS/MS**.

Spot	Accession number	Protein name	Change (fold)	Subcellular localization	Keywords - biological processes
1	MDHC_RAT	Malate dehydrogenase, cytoplasmic (fraction)	↓ 6.2	cytoplasm	tricarboxylic acid cycle
2	PSA1_RAT	Proteasome subunit alpha type-1	↑ 2.4	cytoplasm, nucleus	cleavage of peptide bonds, immunity
3	ACON_RAT	Aconitate hydratase, mitochondrial	↑ 2.2	mitochondrion	tricarboxylic acid cycle

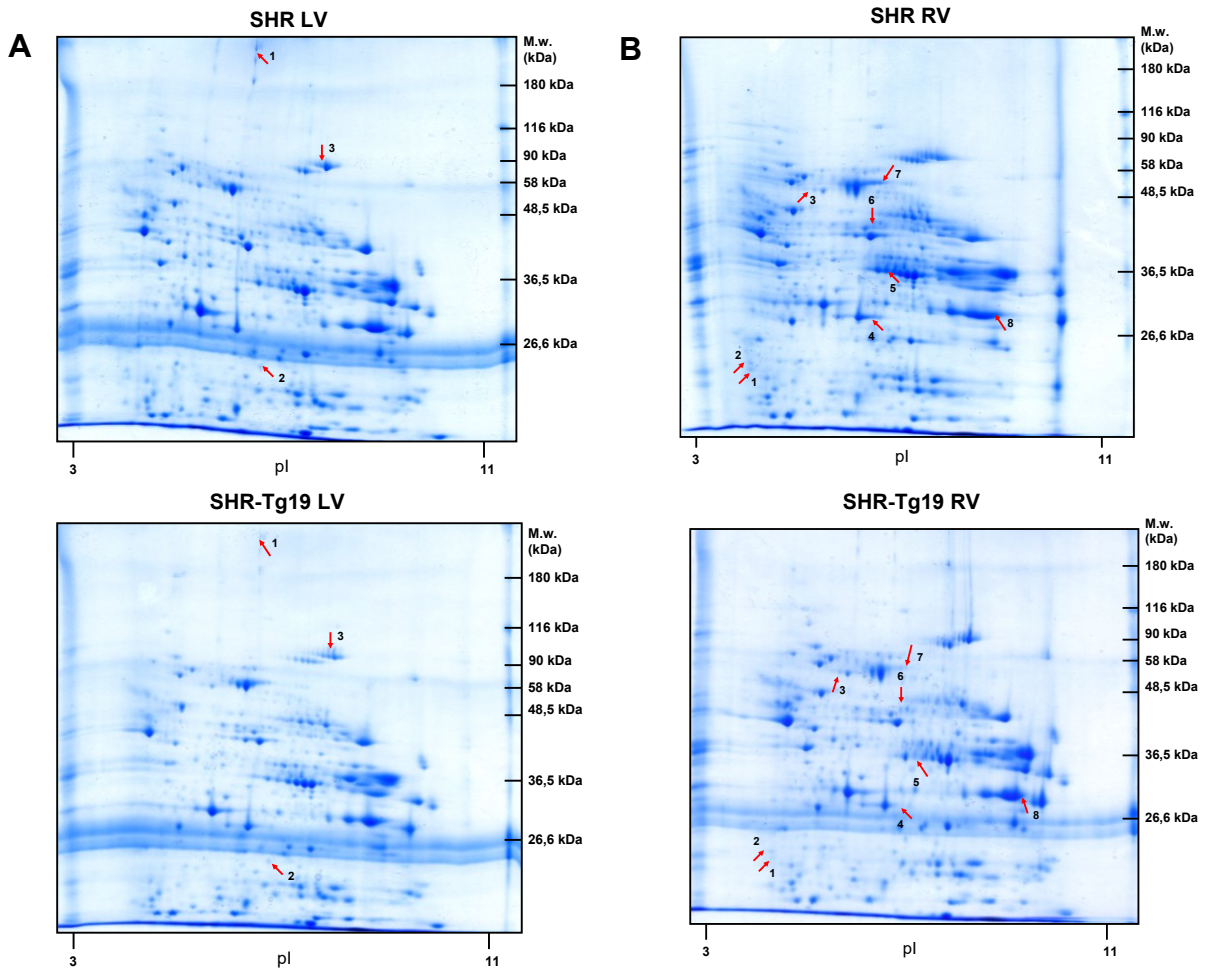

Fig. 10. Two-dimensional gel electrophoresis maps of PNS prepared from SHR (upper panels) and SHR-Tg19 rats (lower panels) stained by colloidal Coomassie Blue, A-left ventricle (LV), B-right ventricle (RV). Protein samples (1 mg) were separated in the first dimension on pH 3-11 IPG strips and then SDS- PAGE on 10% acrylamide gels. The position of molecular weight markers are indicated to the right and the pI at the bottom of each gel. The corresponding identifications of significantly altered protein spots 1-3 (A) and 1-8 (B) by MALDI-TOF MS/MS are listed in Tables 3 and 4. Please refer to supplementary Tables 1 and 2 for a complete list of peptides.

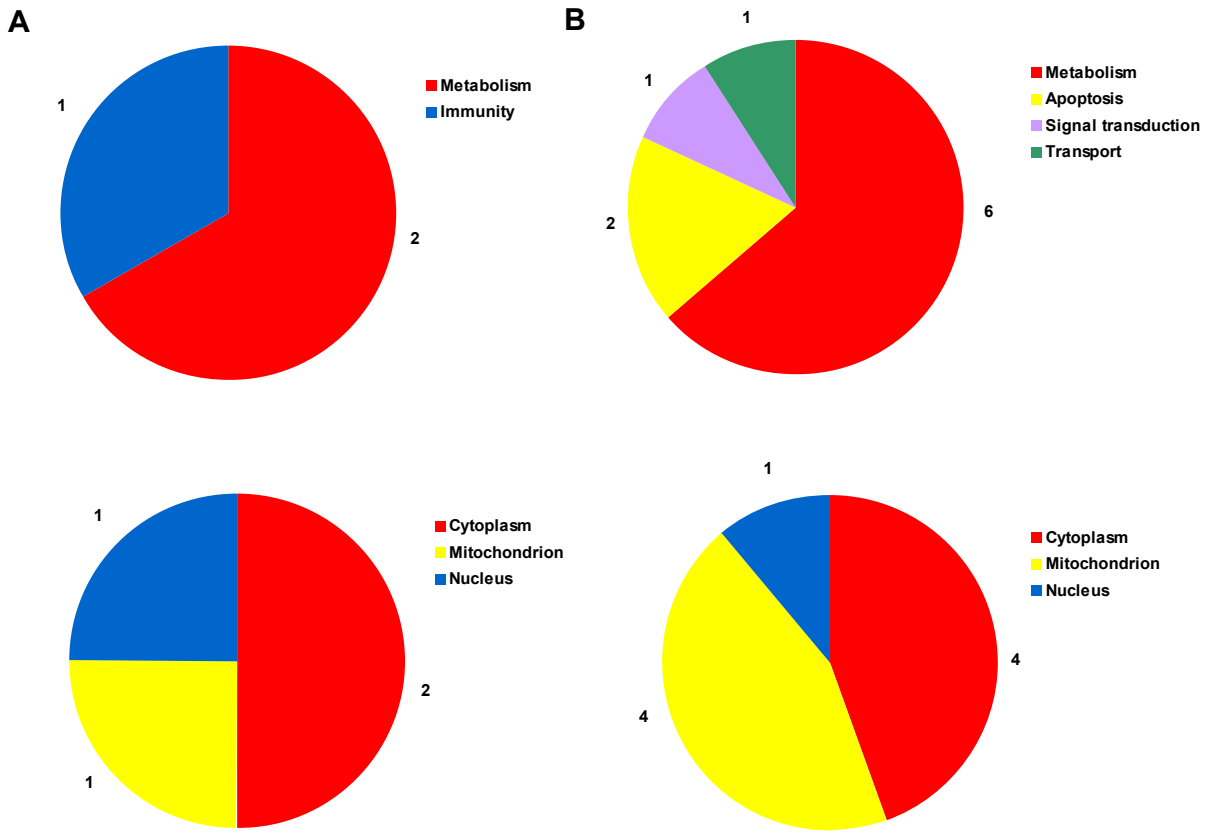

Fig. 11. Protein function (upper panels) and subcellular localization (lower panels) of altered left (A) and right (B) ventricle PNS proteins in SHR and SHR-Tg19 rats identified by MALDI-TOF MS/MS. The functional significance and localization of these proteins was determined according to the current annotations in the UniProt database (tables 3 and 4).

Divergently from the left ventricles, our analysis of 2DE maps revealed a markedly higher number of spots with different intensity between samples isolated from the right ventricles (Fig. 10B and 11B). There were 8 downregulated proteins in the right ventricles of SHR-Tg19 when compared to SHR and these proteins identified by mass spectrometric analysis are listed in Table 5: 14-3-3 protein eta (spot 1, ↓2.2-fold), 14-3-3 protein gamma (spot 2, ↓2.9-fold), dihydrolipoyllysine-residue acetyltransferase component of pyruvate dehydrogenase complex (spot 3, ↓2.4-fold), malate dehydrogenase (spot 4, ↓2.7-fold), long-chain specific acyl-CoA dehydrogenase (spot 5, ↓2.4-fold), aldehyde dehydrogenase (spot 6, ↓4.0-fold), succinate dehydrogenase [ubiquinone] flavoprotein subunit (spot 7, ↓3.2-fold), and glyceraldehyde-3-phosphate dehydrogenase (spot 8, ↓2.9-fold). All these downregulated proteins were related to *energy metabolism* (dihydrolipoyllysine-residue acetyltransferase component of pyruvate dehydrogenase complex, malate dehydrogenase, long-chain specific acyl-CoA dehydrogenase, aldehyde dehydrogenase, succinate dehydrogenase flavoprotein subunit, glyceraldehyde-3-phosphate dehydrogenase), *apoptosis* (aldehyde dehydrogenase, glyceraldehyde-3-phosphate dehydrogenase), *signal transduction* (14-3-3 protein gamma) and *transport* (14-3-3 protein eta) (table 6). A complete list of peptides related to MALDI-TOF MS/MS identification of altered proteins is in supplementary Tables 1 and 2.

Table 5: **MALDI-TOF MS/MS** analysis of altered CBB-stained spots in PNS prepared from the **right ventricles**; difference of protein composition in PNS samples isolated from SHR and SHR-Tg19 rats. Please refer to **supplementary Table 1** for a complete list of peptides.

Spot	Accession number	Protein name	Mascot score	Matched peptides	SC[a] [%]	MW[b] (kDa)	pI[c]	Change (fold)
1	1433F_RAT	14-3-3 protein eta	314	24	60	28.4	4.81	↓ 2.2
2	1433G_RAT	14-3-3 protein gamma	448	26	66	28.5	4.80	↓ 2.9
3	ODP2_RAT	Dihydrolipoyllysine-residue acetyltransferase component of PHD complex, mitochondrial (fraction)	508	31	38	67.6	8.76	↓ 2.4
4	MDHC_RAT	Malate dehydrogenase, cytoplasmic	293	19	38	36.6	6.16	↓ 2.7
5	ACADL_RAT	Long-chain specific acyl-CoA dehydrogenase, mitochondrial	573	38	60	48.2	7.63	↓ 2.4
6	ALDH2_RAT	Aldehyde dehydrogenase, mitochondrial	257	17	27	57.0	6.63	↓ 4.0
7	DHSA_RAT	Succinate dehydrogenase [ubiquinone] flavoprotein subunit, mitochondrial	740	40	58	72.6	6.75	↓ 3.2
8	G3P_RAT	Glyceraldehyde-3-phosphate dehydrogenase	620	37	68	36.1	8.14	↓ 2.9

[a] sequence coverage, [b] theoretical molecular weight, [c] theoretical isoelectric point

Table 6: Subcellular localization and biological processes of altered proteins in the **right ventricle** PNS samples of SHR and SHR-Tg19 rats identified by **MALDI-TOF MS/MS**.

Spot	Accession number	Protein name	Change (fold)	Subcellular localization	Keywords - biological processes
1	1433F_RAT	14-3-3 protein eta	↓ 2.2	cytoplasm	regulation of sodium ion transport
2	1433G_RAT	14-3-3 protein gamma	↓ 2.9	cytoplasm	signal transduction, response to insulin stimulus, regulation of synaptic plasticity
3	ODP2_RAT	Dihydrolipoyllysine-residue acetyltransferase component of pyruvate dehydrogenase complex, mitochondrial (fraction)	↓ 2.4	mitochondrion	carbohydrate metabolism, glucose metabolism, tricarboxylic acid cycle
4	MDHC_RAT	Malate dehydrogenase, cytoplasmic	↓ 2.7	cytoplasm	tricarboxylic acid cycle
5	ACADL_RAT	Long-chain specific acyl-CoA dehydrogenase, mitochondrial	↓ 2.4	mitochondrion	fatty acid metabolism, lipid homeostasis
6	ALDH2_RAT	Aldehyde dehydrogenase, mitochondrial	↓ 4.0	mitochondrion	response to fatty acid, ethanol degradation, negative regulation of apoptosis
7	DHSA_RAT	Succinate dehydrogenase [ubiquinone] flavoprotein subunit, mitochondrial	↓ 3.2	mitochondrion	tricarboxylic acid cycle, respiratory electron transport chain
8	G3P_RAT	Glyceraldehyde-3-phosphate dehydrogenase	↓ 2.9	cytoplasm, nucleus	glycolysis, apoptosis, regulation of translation

4.5. Label-free MS analysis

Information on differently expressed proteins which were determined by label-free quantification in samples of PNS prepared from the left and right ventricles of SHR and SHR-Tg19 is summarized in **Tables 6** and **7**. In total, there were 1591 proteins identified in left ventricle samples and 1894 proteins in right ventricle samples. Changes in expression at least two-fold were considered significant. There were 7 such changes found in left ventricles and 10 in right ventricles of SHR-Tg19 compared to SHR. All these proteins were 2-3 times downregulated in SHR-Tg19. Only one protein was downregulated in both left and right ventricles (Coiled-coil domain-containing protein 51). Proteins with changed expression in the left ventricle of SHR-Tg19 are listed in Table 7. Out of 7 changes, 5 are related to proteins of the mitochondrial respiratory chain (LOC100361144, LOC100362391, LOC688963, LOC100361934 and COX17). As shown in Table 8, there were 10 downregulated proteins in the right ventricles of SHR-Tg19. Three of them are constituents of cytoskeleton. Notable are the 2-fold downregulations of MEK1 and protein kinase inhibitor PKIA.

Table 7: Expression change, subcellular localization and biological characterization of altered proteins in the **left ventricle** PNS samples of SHR and SHR-Tg19 rats identified by **label-free MS**.

Accession number	Protein name	Change (fold)	Subcellular localization	Protein characterization
D4A4P3_RAT and M0RA24_RAT	LOC100361144 and LOC100362391	↓ 2	Mitochondrion inner membrane	Similar to NADH dehydrogenase 1 beta subcomplex subunit 3
F1LPG5_RAT and F1M7T1_RAT	LOC688963 and LOC100361934	↓ 2.2	Mitochondrion inner membrane	Similar to NADH dehydrogenase 1 beta subcomplex subunit 4
Q76MV3_RAT	Cytochrome C oxidase assembly protein COX17	↓ 2.3	Mitochondrial intermembrane space	Assembling subunit of cytochrome c oxidase
D3ZZK1_RAT	LOC100359563	↓ 2	Cytosol	Similar to ribosomal protein S20
CCD51_RAT	Coiled-coil domain-containing protein 51	↓ 3	Plasma membrane	Multipass membrane protein with two isoforms

Table 8: Expression change, subcellular localization and biological characterization of altered proteins in the **right ventricle** PNS samples of SHR and SHR-Tg19 rats identified by **label-free MS**.

Accession number	Protein name	Change (fold)	Subcellular localization	Protein characterization
MP2K1_RAT	Dual specificity mitogen-activated protein kinase kinase 1	↓ 2	Nucleus, cytosol, mitochondrion, endosome	Phosphorylates MAPK3/ERK1 and MAPK1/ERK2 as a part of MAP kinase pathway
IPKA_RAT	cAMP-dependent protein kinase inhibitor alpha	↓ 2,5	Nucleus, cytosol	Inhibits protein kinase A catalytic activity
PAIRB_RAT	Plasminogen activator inhibitor 1 RNA-binding protein	↓ 2,2	Nucleus, cytosol, plasma membrane	Regulates stability of Plasminogen activator inhibitor 1 mRNA
RTN3_RAT	Reticulon-3	↓ 2	ER, Golgi	Involved in membrane trafficking between the endoplasmic reticulum and Golgi
BMP10_RAT	Bone morphogenetic protein 10	↓ 2,4	Plasma membrane	Required for maintaining the proliferative activity of embryonic cardiomyocytes
THIM_RAT	3-ketoacyl-CoA thiolase	↓ 3,3	Mitochondrion	Catalyzes the last reaction in beta-oxidation spiral
SEP11_RAT	Septin-11	↓ 3,3	Cytoskeleton	Cytoskeletal GTPase involved in cytokinesis and vesicle trafficking
M0R8B6_RAT	Tubulin beta 1	↓ 2,5	Cytosol	Major constituents of microtubules
Q4QQV0_RAT	Tubulin beta 6	↓ 2		
CCD51_RAT	Coiled-coil domain-containing protein 51	↓ 3.4	Plasma membrane	Multipass membrane protein with two isoforms

4.6. Mitochondrial respiration

Mitochondrial oxidation rates were determined by high-resolution respirometry. Multiple substrate-inhibitor titration was applied for investigation of mitochondrial function. Maximal respiratory rates were measured with 4 different substrates (glutamate, malate, succinate, and palmitoyl-L-carnitine). Representative plots of oxygen concentration and oxygen flux rate during a stepwise protocol designed for functional assessment of mitochondria are shown in figure 7. Oxygen consumption rates markedly differed between the left and right ventricles of both rat strains. The activities of complex I and complex II, as well as proton leak rate and uncoupled respiration were higher by about 40-60 % in the LV than in the RV (Fig. 12). Rate of proton leak (measured by ATP synthase blocking with oligomycin) was significantly different only between the LV and RV of SHR, but not between the LV and RV of SHR-Tg19. When presented with malate and palmitoyl-carnitine as substrates, mitochondria isolated from the LV of SHR-Tg19 were more active (by 36 %) than those derived from the RV.

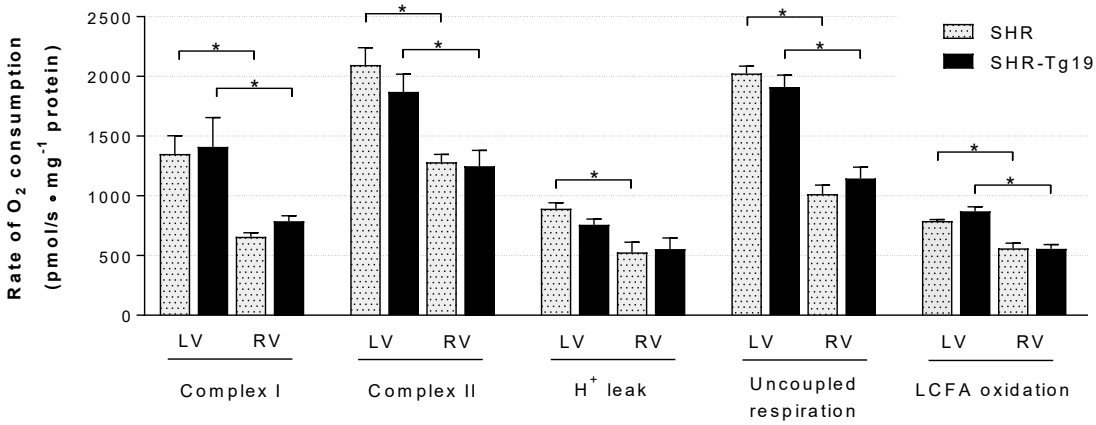

Fig. 12. Oxygen consumption in mitochondria isolated from the left (LV) and right (RV) ventricles of SHR and SHR-Tg19. Average rates of oxygen consumption under different conditions representing the function of CI, CII, proton leak, uncoupled respiration and long-chain fatty acid (palmitoyl-L-carnitine) oxidation are displayed in panel **B**. Each value represents the mean ± SEM of 4 separate experiments, * – $P < 0.05$.

4.7. Activity and expression of selected metabolic and respiratory enzymes

Enzyme activities of hexokinase (HK), malate dehydrogenase (MDH), citrate synthase (CS), NADH:cytochrome c oxidoreductase (NCOR) and succinate:cytochrome c oxidoreductase (SCOR) complexes were measured using a spectrophotometric coupled assay. SCOR complex activity was relatively low (0,0477±0,005 in the LV of SHR and 0,145±0,008 in the RV of SHR compared to values around 0,3 μmol ×min-1 ×mg-1 of protein for NCOR complex). Activity of SCOR complex measured in the RV was significantly higher than in the LV by 205% in SHR and by 125% in SHR-Tg19 (Fig. 13B). Besides that, transgenic expression of Cd36 led to a significant increase (by 57%) in SCOR activity in the LV but not in the RV.

Activities of NCOR and CS did not differ between both the strains and ventricles (Fig. 13A, data not shown for CS).

Mitochondrial MDH activity from both ventricles of SHR-Tg19 was significantly lower (by 22% in the LV and 24% in the RV) than in SHR (Fig. 13C). Total cytoplasmic activity of MDH was decreased (also by about 20%) only in the samples from the LV (but not RV) of SHR-Tg19. Therefore, activity of cytoplasmic MDH was similar in both ventricles of transgenic rats, whereas in SHR it was higher by about 25% in the LV compared to RV (Fig. 13D).

Activity of cytoplasmic HK was decreased by about 30% in the LV of SHR-Tg19 (Fig. 13F). No significant differences were observed between HK activities in isolated mitochondria from SHR and transgenic rats (Fig. 13E).

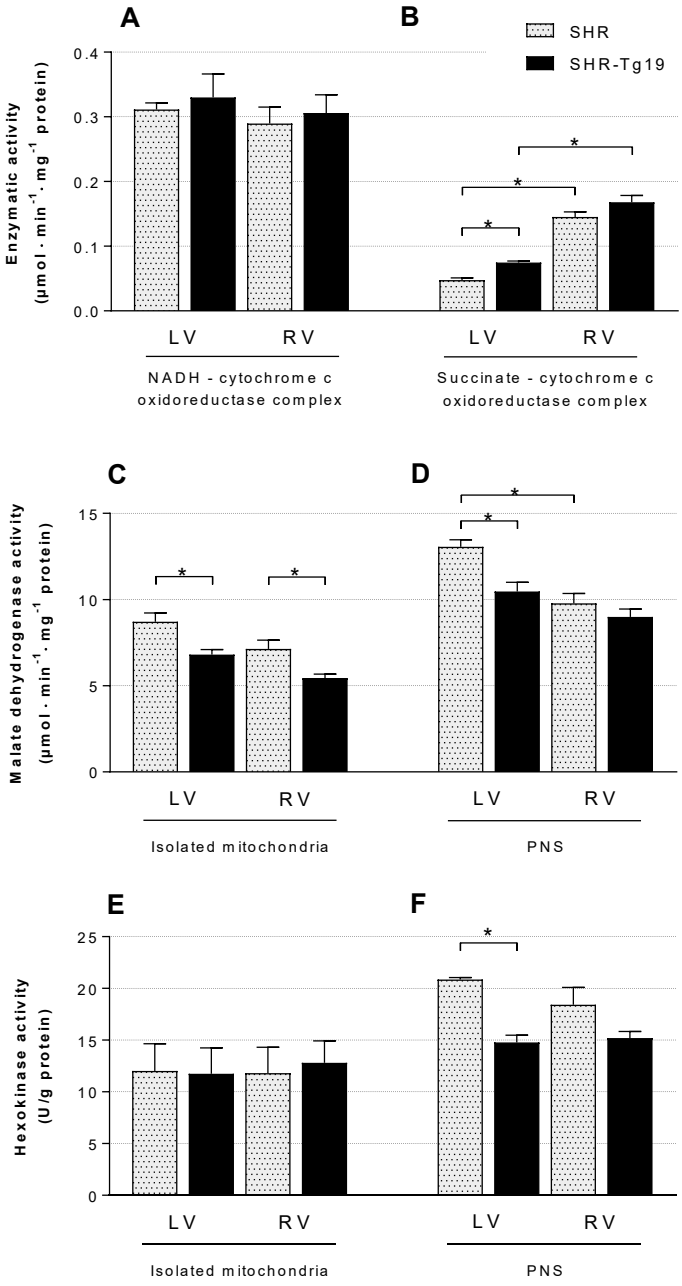

Fig. 13. Activities of selected enzymes involved in substrate oxidation and energy metabolism. Enzymatic activities were determined in mitochondria or post-nuclear supernatant (PNS) prepared from the left and right ventricles of SHR and SHR-Tg19. Activity of NADH-cytochrome c oxidoreductase (A) and succinate cytochrome c oxidoreductase (B) was measured in isolated mitochondria. Activity of malate dehydrogenase was measured in isolated mitochondria (C) and in the PNS (D). Activity of hexokinase was measured in isolated mitochondria (E) and in the PNS (F). Each value represents the mean ± SEM of 3 separate experiments, * – $P < 0.05$.

4.8. Expression of several OXPHOS proteins

Relative expression levels of selected OXPHOS subunits were assessed by western blot analysis. Representative western blots are shown in Fig. 14. The expression of SdhA, ATPA5 and UQCR2 did not differ either between the LV and RV or between samples from SHR and SHR-Tg19. Interestingly, the amount of NADH dehydrogenase subunit Ndufb8 was higher (by about 125%) in the RV than in the LV derived from both rat strains (Fig. 15B). The expression of SDHB, a subunit of succinate dehydrogenase, in the LV was markedly lower (by 41%) in SHR-Tg19, compared to SHR (Fig. 15C). Concomitantly, the expression level of this subunit was higher (by 187%) in the RV than in the LV of SHR-Tg19. Cytochrome c oxidase subunit (MT-CO1) exhibited higher expression (by 20 %) in the RV of SHR compared to the LV of the same rat strain (Fig. 15D). Finally, we checked MT resident protein prohibitin levels in order to ascertain that the observed changes in protein expression did not arise from altered mitochondrial content in the PNS (Ikonen et al., 1995). The expression levels of this mitochondrial protein, which is not a component of the electron transport chain, did not significantly differ between samples from both ventricles of SHR and SHR-Tg19 (Fig. 15E).

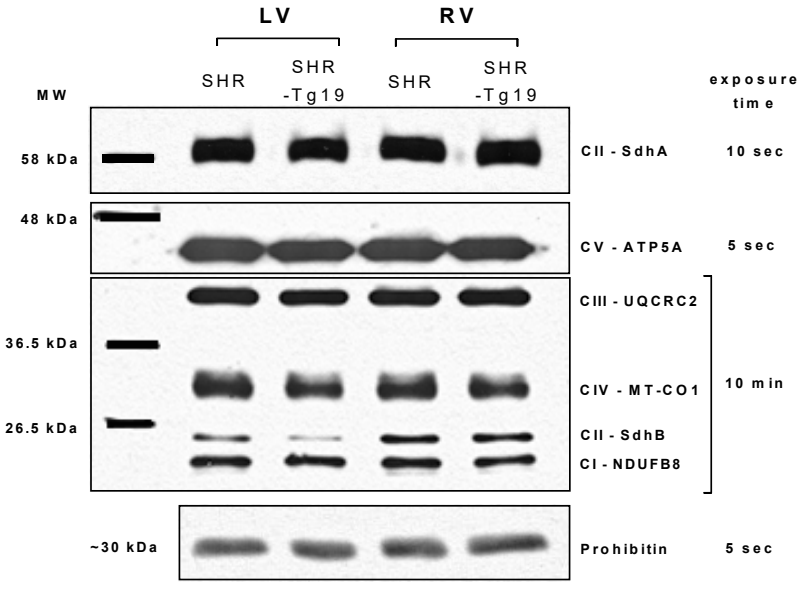

Fig. 14. Representative western blot image of OXPHOS complexes (I-V) and mitochondrial marker protein prohibitin in the PNS from LV and RV of SHR and SHR-Tg19. Subunits of CI (NDUFB8), CII (SdhA and SDHB), CIII (UQCRC2), CIV (MT-CO1) and CV (ATP5A) were probed with appropriate antibodies.

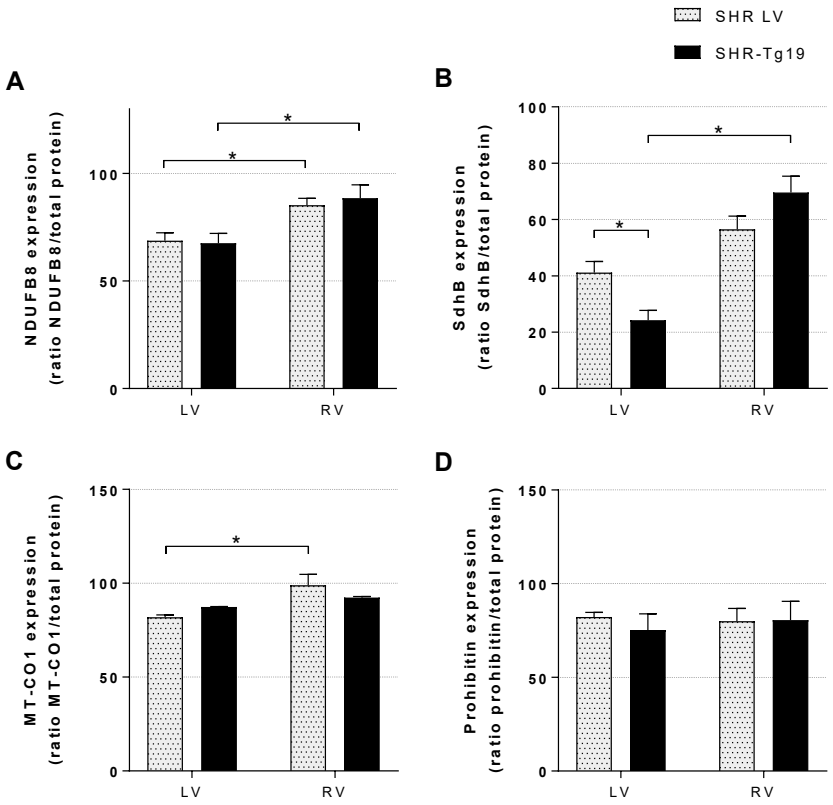

Fig. 15. Western immunoblot quantification of OXPHOS complexes (I-V) and prohibitin in the PNS from LV and RV of SHR and SHR-Tg19. OXPHOS complexes protein expression levels were quantified by densitometric analysis, using normalization of signal intensity to total protein loading (assessed by staining membranes using Ponceau S). There were no significant differences in the relative expression of subunits of OXPHOS complexes between different myocardial preparations except for NDUFB8 (B), SDHB (C) and MT-CO1 (D). The expression levels of prohibitin did not vary between all of the samples tested (E). Data presented are representative of 5 separate experiments, * – $P < 0.05$.

4.9. Expression of peroxisomal proteins

Relative expression levels of catalase and the 70-kDa peroxisomal membrane protein (PMP70) were assessed by western blotting (Fig. 16). Whereas catalase expression did not differ between the groups, the level of PMP70 was markedly higher (by about 50%) in the LV than in the RV of both SHR and SHR-Tg19. Transgenic rescue of *Cd36* in SHR resulted in significantly lower expression (by about 40%) of PMP70 in the LV.

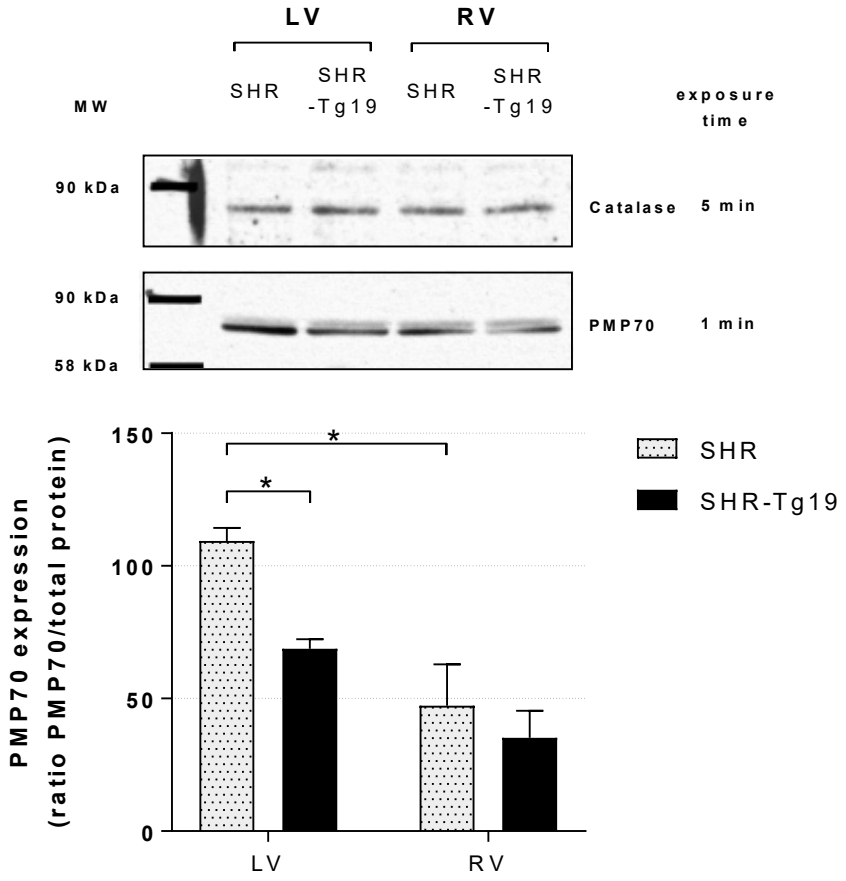

Fig. 16. Expression of selected peroxisomal proteins in ventricles of SHR and SHR-Tg19. Representative immunoblots of catalase and the 70-kDa peroxisomal membrane protein (PMP70) are shown. The distribution of PMP70 in the LV and RV of both rat strains was quantified by densitometric analysis, using normalization of signal intensity to total protein loading. There were no significant differences in the levels of catalase between the groups. Data represents 3 separate experiments, * – $P < 0.05$.

4.10. Distribution of membrane microdomains markers and other proteins in plasma membrane fractions extracted by TX-100

Samples of PM were treated with 1% Triton X-100 and fractionated by centrifugation resulting in an insoluble fraction that presumably contained protein constituents of lipid microdomains and a soluble fraction enriched with bulk membrane proteins. We utilized ChT-HRP dot blot and classic western immunoblotting to analyze the distribution of typical lipid raft markers in these fractions (Fig. 17).

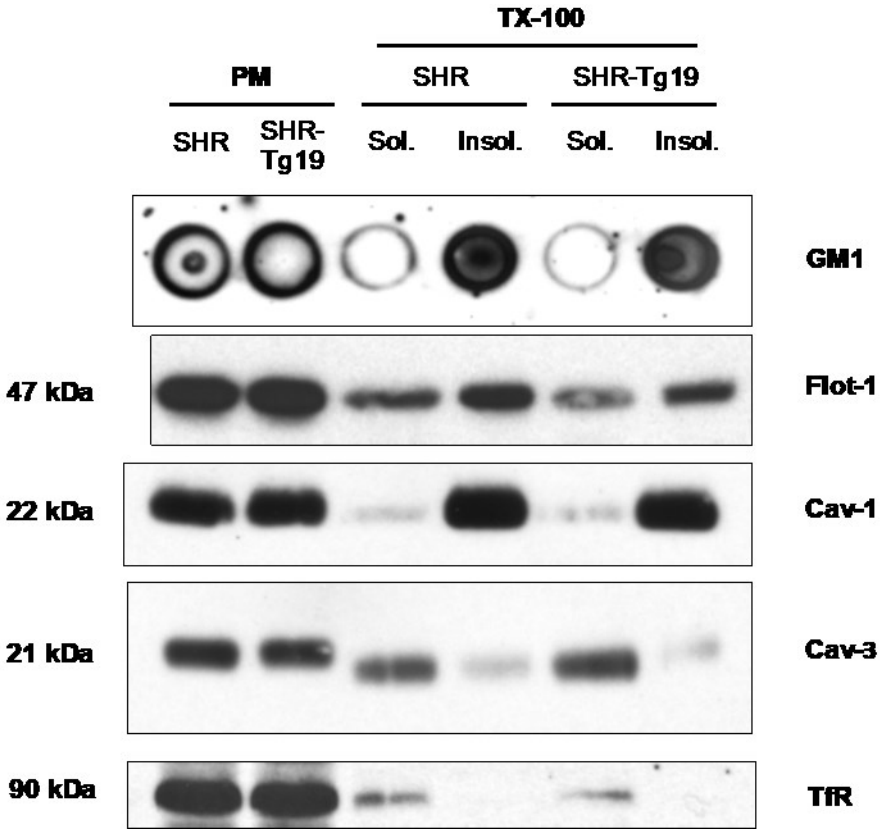

Fig. 17. Expression and distribution of typical lipid raft markers in the samples of plasma membrane and its fractions isolated in 1% Triton X-100 solution. Ganglioside M1 (GM1) distribution assayed with ChT-HRP using dot blot technique. Flot-1, Cav-1, Cav-3 and TfR were detected using corresponding antibodies. An image representative of 3 experiments is shown for each protein. There were no significant differences in expression of these proteins between samples from SHR and SHR-Tg19.

Western immunoblotting was used to evaluate the expression of β-AR (Fig. 18). Quantification analysis did not reveal significant differences in their expressions in the PM samples from the LV of SHR and SHR-Tg19. The receptors were distributed differently in the TX-100 isolated fraction samples. In both strains the β1 receptors were observed only in the soluble fraction, whereas β2 – only in the insoluble. The expression of G protein subunit α_{i2} was observed in both fractions and was similar in both strains, however, it was markedly higher in the DRM samples (Fig. 19).

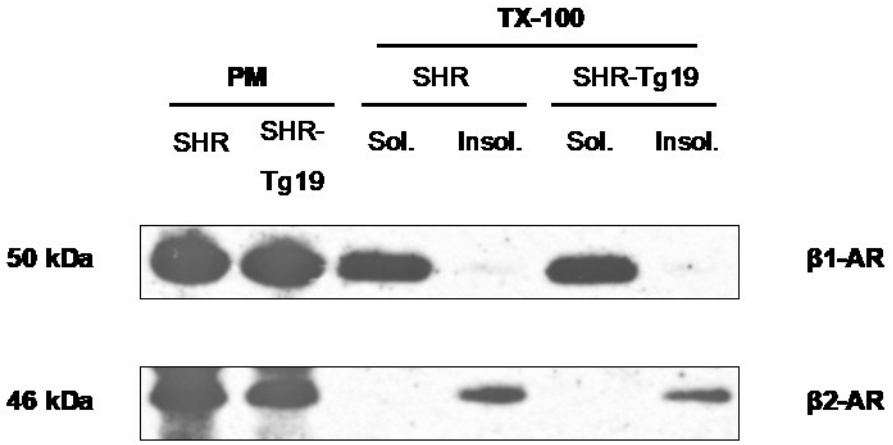

Fig. 18. Distribution of β1 and β2 adrenergic receptor subtypes in the samples of plasma membrane and its fractions isolated using TX-100.

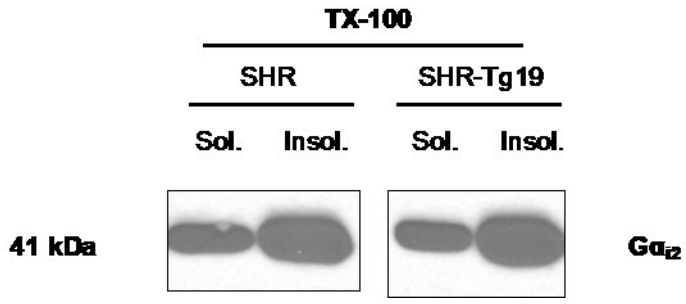

Fig. 19. Distribution of $G\alpha_{i2}$ protein in the samples of fractions isolated using TX-100.

Analysis of G protein β subunit distribution and expression in the membrane fractions showed some significant differences between the studied strains (Fig. 20). In the TX100-insoluble fraction the expression of Gβ was significantly lower by about 85% in SHR-Tg19 ($P < 0.05$). In samples from both SHR and SHR-Tg19 the protein exhibited higher expression in the soluble fraction.

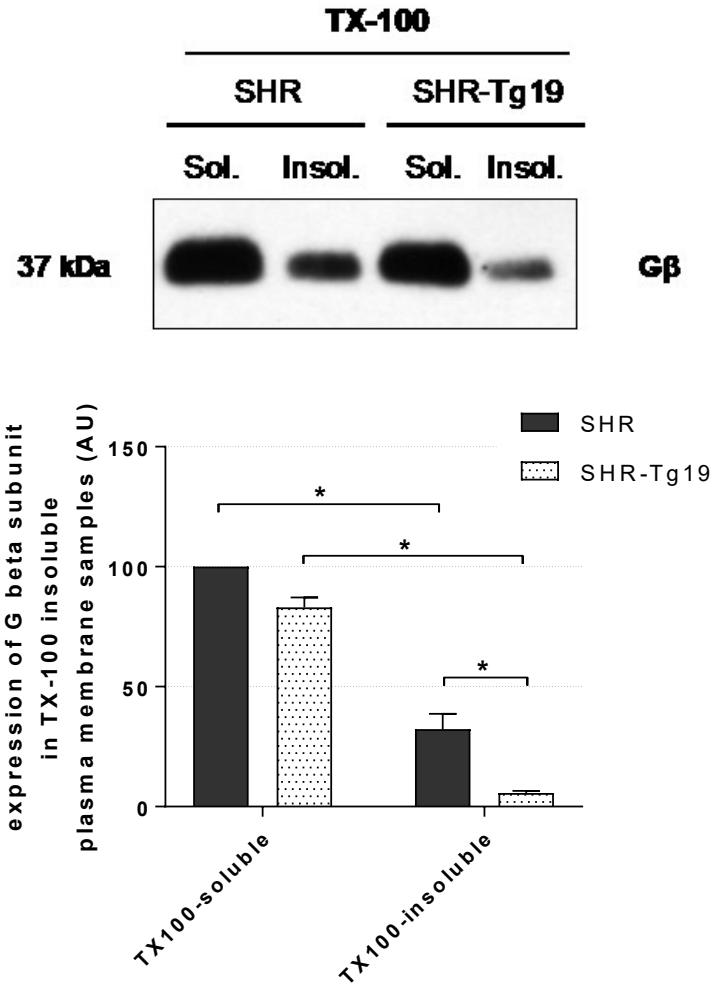

Fig. 20. The upper panel shows the distribution of G protein β subunit in TX100-soluble and -insoluble fractions of SHR and SHR-Tg19 cardiac plasma membranes. Immunoblot is representative of 3 experiments, * – $P < 0.05$.

The expression of connexin 43 in the left ventricles was higher by about 50% in the PNS and PM isolated from SHR-Tg19 than from SHR (Fig. 21). Our experiments have also shown that connexin 43 is located exclusively in TX100-insoluble fraction of the hearts of both strains of rats. However, its expression in the TX100-insoluble fraction of SHR-Tg19 was lower by 65% than in the same fraction of SHR. Additionally, only one band was observed in the samples treated with TX-100, unlike the PNS and PM samples where a second, higher band was visible. This band corresponds to the phosphorylated connexin 43.

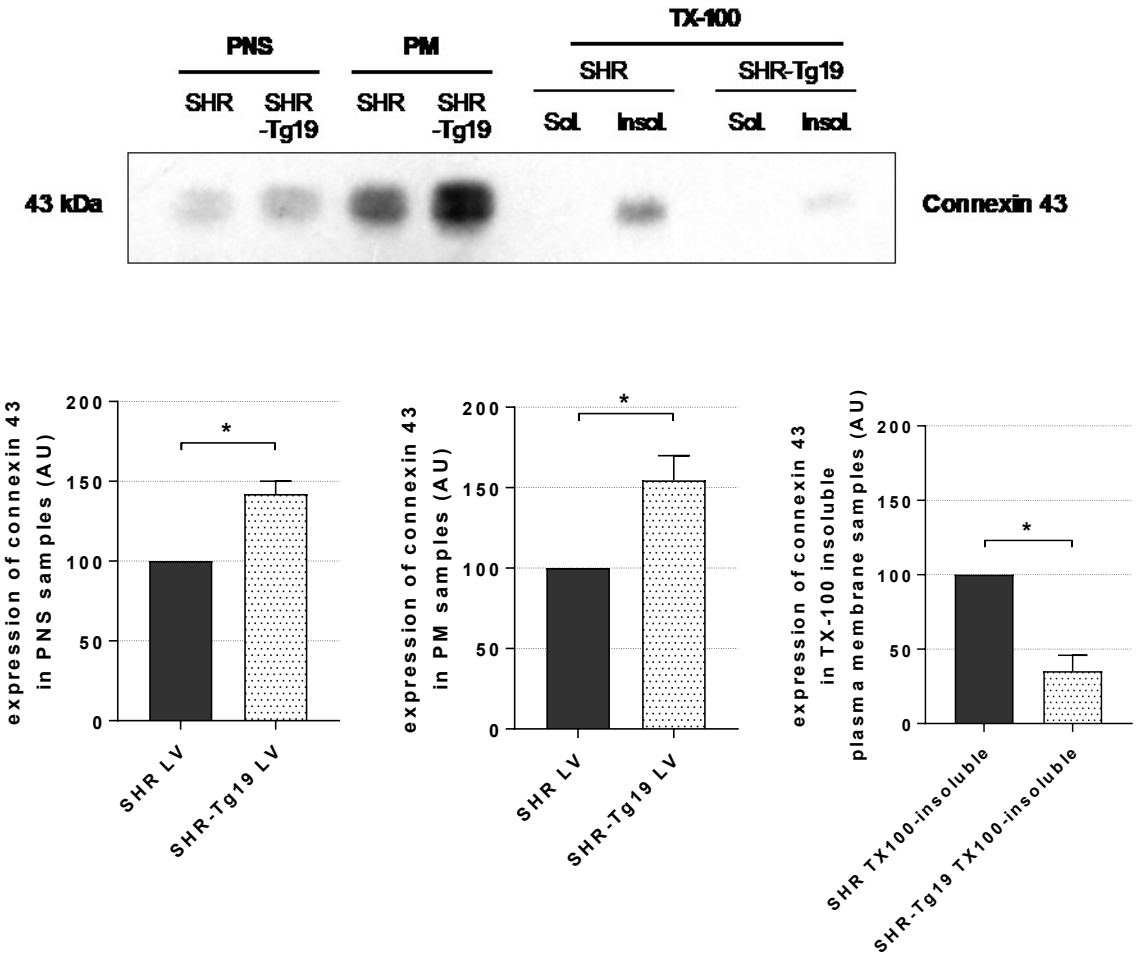

Fig. 21. Expression and distribution of connexin 43 protein in left ventricular PNS, PM and TX100-soluble and insoluble fractions of SHR and SHR-Tg19. Representative immunoblot of 6 experiments is shown in the upper panel. The signal was normalized using Ponceau stain and quantified. The resulting graphs are shown in the lower panel, * – $P < 0.05$.

4.11. Proteomic analysis of plasma membrane fractions extracted by TX-100

We used label-free quantification to compare protein composition of TX-100 resistant and soluble plasma membranes of SHR. Among total of 1676 identified protein fragments those were chosen that exhibited at least 2-fold change. 81 proteins were enriched in the DRM fraction and 97 resided in the soluble fraction. Proteins are presented in supplementary Tables 3 (DRM) and 4 (DSM) divided into groups based on their localization and function in the cell. Figure 22 provides visualization of the grouping, which was based on functional annotation tools from DAVID Bioinformatics Resources and current UniProt database annotations.

Notably, functional clustering revealed DSM fraction enrichment with cytoskeleton organization (26) and vesicular transport proteins (13) along with contractility (10) and extracellular matrix proteins (7). Commonly used lipid raft markers such as caveolin-1 and flotillin-1, as well as caveolar proteins cavin-1 and -2 were present in the DRM fraction.

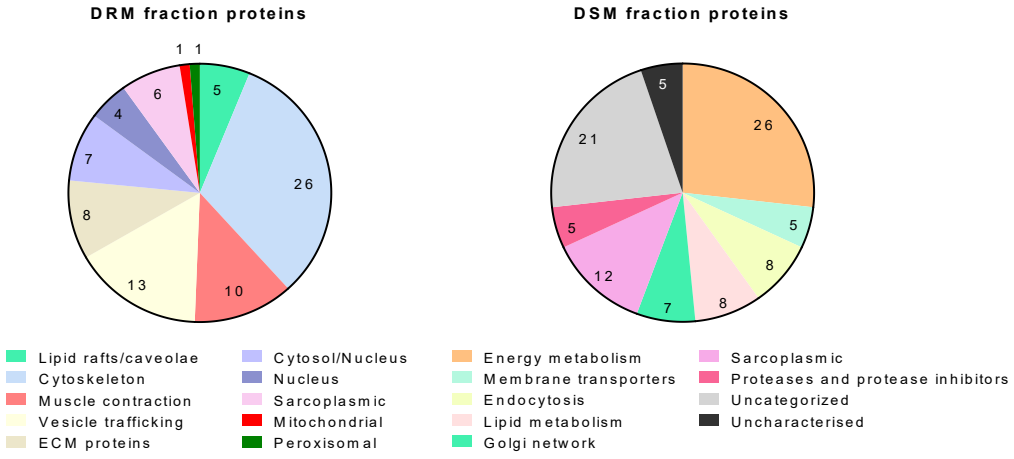

Fig. 22. Functional and localizational clustering of proteins in TX-100 resistant (DRM) and soluble (DSM) membrane fractions based on current annotations in the UniProt database.

The DSM fraction contained a large number of energy metabolism enzymes (26, including glycolysis, FA oxidation enzymes and creatine kinases) and sarcoplasmic proteins (12, including calnexin). 8 proteins from this fraction are responsible for lipid uptake and metabolism, another 8 for endocytosis. Several members of Rab GTPase family were present among the latter, as well as in group of 7 proteins belonging to the Golgi network. A group of 21 proteins possessed different functions and therefore could not be categorized into a particular cluster. Function of last 5 proteins listed in the table is unknown.

4.12. Immunofluorescence imaging analysis

We employed immunofluorescence imaging technique to characterize the difference in cellular expression of connexin 43 and β2 adrenergic receptors and their colocalization with caveolin proteins within the LV of SHR and SHR-Tg19. Membrane association of caveolin-1 and caveolin-3 proteins is visualized in Fig. 23. While caveolin-1 was localized to the sarcolemma and some of the observed cell nuclei, caveolin-3 was observed in sarcolemma and in what appears to be the transverse-tubular system.

We then used a combination of β2-AR or connexin 43 antibodies with caveolin 3 which served as a marker of the t-tubular system. As expected, connexin 43 signal was observed predominantly within areas of cell-cell contacts as clusters of spots corresponding to gap junctions localized at the intercalated disks. We were surprised, however, to see the β2-AR signal interleaving with caveolin 3 striations and not overlapping. Analysis using Manders overlap coefficient revealed no significant differences between SHR and SHR-Tg19 in the extent of co-localization of both connexin 43 and β2-AR with caveolin 3 (Fig. 24).

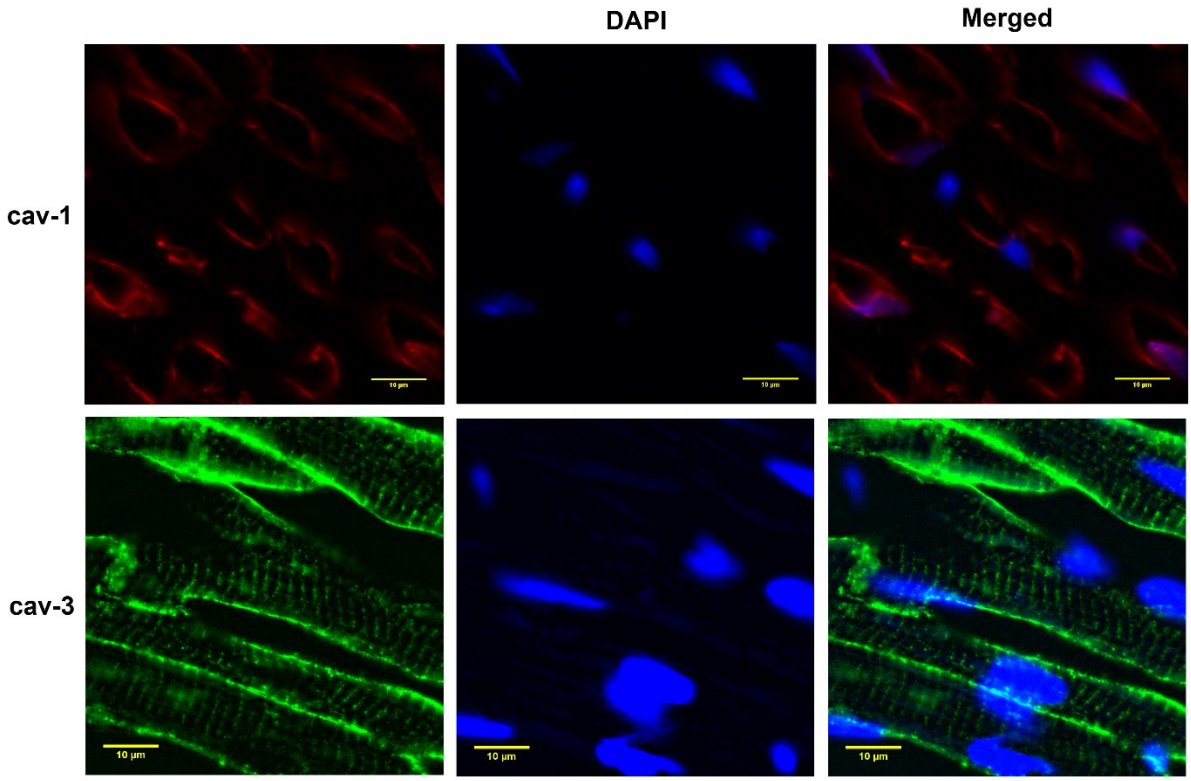

Fig. 23. Expression of caveolin-1 in endothelium and fibroblasts and caveolin-3 in cardiomyocytes of SHR. DAPI was used to stain the nuclei. Scale bar is 10 µm.

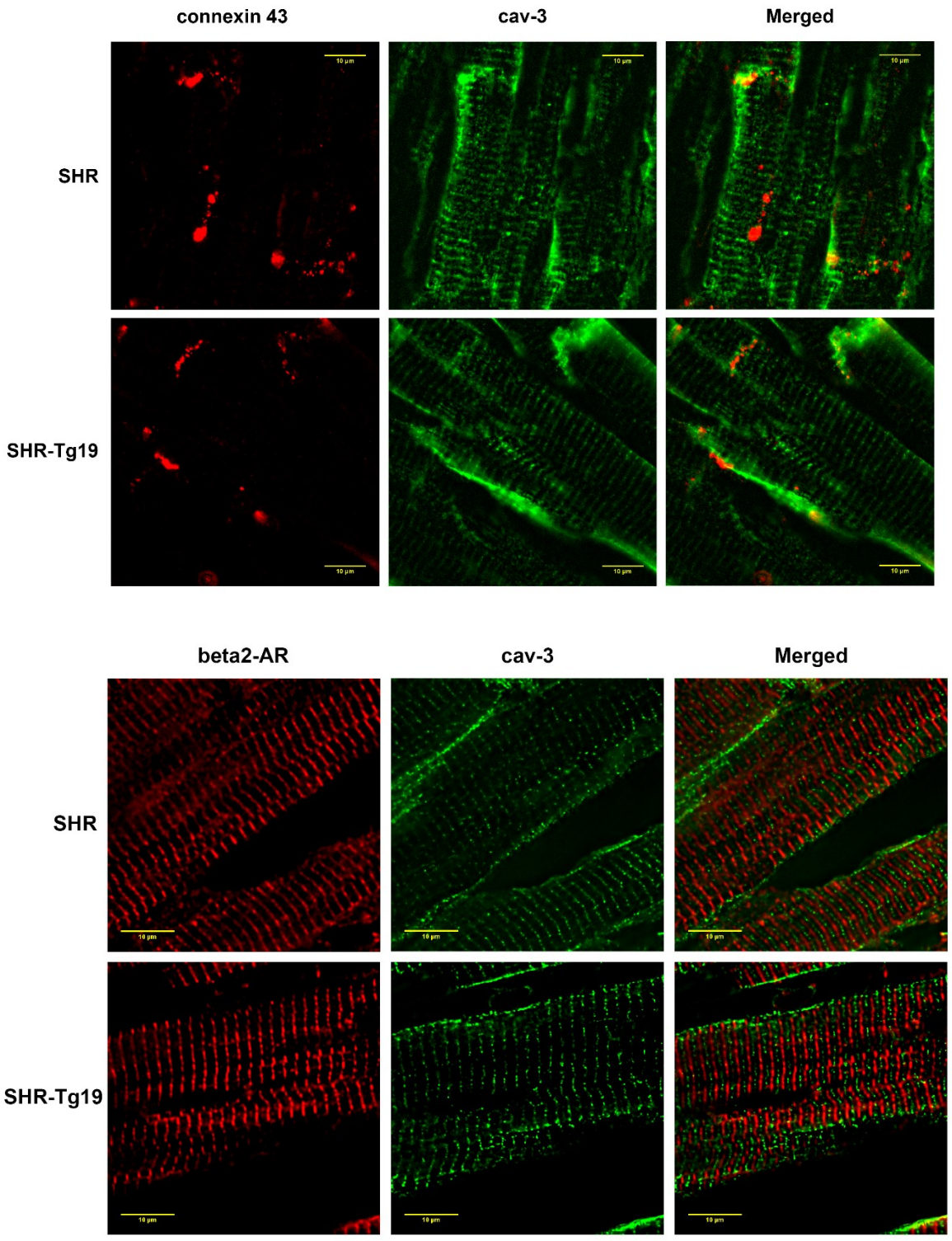

Fig. 24. Localization of connexin 43 and β2-AR proteins in cardiomyocytes of SHR and SHR-Tg19 merged with the signal of anti-caveolin-3 antibody. Scale bar is 10 μm.

4.13. Expression of regulatory proteins in the PNS from LV and RV

We used Western blotting to compare the expression of some regulatory proteins in the PNS of LV and RV between SHR and SHR-Tg19. Level of phosphorylated RhoA kinase was increased by about 15% in the LV of SHR-Tg19. Total level of RhoA in both ventricles as well as phospho-RhoA level in the RV did not change significantly (Fig. 25). Kinase ERK1 was upregulated in the LV of SHR-Tg19 by 30%, whereas there was no significant change in its expression in the RV. Expression of its close homolog, kinase ERK2, did not differ significantly between the strains. Level of phosphorylated form of ERK1 was similar between the strains, but about 60% lower in the RV than in the LV. Similar differences were observed for ERK2 but due to higher dispersion of the measured values they were not statistically significant (Fig. 26). No changes were found in the epac1 expression (Fig. 27).

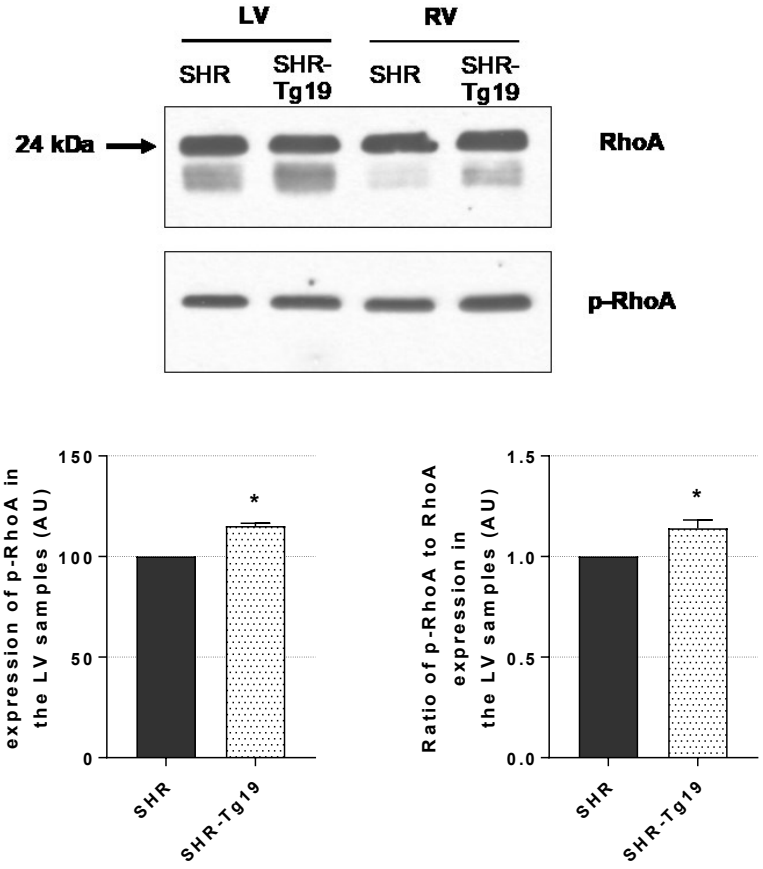

Fig. 25. Expression of RhoA and phospho-RhoA determined in the PNS from LV and RV of SHR and SHR-Tg19. Lower panel shows graphs of p-RhoA expression (*left*) and ratio of p-RhoA/RhoA expression (*right*) in the LV of both strains (* – $P < 0.05$).

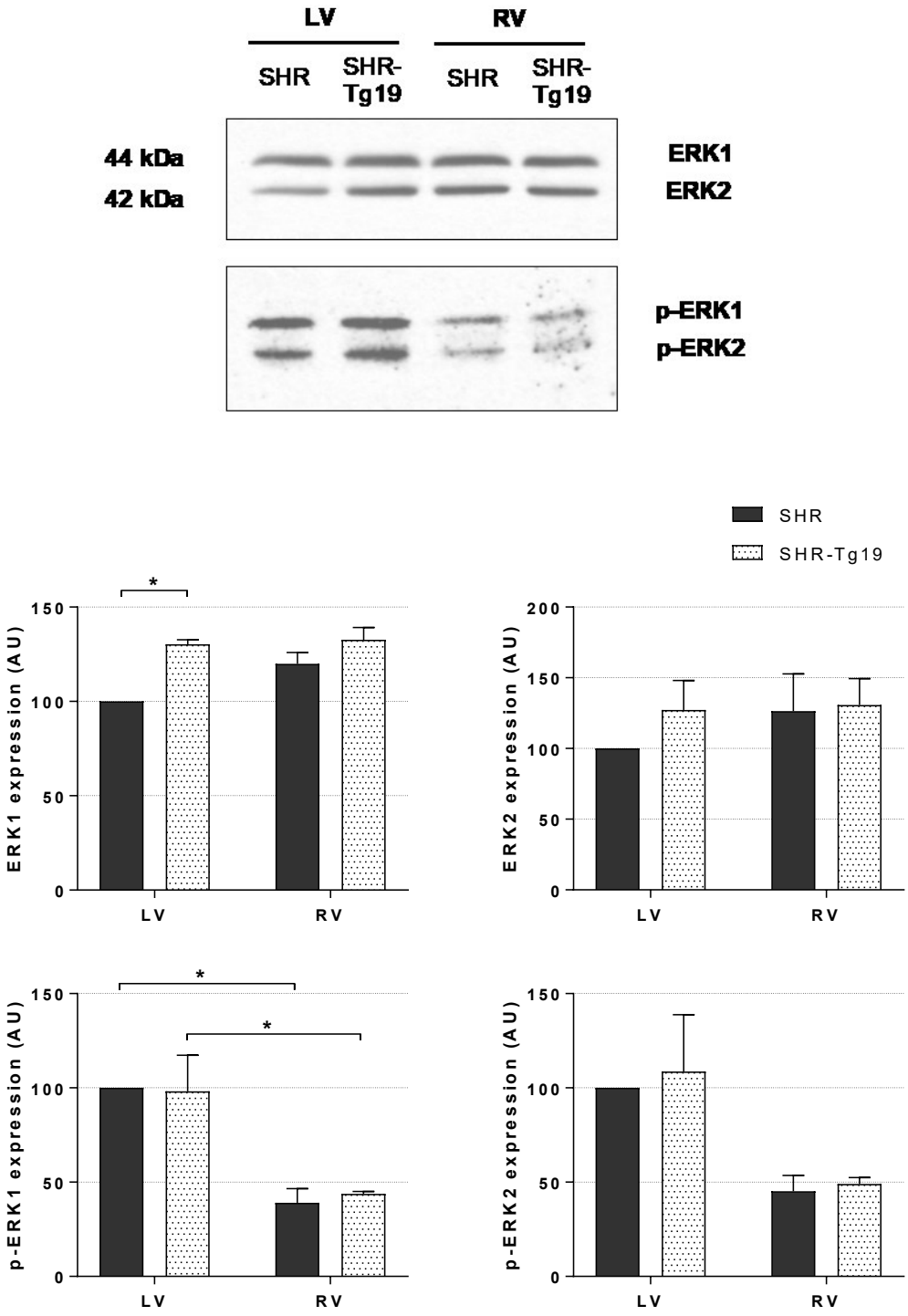

Fig. 26. Expression of ERK1/2 and phospho-ERK1/2 in the PNS from LV and RV of SHR and SHR-Tg19. Lower panel shows graphs of protein expressions plotted after three repeated measurements (* – $P < 0.05$).

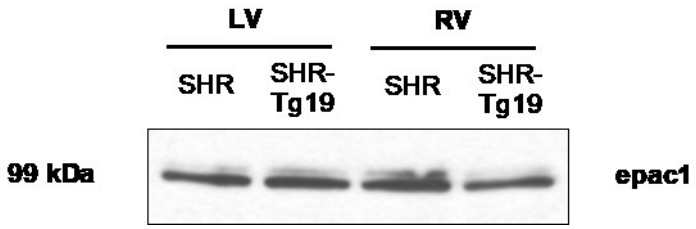

Fig. 27. Expression of epac1 protein in the PNS from LV and RV of SHR and SHR-Tg19. No significant changes were found between the samples after 5 repeated measurements.

5. DISCUSSION

Constantly active heart muscle requires a steady supply of energy substrates. It prefers fatty acids as the most energy-dense fuel, but can utilize a broad range of substrates, including glucose, ketone bodies, pyruvate, lactate and amino acids. One of the deciding factors in substrate preference is availability. Here FA transport facilitating proteins come into play. FA translocase Cd36 is responsible for at least 50% of cardiomyocytic LCFA uptake and possesses signaling capabilities influencing AMPK activity. Comparison of SHR, which does not express functional Cd36 due to a deletional mutation, and its progenitor WKY showed upregulation of glycolytic and downregulation of beta-oxidation enzymes (Iemitsu et al., 2003; Zamorano-León et al., 2010). When the switch to glycolytic metabolism that is normal for the fetal heart occurs in the adult heart it can be seen as a sign of progression towards heart failure as it is not sufficient to meet cardiac muscle energy needs. This metabolic pattern in adult heart is associated with hypertrophy and insulin resistance (Allard et al., 2000; Barger and Kelly, 1999).

5.1. Proteomic comparison

One of the goals of this study was to identify broader effects of transgenic Cd36 expression on protein composition of ventricular cardiomyocytes of SHR. We also compared the protein profiles of the left and right ventricles. The predominant number of the hypertension and failing heart metabolism studies have been done on the left ventricle, as evident by NCBI PubMed database search that excludes either “left” or “right” ventricle metabolism keywords. Meanwhile, right ventricular dysfunction is a powerful prognostic factor in patients with congestive heart failure (Di Salvo et al., 1995; Tadic et al., 2017).

We did not observe same differences in the proteomes of SHR and SHR-Tg19 as were found between SHR and WKY by Zamorano-León et al. (2010). These authors observed that most of the beta-oxidation enzymes were downregulated in the LV of SHR and pyruvate dehydrogenase was upregulated. Our comparison of SHR and SHR-Tg19 proteomes revealed significant downregulation of malate dehydrogenase in both ventricles using MALDI-TOF MS, which also identified an increase in mitochondrial aconitate hydratase and proteasome subunit alpha type-1 expressions in the LV of SHR-

Tg19. Aconitate hydratase (aconitase) is a TCA cycle initiating enzyme highly expressed in the heart. It is very sensitive to ROS accumulation, which lowers its activity and thus slows downstream respiratory reactions that are primary producers of ROS in mitochondria (Matasova and Popova, 2008). Upregulation of aconitase in SHR-Tg19 can be seen as a sign of increased activity of the TCA cycle and improved heart function. Concurrent downregulation of MDH is discussed in section 5.2. Proteasome subunit alpha type-1 (PSMA1) together with other alpha subunits creates heptameric outer ring of 20S proteasome core particle which after binding of two regulatory particles maintains specific degradation of ubiquitinated proteins. Alpha subunits essentially serve as a gate which allows access of degradation-destined proteins to catalytic center of 20S proteasome. PSMA1 was found to be overexpressed in breast cancer cells which also display an enhanced activity of the ubiquitin-proteasome system (Deng et al., 2007). Unfortunately, to our knowledge there are no available studies regarding the functions of individual proteasomal alpha subunits. As a whole, the ubiquitin-proteasome system is indeed known to regulate apoptosis by acting on p53, NF-κB and HIF-1α (Thompson et al., 2008). This regulation is considered cardioprotective as proteasomal degradation of p53 prevents excessive apoptosis during such events as ischemic injury (Powell et al., 2012). Proteasomes also degrade mis-targeted mitochondrial proteins that otherwise could trigger apoptosis, e.g. EndoG. Additionally, assembly of 20S particles is enhanced by increased ROS levels (Bragoszewski et al., 2017).

Although label-free proteomic analysis did not reveal any of the changes identified by MALDI-TOF MS, the results obtained in the latter analysis were confirmed by enzymatic activity assays. The observed discrepancy between the two proteomic approaches arises from their respective limitations. 2-Dimensional electrophoresis has well-known problems associated with inaccurate characterization of the molecular mass and isoelectric point and inability to properly resolve membrane proteins due to their hydrophobicity. Another problem is that small proteins or proteins with low abundance can be omitted by the analysis, resulting in only high-abundant relatively big and well-soluble proteins being detected (Gygi et al., 2000). Therefore, it is important to cross-validate 2DE analysis data using other methods. Despite its limitations, gel-based proteomics have the advantage of resolving post-translationally

modified proteins, which is important in cardiac research as 62% of heart cell proteins possess at least 1 covalent modification (Van Eyk, 2011).

However, 2DE is also labor-intensive and results are prone to gel-to-gel variability. A variety of liquid chromatography-based MS (LC-MS) methods became widely available due to technological advances in high-throughput proteomics. These methods were originally dependent on stable isotopic labeling of samples, but development of quantitative approaches allowed accurate protein detection using label-free MS. Unlike 2DE paired with MALDI-TOF, label free MS allows for higher dynamic range of detected proteins. Unfortunately, it is not without its own limitations which are based on resolving power of a spectrometer and data normalization and interpretation (Sandin et al., 2015). Here we applied MaxLFQ algorithm, which is aimed at quantifying proteins signal intensities using an improved normalization procedure (Cox et al., 2014).

Using label-free LC-MS we identified a total of 7 changes in SHR-Tg19 LV proteome compared to SHR. Five of these proteins were unannotated entries with only provisory names in the UniProt database. Looking these entries up in rat genome database (RGD) revealed their pseudogene status, further confirmed by running BLAST two sequence comparison algorithm (Pundir et al., 2016; Shimoyama et al., 2015). However, judging by detectability of their protein products we should use a term "pseudo-pseudogenes", which was coined during research of similar phenomenon in *D. melanogaster* (Prieto-Godino et al., 2016). Two of them, currently filed in RGD under provisory names LOC103691697 and LOC103694107 cover 4% of the *Ndufb3* gene sequence with 90% identity. That gene encodes NADH dehydrogenase 1 beta subcomplex subunit 3 that plays an accessory role in the respiratory chain Complex I of the inner mitochondrial membrane. Second pair consists of proteins LOC100361934 and LOC688963, genes of which share 6% of their length with *Ndufb4* (96% identity), which codes for NADH dehydrogenase 1 beta subcomplex subunit 4. And protein LOC100359563 is encoded by gene that 99% similar to 33% of the length of ribosomal protein S20 (*Rps20*) gene sequence. RPS20 is a small protein of the 40S ribosomal subunit, which is homologous in rat and human. Aside from being an artifact of proteomic analysis, we hypothesize that either these proteins or their mRNA can have functional impact on the cell. Studies of gene expression in tumor cells suggest that pseudogene mRNA products may regulate expression of cognate proteins by acting as a

"decoy" for binding of inhibitory miRNA (Poliseno et al., 2010). Additionally, some pseudogenes were found to produce functional siRNA thus playing a role in transcriptional regulation (Chan and Chang, 2014). Both NDUFB3 and NDUFB4 subunits are not directly involved in catalysis of respiratory reactions and may serve an accessory role during Complex I assembly. Dysfunction of the *Ndufb3* gene was shown to induce Complex I deficiency (Calvo et al., 2012). NDUFB4 protein is highly susceptible to nitration by reactive oxygen species (Murray et al., 2003). RPS20 is a small protein of the 40S ribosomal subunit, which is homologous in rat and human (Wool et al., 1995). RPS20 was shown to promote p53-mediated apoptosis by inhibiting Mdm2 ubiquitin ligase activity (Daftuar et al., 2013). Tumor suppressor protein p53 is functionally linked to stretch-induced cardiomyocyte apoptosis, which may be implicated in progression of cardiac hypertrophy to heart failure (Leri et al., 2000). Interestingly, cytoplasmic MDH, which was downregulated in the LV of SHR-Tg19, possesses p53-binding and activating capability thus being able to serve as a transcriptional activator of p53-mediated cell cycle arrest and apoptosis, thus linking metabolism and apoptotic stress response (Lee et al., 2009). Protein COX17 is a copper-binding chaperone necessary for the assembly of cytochrome c oxidase (COX) (Kako et al., 2004). COX levels are known to be decreased in SHR and in artificially induced hypertrophy by coarctation of the abdominal aorta (Kuo et al., 2005).

Both 2DE/MALDI-TOF MS and LC-MS analyses found more changes in the RV than in the LV of SHR-Tg19, all of which were downregulations. The first approach allowed us to identify changes in several metabolic dehydrogenase enzymes, including malate, succinate, aldehyde, glyceraldehyde-3-phosphate (GAPDH) and long-chain specific acyl-CoA dehydrogenase (LCAD) as well as dihydrolipoyl transacetylase (DLAT) component of pyruvate dehydrogenase complex. All of these except MDH and GAPDH were mitochondrial proteins. Expression of aldehyde dehydrogenase (ALDH) had lowered 4-fold in SHR-Tg19. This is the most striking change in RV proteins, most of which were downregulated 2- to 3-fold. Catalysis of aldehydes to non-reactive forms by ALDH is cardioprotective and helps lower oxidative stress (Chen et al., 2010). As aldehydes can form in cells as products of lipid peroxidation, the downregulation of ALDH in SHR-Tg19 may be associated with lower cardiac TG contents. Research indicates that ALDH expression can be suppressed by PKA activity, which is elevated in SHR-Tg19 due to enhanced β2-AR signaling (You et al., 2002). GAPDH is a key

glycolytic enzyme and DLAT as a part of PDH complex mediates entry of glycolysis end product pyruvate into the TCA cycle. Their downregulation may be a sign of shift towards more energy-sufficient beta-oxidation. Additionally, GAPDH has pro-apoptotic function mediated via mitochondrial membrane permeabilization, thus lower levels of this enzyme may induce cardioprotection in SHR-Tg19 (Tarze et al., 2007). On the other hand, downregulation of SDH is detrimental in the context of heart disease (Chouchani et al., 2014). SDH subunit A participates in the TCA cycle where it catalyzes oxidation of succinate to fumarate. Downregulation of its activity results in increased succinate levels and lower mitochondrial complex II respiration rates. It was shown to be positively regulated by SIRT3 via NAD^+-dependent deacetylation, a mechanism that is compromised during heart failure (Horton et al., 2016). The same mechanism also regulates activity of LCAD, which is a major beta-oxidative enzyme (Hirschey et al., 2010). Its gene expression is dependent on PPARα transcription factor which is activated by increase in FA levels. On the other hand, Cd36 expression has a positive correlation with that of LCAD, making it hard to draw a decisive conclusion from this result (García-Rúa et al., 2012). Proteins of the 14-3-3 family interact with over 200 phosphoproteins and affect a broad range of pathways, including cell cycle and apoptosis. It is hypothesized that 14-3-3 proteins act by docking onto dual-phosphorylated sites on their targets, facilitating conformation change or interactions of some proteins and preventing interactions of others by masking their active domains (Cau et al., 2018). They were shown to be involved in mediating insulin intracellular actions by interfering with signaling proteins (Chen et al., 2011). 14-3-3 can participate in apoptosis regulation by activating MAPK pathway protein Raf-1, inhibit pro-apoptotic effect of Bad and integrate anti-apoptotic effects of Akt (Dong et al., 2007).

Analysis of RV changes by LC-MS identified 10 proteins, all of which were downregulated in SHR-Tg19. Three of them were either regulatory or structural cytoskeletal proteins, others were connected to regulation of apoptosis.

Ubiquitously expressed cytoskeletal GTPase Septin-11 co-localizes with microtubules and is involved in multiple cellular functions including vesicular trafficking and cytokinesis (Hanai et al., 2004). Beta-tubulin isoforms 1 and 6 are major counterparts of microtubules, formations that consist of repeating alpha- and beta-tubulin units, where alpha-tubulins always located at elongating end of the microtubule and beta- are at the dissolving end. Earlier measurements of tubulins mRNA expression

showed that beta-tubulin 1 is confined to hematopoietic cells and later it was discovered that it indeed have significant functions in white blood cells and platelets (Lecine et al., 2000; Wang et al., 1986). Despite that, beta-tubulin 1 expression was observed in the heart where its upregulation is contributing to hypertrophy development by aggressive microtubule formation, this effect was especially prominent in the right ventricle (Narishige et al., 1999).

Dual specificity mitogen-activated protein kinase kinase 1 (Map2k1 or MEK1) is an essential component of classical MAPK pathway which forms heterodimers with MEK2 that are crucial to performing negative feedback regulation of said pathway (Catalanotti et al., 2009). Its phosphorylation by MAPKKK c-Raf leads to activation and phosphorylation of downstream kinases MAPK3/ERK1 and MAPK1/ERK2 whose targets are multiple cytosolic proteins and nuclear transcription factors (Macdonald et al., 1993). MEK1 is implicated in promoting cell survival as part of the MAPK pathway (Gise et al., 2001). Cyclic AMP-dependent protein kinase inhibitor alpha (PKIα) is a strong suppressor of both α and β catalytic subunits of PKA (Olsen and Uhler, 1991). Loss of PKIα may be linked to enhanced β-adrenergic signaling in SHR-Tg19. RNA-binding protein (PAI-RBP1) binds to 3′-most 134 nt of plasminogen activator inhibitor-1 (PAI-1) mRNA and regulates its stability (Peluso et al., 2004). PAI-1 prevents apoptosis by inhibiting serine proteases. Its expression is increased in disease states such as metabolic syndrome (Juhan-Vague and Alessi, 1997). Reticulon-3 (RTN3) is expressed in the endoplasmic reticulum (ER) and Golgi apparatus where it is necessary for transport of membrane vesicles in the early secretory pathway (Wakana et al., 2005). RTN3 is activated in response to ER stress and exhibits anti-apoptotic activity by accumulating Bcl-2 in mitochondria (Wan et al., 2007). Bone morphogenetic protein 10 (BMP-10) is maintaining proliferative activity of cardiomyocytes during embryonic development (Sun et al., 2014). Overexpression of BMP-10 in human prostate cancer cells was shown to inhibit cell growth via activation of ERK1/2, implying its possible role in regulation of apoptosis (Ye et al., 2009). Mitochondrial 3-oxoacyl-coenzyme A thiolase, also known as acetyl-CoA acyltransferase 2 (ACAA2), catalyzes the last reaction of the mitochondrial fatty acid beta-oxidation spiral by transferring acetyl group to coenzyme A. ACAA2 was shown to interact with BCL2/adenovirus E1B 19kDa interacting protein 3 (BNIP3) and suppress its pro-apoptotic activity (Cao et al., 2008).

Pressure overload induced cardiac hypertrophy is associated with increased cardiomyocyte apoptosis observed in both LV and RV (González et al., 2002; Teiger et al., 1996). This is especially apparent in SHR when transition from hypertrophy to heart failure occurs. Expression of Cd36 and resultant changes could be speculated to have anti-apoptotic and anti-hypertrophic effects in the RV of SHR heart.

Coiled-coil domain-containing protein 51 (ccdc51) was downregulated in samples from both the left and right ventricles of SHR-Tg19 according to LC-MS analysis. Preliminary data found in Ensembl database describe Ccdc51 as a multi-pass membrane protein localized in mitochondrial matrix and nucleoplasm that is homologous in rat and human. It exhibits ubiquitin c binding activity and was shown to be absent in human newborns with intrauterine grows restriction (Emanuele et al., 2011; Ruis-González et al., 2015). There is still limited information about the function of this protein.

To the best of our knowledge, proteomic studies have been done only on the left ventricles of SHR so far. In general, relatively little is known about differences between the left and right ventricle proteomes. In the heart, the left ventricle plays a key role in the circulatory system and is therefore the subject of greater interest when compared to the right ventricle or atria. Here we observed 257 unique proteins in the left ventricles and 560 unique proteins in the right ventricles of SHR, along with 1334 proteins in both ventricles. These proportions correspond well with the results of other proteomic studies on left and right ventricular tissue (Cadete et al., 2012; Comunian et al., 2011; Zhou et al., 2006).

5.2. Analysis of respirational parameters

There are reports that Cd36 along with many other membrane-bound receptors can be subjected to ectodomain cleavage by metalloproteases in SHR (Santamaria et al., 2014). Therefore, we were curious about the distribution of Cd36 in heart tissue of SHR and transgenic Cd36-expressing rats. Our immunoblotting experiments showed that expression of Cd36 transgene in SHR was associated with markedly increased Cd36 content in heart plasma membranes, indicating that the membrane Cd36 population of cardiac cells is rescued in SHR-Tg19. Furthermore, wild-type Cd36 was previously observed in adipocyte plasma membranes of WKY and SHR-Tg19, but not SHR (Pravenec et al., 2001). We also detected some Cd36 expression in the mitochondrial fractions prepared from the LV of both rat strains, albeit in much lower amounts than in

the PM. Localization of Cd36 in the mitochondrial membrane was previously reported by Campbell et al. (2004), however, FA oxidation is apparently not influenced by Cd36 presence in mitochondria (King et al., 2007). Our results agree with this study as our respirometric measurements did not reveal any significant differences between the oxygen fluxes in mitochondria isolated from SHR and SHR-Tg19. On the other hand, LV tissue homogenates from SHR-Tg19 exhibited higher respiratory activity (by about 20%) than those from SHR (Neckář et al., 2012). A similar discrepancy between the properties of isolated mitochondria and skinned heart fibers was observed by Jüllig et al. (2008). They reported that skinned fibers isolated from SHR exhibited lower respiratory activity (by about 40%) than those derived from WKY. Although isolated mitochondria displayed higher respiratory fluxes, their activity did not significantly differ between the two groups of rats; only complex II activity and respiration in FCCP-uncoupled state were reduced in isolated mitochondria of SHR compared to WKY. It should be noted, however, that these rats were 20 months old at the time of the experiment, and thus influenced by progressive metabolic dysfunctions.

In accordance with our proteomic analysis, the spectrophotometric assay of MDH showed a significant reduction of its activity in both PNS and isolated mitochondria from the LV of SHR-Tg19. Interestingly, investigations of different cancer cell lines revealed a novel role of MDH as a provider of NAD for glycolysis (Hanse et al., 2017). Indeed, the excessive NADH produced in glycolysis in hypertrophied SHR heart was shown to be oxidized by MDH via either malate/aspartate or novel malate/oxaloacetate shuttle (Atlante et al., 2006; Nielsen et al., 2011). Therefore, it might be speculated that a relatively high glycolytic activity in the LV of SHR may require more effective functioning of MDH. Furthermore, we observed a significantly reduced activity of HK (by about 30%) in samples from the LV of SHR-Tg19 compared to SHR, indicating suppression of glycolytic metabolism. In line with this, SHR heart was reported to exhibit markedly higher activity of HK (by 60%) when compared to WKY (Paternostro et al., 1995). Moreover, Hajri et al. (2002) found several-fold increase in glucose uptake by the heart of Cd36-/- mice. Taken together these data imply that transgenic expression of Cd36 in SHR may contribute to a shift from glycolysis to beta-oxidation.

Cd36-mediated entry of FA into cells regulates energy substrate metabolism through PPARs (Drover and Abumrad, 2005). Despite the presence of a functional Cd36 transporter and thus a possibility of PPARα upregulation in SHR-Tg19, we

observed a significant downexpression of the 70-kDa peroxisomal membrane protein (PMP70) (by 40%) in the LV of SHR-Tg19 compared to SHR. However, we did not detect any difference in the expression of peroxisome resident enzyme catalase, thus concluding that total number of peroxisomes might remain unchanged. PMP70 participates in transport of LCFA-CoA molecules across the peroxisomal membrane. Given that peroxisomes are capable of oxidizing a wider range of substrates than mitochondria, it could be speculated that in Cd36-deficient animals peroxisomal oxidation of lipids becomes more pronounced as the heart continues to rely heavily on beta-oxidation. In this context, it is worth mentioning that overexpression of PMP70 has been demonstrated to lower mitochondrial beta-oxidation (Imanaka et al., 1999).

SHR tissues express increased levels of oxidative stress markers. Recently it has been shown that lipid peroxidation in the heart can be alleviated by dietary medium-chain triglyceride supplementation (Saifudeen et al., 2017). The previous study by Neckář et al. (2012) did not find any difference between SHR and SHR-Tg19 in the activities of antioxidant enzymes and levels of different oxidation products except for the reduced glutathione which was lower in SHR-Tg19. OXPHOS complex II is a major ROS production center and it was shown that the loss of iron-sulfur protein subunit SDHB from this complex could aggravate ROS formation (Guzy et al., 2008). We detected lower expression of SDHB and elevated activity of SCR in the LV of SHR compared to SHR-Tg19. This discrepant result may be explained by the decrease in the expression of SDHB subunit unassociated with Complex II.

Here, we revealed a significant difference in the efficiency of respiration in isolated mitochondria between the LV and RV from SHR rats. Our results concur with high-resolution respirometric measurements of permeabilized cardiac muscle fibers from WKY rats. The difference between the ventricles was similar, although permeabilized fibers exhibited overall lower respiratory rates (Grundmanová et al., 2016). Our data also revealed higher SCR activity and higher expression of NDUFB1 and SDHB in the RV from both SHR and SHR-Tg19. However, in the RV the contribution of complex II (after the addition of rotenone) to O2 utilization was almost 2 times lower than in the LV. Complex IV could be suspected in producing this discrepancy as its activity does not directly influence measurements of enzymatic activity. It could also be speculated that the surplus of succinate dehydrogenase complexes exists in the RV of SHR independently of Cd36 function and that those

complexes are uncoupled from the rest of the oxidative phosphorylation system and could be linked to ROS production in the RV mitochondria. Concurringly to that, ROS production in the failing right ventricle of the rat heart is attributed to heightened Complex II activity and expression (Redout et al., 2007). Although rats in our study did not enter the chronic heart failure state, our results show that pathological changes are already present in cardiac mitochondria. As mentioned above, we detected a markedly higher PMP70 level in the LV than in the RV from SHR and transgenic expression of wild-type Cd36 in SHR reduced the content of this protein in the LV nearly to the RV level. Interestingly, Colasante et al. (2015) reported that the expression of peroxisome-related genes was mostly higher in the LV, probably due to the higher workload and hence energy requirements when compared to the RV and atria. However, the expression of mRNA coding for PMP70 was the same in both ventricles. This could mean that PMP70 is abnormally high in the LV of SHR and that its expression can be modulated by the expression of functional Cd36.

5.3. Simplified method for preparation of membrane fractions

Currently, sucrose density gradient centrifugation is the most commonly used method to isolate and study membranes enriched in lipid rafts. This procedure may involve treatment with nonionic detergents like Triton X-100, in which sphingolipid-cholesterol rafts are insoluble at 4°C (Brown and Rose, 1992) or sonication in pH 11 sodium carbonate buffer (Song et al., 1996a). Both methods require long (16-20 h) centrifugation times, which is undesirable as it strains the equipment. Another approach relies on iodixanol density gradient centrifugation. First introduced by Smart et al. (1995), this method required multiple centrifugation steps and produced low amounts of sample material. An improved process described in an article by Macdonald and Pike (2005) required only 1.5 h of centrifugation time and resulted in higher yields. However, the distribution of the membrane proteins in the fractions obtained by this method raises some concerns as flotillin and caveolin were located in fractions 1-8 and 7-12, respectively, but transferrin receptor (which is regarded as a non-raft protein) resides in fractions 5-8, between these typical raft proteins as shown in Fig. 2 of the said article. Additionally, this study was done on cultured cells and we have not been able to reproduce this separation using the plasma membranes derived from cardiac tissue.

Instead, we used an approach based on TX-100 solubilization, which also requires only 1 h of centrifugation, as described by Rubin and Ismail-Beigi (2003). Unlike methods that use sucrose gradients this separates only two fractions – a supernatant that contains TX-100 soluble membranes and a pellet that ought to be resuspended and contains membranes resistant to TX-100 solubilization. We tested the quality of this separation using Western blotting for major protein markers and found that most of them were distributed in the relevant fractions, including Cav-1 and TfR (Fig. 17). Additional analysis of GM1 distribution using cholera toxin subunit B also corroborated these results. However, protein flotillin-1, which is routinely used as a raft marker, was distributed rather evenly between these fractions. Flotillin-1 is a 47 kDa protein that is anchored in the membrane by two loops on its N-tail as well as with a palmytoilation (Morrow and Parton, 2005). Studies in the B cells indicate it is a non-caveolar raft-associated protein and showed clear localization of Flot-1 in these structures (Solomon et al., 2002). Indeed, experiments involving cholesterol depletion from the sarcolemma of skeletal myofibers resulted in disrupted caveolar morphology but had no effect on the distribution of Flot-1 (Kaakinen et al., 2012). The fact that flotillin-1 localizes predominantly in the planar rafts may explain our present findings.

However, judging by the localization of the Cav-3 protein in TX-100 soluble fractions we conclude that this method does not isolate all microdomain membranes evenly and may be too harsh in dissolving some of them. In the aforementioned study on skeletal myofibers, Cav-3 was mostly localized in the insoluble fraction, however, the detergent was able to solubilize a large amount of the protein (Kaakinen et al., 2012). These myofibers were incubated in ice-cold TX-100 for 10 min before 2.5 h centrifugation versus 1 h incubation and 1 h centrifugation in our study. Conditions used in our experiment resulted in almost complete solubilization of Cav-3 but not Cav-1 which remained only in the TX-100 insoluble fraction (Fig. 17). Both caveolin isoforms are expressed in the heart, but as indicated in studies on KO mice models, Cav-3 is muscle cell specific and Cav-1 is localized in cardiac fibroblasts and endothelial cells (Razani and Lisanti, 2001). Indeed, immunofluorescent staining using Cav-1 antibody revealed non-striated heart cells most of which were distinctly tube-shaped and thus likely belonging to endothelial cell population (Fig. 23).

This may indicate that the method that we chose to isolate microdomain-enriched membranes is more suited to separate fibroblast and endothelium membrane

microdomains as cardiomyocytic Cav-3 is solubilized. However, this does not explain the localization of β2-AR in the TX-100 insoluble fraction. These receptors are normally co-localized with t-tubules and caveolae in cardiomyocytes (Head et al., 2005). As a part of the sarcolemma, t-tubules are rich in Cav-3, which is also implicated in their formation (Carozzi et al., 2000). Therefore, it is difficult to explain that TX-100 solubilized membranes rich in Cav-3 but not β2-AR in our experimental conditions. It can be speculated that Cav-3 is more susceptible to TX-100 solubilization than other components of cardiomyocyte caveolae.

To elucidate the proteomic composition of TX-100 fractionated membranes we used label-free LC/MS. Unlike other proteomic methods, this one is particularly suited to identify membrane-bound proteins (Matta et al., 2015). There were 1676 proteins identified in both separated fractions. We chose only those that were expressed 2-fold change between the samples of membrane fractions. By using DAVID Bioinformatics Resources, we clustered these proteins into functional-localizational groups (Fig. 22 and supplementary Table 3 and 4).

Eighty-one proteins were identified to be enriched in the DRM fraction. Five of them (Cav-1, Flot-1, Cx43 and two isoforms of cavin) belonged to lipid raft fraction. Twenty-six of the proteins identified in the DRM fraction were cytoskeletal. Lipid rafts and caveolae are indeed known to tether with many cytoskeletal elements in cardiomyocytes (Head et al., 2014). Our proteomic analysis identified enrichment of gamma-actin and many tubulin isoforms in the DRM fraction. These proteins are structural components of actin filaments and microtubules respectively. Caveolin-1 is known to co-localize with microtubules and affect their polymerization (Kawabe et al., 2006). Additionally, disruption of microtubules or actin microfilaments may reduce the amount of DRM-associated Cav-1 and Cav-3 (Head et al., 2006) and raft formation (Plowman et al., 2005). Disruption of either microtubules or actin filaments also leads to exclusion of β-AR, Gα and AC proteins from buoyant fraction isolated using sodium carbonate buffer (Head et al., 2006). Our DRM fraction also contained many proteins related to cardiac contractility machinery, such as dystrophin, desmin, troponin, tropomyosin, myosin and alpha-actin. Desmin is a 53.5 kDa protein that polymerizes to form intermediate filaments. These structures surround the myofibrils at Z-discs and anchor in to the sarcolemma via the costamere protein complex (Capetanaki et al., 2007). The costameres are integral membrane protein complexes that bind to laminin in

the ECM. Protein dystrophin is associated with costameres on the intracellular membrane and alpha-actinin at the I-band of the myofibril (Minetti et al., 1992). By binding them dystrophin is providing a structural link between cell membrane and the intracellular contractile machinery. Costameres are known to include GPI-anchored proteins and Cav-3 which imply their lipid raft distribution (Sotgia et al., 2000). Additionally, we observed many proteins constituting the vesicular transport machinery. It is proposed that lipid rafts participate in vesicular trafficking not only as membrane regions that bind cytoskeleton filaments along which the vesicles travel, but also as domains of the said vesicles membranes (Ikonen, 2001). To summarize these findings, it may be correct to assume that the DRM fraction that we obtained indeed contains lipid rafts with their integral proteins. It includes the ECM and contractility proteins because they were bound to these raft-associated proteins during fractionation.

However, there were also nuclear and SR proteins present in this fraction. It might raise concerns for the viability of the fractionation method due to alternative explanation of observed results: the pellet might consist not of TX-100 solubilization-resistant fraction but of heavy cytoskeleton and contractile proteins that were sedimented during the centrifugation. The observed distribution of Cav-3 in the soluble fraction corroborates this interpretation of the data. On the other hand, we used the PM-enriched fraction prepared from the post-nuclear supernatant which should exclude heavy myofibrils and nuclei. Further experiments are needed to ascertain the nature of contaminating nuclear and SR proteins, but it should be noted that lipid microdomains are postulated to exist in intracellular compartments, such as Golgi and nucleus (Cascianelli et al., 2008; Stüven et al., 2003). Thus, it would not be unreasonable to suggest that the chosen fractionation resulted in proteins from the intracellular membranes as well as from the PM to be included in the DRM fraction.

Second group contains 97 proteins identified to be enriched in the TX-100 soluble fraction. Unlike the first group, it was much more diverse and not all of the proteins could be decisively categorized. Moreover, the DSM fraction contained 5 yet uncharacterized proteins including aforementioned coiled-coil domain-containing protein 51.

The largest category contains proteins participating in energy metabolism followed by group of sarcoplasmic reticulum residents. Mitochondria are generally considered to lack lipid rafts in their membranes as mitochondrial proteins are not

affected by cholesterol depletion and show different gradient distribution profiles (Zheng et al., 2009). There are regions of the ER membrane termed mitochondria-associated membranes (MAM) for their close association with mitochondria. A study of proteomic composition of TX-100 solubilized MAM preparations from rat neuronal cell line revealed they contain lipid raft proteins (Poston et al., 2011). We compared their protein listings with ours to find some overlap. Indeed, such entries as calnexin, hypoxia up-regulated protein 1 and NADH-cytochrome b5 reductase 1 were present in both our DSM fraction and in the MAM study where they were marked as non-raft. However, the DSM fraction contains calreticulin which was also found in the MAM but marked as a raft protein. Moreover, a cytoskeleton-associated protein 4 that we observed in the DRM fraction was marked as a non-raft protein by the authors of that study.

The DSM fraction have several membrane transporters including one of Na^+/K^+-ATPase subunits. Na^+/K^+-ATPase activity is dependent on membrane fluidity and was shown to be inhibited by high cholesterol to phospholipid ratio (Kimelberg, 1975; Sutherland et al., 1988). Four GTPase members of the Rab family were present in the DSM fraction. They regulate endosomal motility and were also known to be regulated by cholesterol level (Chen et al., 2008). This could explain the association of these proteins with less cholesterol-dense regions of the membrane outside of lipid rafts while also confirming the feasibility of chosen fractionation approach.

5.4. Comparison of selected proteins between SHR and SHR-Tg19

We used regular Western blotting to compare expression of selected proteins of myocardial β-adrenergic pathway in TX-100 soluble and insoluble fractions from the LV tissue of SHR and SHR-Tg19. The β-adrenergic receptor 1 and 2 expression was on the same level in both strains. This is consistent with the results from our previous experiments where we observed the difference between the expressions of β-AR in SHR and SHR-Tg19 using radioligand binding experiments but not by Western blotting (Klevstig et al., 2013). In the present work the β1-AR signal was detected only in the DSM fraction, while the β2-AR signal only in the DRM (Fig. 18). According to mammalian lipid raft database RaftProt there is no evidence that β1-AR are localized to lipid rafts (Shah et al., 2015). However, their distribution in the membrane is confined due to association with scaffolding proteins (Valentine and Haggie, 2011). On the other hand, β2-AR are proposed to localize in lipid rafts and leave them upon activation to be

internalized via lipid raft-independent mechanism (Allen et al., 2005). Another study highlighted differences in results provided by individual lipid raft fractionation methods. It showed that β2-AR were observable in the raft fraction prepared using the methods by Song et al. (1996a) or Macdonald et al. (2005) but not using 1% or 0.1% TX-100 sucrose gradient (Pontier et al., 2008). This was done in cultured neuronal cells (C6 line) but when cardiomyocytes was subjected to similar procedure β2-AR was co-isolated in the same fraction as Cav-3 (Rybin et al., 2003).

We employed immunofluorescence imaging to determine the extent of co-localization of Cav-3 and β2-AR (Fig. 24, lower panel). Interestingly, there was almost no visible overlap between Cav-3 and β2-AR as seen in the merged image. This result is consistent with the observed difference in the distribution of Cav-3 and β2-AR between the fractionated membranes separated using TX-100. However, the observed lack of co-localization conflicts with the consensus which shown β2-AR association with Cav-3 caveolae in cardiomyocytes (Ostrom and Insel, 2004). A possible explanation for this discrepancy could be that antibodies to extracellular epitopes of β2-AR that we used could not bind to those receptors inside the caveolae. This could also be an artefact of formaldehyde fixation.

The study by Pontier et al. (2008) showed that β-adrenergic signaling proteins like Gα and AC localize to lipid rafts in a cholesterol-dependent manner. This corroborates our results of the distribution of $G\alpha_i$ protein that was predominantly observed in the DRM fraction in both strains. On the other hand, we observed most of the Gβ subunit expression in the DSM fraction. This result is supported by the study of different G protein subunits association with Cav-1 which found that among them Gβ was the most weakly associated with caveolar microdomains (Oh and Schnitzer, 2001). Gβγ complex have multiple inhibitory effects on GPCR signaling. Its binding with Gα subunit prohibits activation of the latter by increasing the affinity to GDP (Brandt and Ross, 1985). After GPCR activation the Gβγ complex dissociates and conveys its signaling effects which include AC isoforms V and IV inhibition and activation of GRK2 (Pitcher et al., 1992; Tang and Gilman, 1991). The phosphorylation by the latter kinase leads to β-AR deactivation. Therefore, the decrease in raft-associated Gβ could be in line with our previous observations of increased AC activity and PKA phosphorylation in SHR-Tg19 (Klevstig et al., 2013).

Additionally, we performed a radioligand assay to determine a total number of α-AR in both LV and RV but found no differences between SHR and transgenic rats. Changes in α-AR occur in the failing hearts (Jensen et al., 2014), however due to much smaller number of these receptors compared to β-AR they may not be as profound at the age of animals in our study.

Connexin 43 is the most abundant gap junctional protein in the ventricular myocytes. We observed a significant increase in its expression in both PNS and PM samples from the LV of SHR-Tg19. This result was expected as previous studies have shown that this strain have a higher susceptibility to arrhythmias which as we hypothesized might arise from increased conductivity (Neckář et al., 2012). There is evidence that both cAMP effectors PKA and epac1 positively influence gap junction function. Protein epac1 upregulates the accumulation of Cx43 in the plasma membrane and PKA has a significant effect on gap junctional gating function (Somekawa et al., 2005). Therefore Cx43 upregulation could be a consequence of elevated AC activity that was observed in SHR-Tg19 (Klevstig et al., 2013). Although we suspect elevated activity of epac1 in the heart of SHR-Tg19, the expression of this protein measured using Western blotting did not differ from SHR.

However, we struggle to find explanation to a significant decrease in Cx43 expression in TX-100 fractionated samples other than it was an artefact of the preparation since it contradicts the result observed in the PM samples. In order to elucidate these results, we used immunostaining to inspect co-localization of Cav-3 and Cx43 in both strains but found no visible or quantifiable differences between them (Fig. 24, upper panel). As expected, Cx43 expression is seen in the intercalated disc area but similarly shaped Cx43 expression areas were also observed on the lateral sides of the cells.

Another PKA phosphorylation target is small GTPase RhoA. We detected a small but significant increase in expression of its phosphorylated form (Fig. 25). As described in chapter 1.4, RhoA signaling is prohypertrophic and modulated by phosphorylation on Ser188 which induces its translocation to cytosol and protects RhoA from degradation. Finally, we found that the expression of ERK1 was significantly higher in the LV of SHR-Tg19. ERK1 is a third kinase in canonical MAPK cascade (Raf → MEK1/2 → ERK1/2); when activated it phosphorylates many transcription factors thus having a diverse cellular and physiological repertoire, including proliferative and anti-apoptotic

effects. Studies in transgenic mice models show that expression of constitutively active MEK1 isoform enhances I/R injury protection while leading to increases in heart wall thickness and ERK1 expression (Lips et al., 2004). Additionally, activation of epac1 by cAMP was shown to lead to Rap1 and MEK1 mediated regulation of ERK (Enserink et al., 2002). Proliferative effect of cAMP signaling through RhoA and epac1 effects could therefore explain a small but significant increase in heart to body weight ratio observed in SHR-Tg19 in previous studies (Klevstig et al., 2013).

6. CONCLUSIONS

In previous studies we provided the evidence that restoration of Cd36 expression in SHR leads to enhancing of β-adrenergic signaling which includes an increase in total receptor number in the plasma membrane as well as in expression of AC5 isoform and total AC activity. Expression and phosphorylation of this signaling pathway effector PKA was also increased (Klevstig et al., 2013). The present work corroborated this data with new results. In the transgenic strain we observed an increase in connexin 43 expression and RhoA phosphorylation both of which are dependent on PKA activity (Atkinson et al., 1995; Rolli-Derkinderen et al., 2005). Previous results also showed increased arrhythmogenicity in SHR-Tg19 which may be linked to the increase in connexin 43 expression identified in this study. Additionally, in previous work we observed a slight but significant increase in heart mass in SHR-Tg19. While this could be related to more efficient energy utilization, our current work also examined the possible underlying molecular mechanisms and showed cAMP-mediated amplification of RhoA and ERK1.

We also utilized both bottom-up and top-down proteomic strategies in order to investigate the myocardial proteomes of SHR and SHR-Tg19 rats. Both approaches indicated that transgenic expression of CD36 affected protein levels more strongly in right than left ventricles. Except two proteins, all of the observed changes were downregulations. Many of the identified changes relate to energy metabolism proteins. The observed results could be linked to a shift in energy metabolism and alterations in apoptotic signaling which could lead to improvement of energy utilization particularly in the right ventricle. The observed downregulation of some pro-survival proteins may reflect lower lipotoxicity and oxidative stress in transgenic animals.

Respiration enzymes activity measurements corroborated our proteomic analysis and revealed downregulation of mitochondrial malate dehydrogenase activity in both left and right heart ventricles of SHR-Tg19. Together with lower cytosolic hexokinase activity in the left ventricles this result suggests a role of functional Cd36 expression in metabolic substrate preference. This is supported by the observed downregulation of peroxisomal membrane protein 70, which facilitates β-oxidation in peroxisomes. We also observed changes in the expression of some OXPHOS complexes subunits that are suspected in ROS production.

In conclusion, our results support the assumption that Cd36 functioning underlies cardiac metabolic substrate flexibility and suggest a contribution of this translocase to cardiac substrate selection and regulation of ROS production by mitochondria. The present findings regarding changes induced by of Cd36 restoration in SHR could help elucidate the effects of this protein in cardiomyocyte signaling.

7. REFERENCES

Abumrad, N.A., el-Maghrabi, M.R., Amri, E.Z., Lopez, E., Grimaldi, P.A., 1993. Cloning of a rat adipocyte membrane protein implicated in binding or transport of long-chain fatty acids that is induced during preadipocyte differentiation. Homology with human CD36. J. Biol. Chem. 268, 17665–17668.

Agarwal, S., Caldwell, K., Owens, A., Singer, C., Nikolaev, V., Lohse, M., Harvey, R., 2012. Membrane microdomains and cAMP compartmentation. FASEB J. 26, 666.6-666.6.

Aitman, T.J., Glazier, A.M., Wallace, C.A., Cooper, L.D., Norsworthy, P.J., Wahid, F.N., Al-Majali, K.M., Trembling, P.M., Mann, C.J., Shoulders, C.C., Graf, D., St. Lezin, E., Kurtz, T.W., Kren, V., Pravenec, M., Ibrahimi, A., Abumrad, N.A., Stanton, L.W., Scott, J., 1999. Identification of Cd36 (Fat) as an insulin-resistance gene causing defective fatty acid and glucose metabolism in hypertensive rats. Nat. Genet. 21, 76–83.

Aitman, T.J., Gotoda, T., Evans, A.L., Imrie, H., Heath, K.E., Trembling, P.M., Truman, H., Wallace, C.A., Rahman, A., Dore, C., Flint, J., Kren, V., Zidek, V., Kurtz, T.W., Pravenec, M., Scott, J., 1997. Quantitative trait loci for cellular defects in glucose and fatty acid metabolism in hypertensive rats. Nat. Genet. 16, 197–201.

Allard, M.F., Schönekess, B.O., Henning, S.L., English, D.R., Lopaschuk, G.D., 1994. Contribution of oxidative metabolism and glycolysis to ATP production in hypertrophied hearts. Am. J. Physiol. 267, H742-750.

Allard, M.F., Wambolt, R.B., Longnus, S.L., Grist, M., Lydell, C.P., Parsons, H.L., Rodrigues, B., Hall, J.L., Stanley, W.C., Bondy, G.P., 2000. Hypertrophied rat hearts are less responsive to the metabolic and functional effects of insulin. Am. J. Physiol. Endocrinol. Metab. 279, E487-493.

Allen, J.A., Yu, J.Z., Donati, R.J., Rasenick, M.M., 2005. Beta-adrenergic receptor stimulation promotes G alpha s internalization through lipid rafts: a study in living cells. Mol. Pharmacol. 67, 1493–1504.

Alvarez, M.C., Caldiz, C., Fantinelli, J.C., Garciarena, C.D., Console, G.M., Chiappe de Cingolani, G.E., Mosca, S.M., 2008. Is cardiac hypertrophy in spontaneously

hypertensive rats the cause or the consequence of oxidative stress? Hypertens. Res. Off. J. Jpn. Soc. Hypertens. 31, 1465–1476.

Anderson, M.E., Brown, J.H., Bers, D.M., 2011. CaMKII in myocardial hypertrophy and heart failure. J. Mol. Cell. Cardiol. 51, 468–473.

Anidi, I.U., Servinsky, L.E., Rentsendorj, O., Stephens, R.S., Scott, A.L., Pearse, D.B., 2013. CD36 and Fyn Kinase Mediate Malaria-Induced Lung Endothelial Barrier Dysfunction in Mice Infected with Plasmodium berghei. PLoS ONE 8.

Asch, A.S., Barnwell, J., Silverstein, R.L., Nachman, R.L., 1987. Isolation of the thrombospondin membrane receptor. J. Clin. Invest. 79, 1054–1061.

Asch, A.S., Liu, I., Briccetti, F.M., Barnwell, J.W., Kwakye-Berko, F., Dokun, A., Goldberger, J., Pernambuco, M., 1993. Analysis of CD36 binding domains: ligand specificity controlled by dephosphorylation of an ectodomain. Science 262, 1436–1440.

Atkinson, M.M., Lampe, P.D., Lin, H.H., Kollander, R., Li, X.R., Kiang, D.T., 1995. Cyclic AMP modifies the cellular distribution of connexin43 and induces a persistent increase in the junctional permeability of mouse mammary tumor cells. J. Cell Sci. 108 (Pt 9), 3079–3090.

Atlante, A., Seccia, T.M., De Bari, L., Marra, E., Passarella, S., 2006. Mitochondria from the left heart ventricles of both normotensive and spontaneously hypertensive rats oxidize externally added {NADH} mostly via a novel malate/oxaloacetate shuttle as reconstructed in vitro. Int. J. Mol. Med. 18, 177–186.

Augustus, A.S., Kako, Y., Yagyu, H., Goldberg, I.J., 2003. Routes of FA delivery to cardiac muscle: modulation of lipoprotein lipolysis alters uptake of TG-derived FA. Am. J. Physiol. Endocrinol. Metab. 284, E331-339.

Bai, D., Yue, B., Aoyama, H., 2018. Crucial motifs and residues in the extracellular loops influence the formation and specificity of connexin docking. Biochim. Biophys. Acta Biomembr. 1860, 9–21.

Baillie, A.G., Coburn, C.T., Abumrad, N.A., 1996. Reversible binding of long-chain fatty acids to purified FAT, the adipose CD36 homolog. J. Membr. Biol. 153, 75–81.

Barger, P.M., Kelly, D.P., 1999. Fatty acid utilization in the hypertrophied and failing heart: molecular regulatory mechanisms. Am. J. Med. Sci. 318, 36–42.

Barth, E., Stämmler, G., Speiser, B., Schaper, J., 1992. Ultrastructural quantitation of mitochondria and myofilaments in cardiac muscle from 10 different animal species including man. J. Mol. Cell. Cardiol. 24, 669–681.

Bélichard, P., Pruneau, D., Rochette, L., 1988. Influence of spontaneous hypertension and cardiac hypertrophy on the severity of ischemic arrhythmias in the rat. Basic Res. Cardiol. 83, 560–566.

Birnbaumer, L., 2007. Expansion of signal transduction by G proteins The second 15 years or so: From 3 to 16 α subunits plus βγ dimers. Biochim. Biophys. Acta 1768, 772–793.

Bonen, A., Han, X.-X., Tandon, N.N., Glatz, J.F.C., Lally, J., Snook, L.A., Luiken, J.J.F.P., 2009. FAT/CD36 expression is not ablated in spontaneously hypertensive rats. J. Lipid Res. 50, 740–748.

Borra, M.T., Smith, B.C., Denu, J.M., 2005. Mechanism of human SIRT1 activation by resveratrol. J. Biol. Chem. 280, 17187–17195.

Bos, J.L., 2006. Epac proteins: multi-purpose cAMP targets. Trends Biochem. Sci. 31, 680–686.

Boularan, C., Gales, C., 2015. Cardiac cAMP: production, hydrolysis, modulation and detection. Front. Pharmacol. 6.

Bragoszewski, P., Turek, M., Chacinska, A., 2017. Control of mitochondrial biogenesis and function by the ubiquitin-proteasome system. Open Biol. 7.

Brandt, D.R., Ross, E.M., 1985. GTPase activity of the stimulatory GTP-binding regulatory protein of adenylate cyclase, Gs. Accumulation and turnover of enzyme-nucleotide intermediates. J. Biol. Chem. 260, 266–272.

Brooksby, P., Levi, A.J., Jones, J.V., 1993. Investigation of the mechanisms underlying the increased contraction of hypertrophied ventricular myocytes isolated from the spontaneously hypertensive rat. Cardiovasc. Res. 27, 1268–1277.

Brown, D.A., Rose, J.K., 1992. Sorting of GPI-anchored proteins to glycolipid-enriched membrane subdomains during transport to the apical cell surface. Cell 68, 533–544.

Cadete, V.J.J., Lin, H., Sawicka, J., Wozniak, M., Sawicki, G., 2012. Proteomic analysis of right and left cardiac ventricles under aerobic conditions and after ischemia/reperfusion. Proteomics 12, 2366–2377.

Calvo, S.E., Compton, A.G., Hershman, S.G., Lim, S.C., Lieber, D.S., Tucker, E.J., Laskowski, A., Garone, C., Liu, S., Jaffe, D.B., Christodoulou, J., Fletcher, J.M., Bruno, D.L., Goldblatt, J., Dimauro, S., Thorburn, D.R., Mootha, V.K., 2012. Molecular diagnosis of infantile mitochondrial disease with targeted next-generation sequencing. Sci. Transl. Med. 4, 118ra10.

Campbell, S.E., Tandon, N.N., Woldegiorgis, G., Luiken, J.J.F.P., Glatz, J.F.C., Bonen, A., 2004. A novel function for fatty acid translocase (FAT)/CD36: involvement in long chain fatty acid transfer into the mitochondria. J. Biol. Chem. 279, 36235–36241.

Cao, W., Liu, N., Tang, S., Bao, L., Shen, L., Yuan, H., Zhao, X., Lu, H., 2008. Acetyl-Coenzyme A acyltransferase 2 attenuates the apoptotic effects of BNIP3 in two human cell lines. Biochim. Biophys. Acta 1780, 873–880.

Capetanaki, Y., Bloch, R.J., Kouloumenta, A., Mavroidis, M., Psarras, S., 2007. Muscle intermediate filaments and their links to membranes and membranous organelles. Exp. Cell Res. 313, 2063–2076.

Carozzi, A.J., Ikonen, E., Lindsay, M.R., Parton, R.G., 2000. Role of cholesterol in developing T-tubules: analogous mechanisms for T-tubule and caveolae biogenesis. Traffic Cph. Den. 1, 326–341.

Cartee, G.D., Wojtaszewski, J.F.P., 2007. Role of Akt substrate of 160 kDa in insulin-stimulated and contraction-stimulated glucose transport. Appl. Physiol. Nutr. Metab. Physiol. Appl. Nutr. Metab. 32, 557–566.

Cascianelli, G., Villani, M., Tosti, M., Marini, F., Bartoccini, E., Viola Magni, M., Albi, E., 2008. Lipid Microdomains in Cell Nucleus. Mol. Biol. Cell 19, 5289–5295.

Castro, B.M., Torreno-Piña, J.A., van Zanten, T.S., Gracia-Parajo, M.F., 2013. Biochemical and imaging methods to study receptor membrane organization and association with lipid rafts. Methods Cell Biol. 117, 105–122.

Catalanotti, F., Reyes, G., Jesenberger, V., Galabova-Kovacs, G., Simoes, R. de M., Carugo, O., Baccarini, M., 2009. A Mek1–Mek2 heterodimer determines the strength and duration of the Erk signal. Nat. Struct. Mol. Biol. 16, 294–303.

Cau, Y., Valensin, D., Mori, M., Draghi, S., Botta, M., 2018. Structure, Function, Involvement in Diseases and Targeting of 14-3-3 Proteins: An Update. Curr. Med. Chem. 25, 5–21.

Chabowski, A., Coort, S.L.M., Calles-Escandon, J., Tandon, N.N., Glatz, J.F.C., Luiken, J.J.F.P., Bonen, A., 2005. The subcellular compartmentation of fatty acid transporters is regulated differently by insulin and by AICAR. FEBS Lett. 579, 2428–2432.

Chan, W.-L., Chang, J.-G., 2014. Pseudogene-derived endogenous siRNAs and their function. Methods Mol. Biol. Clifton NJ 1167, 227–239.

Chen, C.H., Sun, L., Mochly-Rosen, D., 2010. Mitochondrial aldehyde dehydrogenase and cardiac diseases. Cardiovasc. Res. 88, 51–57.

Chen, H., Yang, J., Low, P.S., Cheng, J.-X., 2008. Cholesterol Level Regulates Endosome Motility via Rab Proteins. Biophys. J. 94, 1508–1520.

Chen, S., Synowsky, S., Tinti, M., MacKintosh, C., 2011. The capture of phosphoproteins by 14-3-3 proteins mediates actions of insulin. Trends Endocrinol. Metab. 22, 429–436.

Chen, Y., Chang, Y., Zhang, N., Guo, X., Sun, G., Sun, Y., 2018. Atorvastatin Attenuates Myocardial Hypertrophy in Spontaneously Hypertensive Rats via the C/EBPβ/PGC-1α/UCP3 Pathway. Cell. Physiol. Biochem. Int. J. Exp. Cell. Physiol. Biochem. Pharmacol. 46, 1009–1018.

Choisy, S.C.M., Arberry, L.A., Hancox, J.C., James, A.F., 2007. Increased susceptibility to atrial tachyarrhythmia in spontaneously hypertensive rat hearts. Hypertens. Dallas Tex 1979 49, 498–505.

Chouchani, E.T., Pell, V.R., Gaude, E., Aksentijević, D., Sundier, S.Y., Robb, E.L., Logan, A., Nadtochiy, S.M., Ord, E.N.J., Smith, A.C., Eyassu, F., Shirley, R., Hu, C.-H., Dare, A.J., James, A.M., Rogatti, S., Hartley, R.C., Eaton, S., Costa, A.S.H., Brookes, P.S., Davidson, S.M., Duchen, M.R., Saeb-Parsy, K., Shattock, M.J., Robinson, A.J., Work, L.M., Frezza, C., Krieg, T., Murphy, M.P., 2014. Ischaemic accumulation of succinate controls reperfusion injury through mitochondrial ROS. Nature 515, 431–435.

Christe, M.E., Rodgers, R.L., 1994. Altered Glucose and Fatty Acid Oxidation in Hearts of the Spontaneously Hypertensive Rat. J. Mol. Cell. Cardiol. 26, 1371–1375.

Clemetson, K.J., Pfueller, S.L., Luscher, E.F., Jenkins, C.S., 1977. Isolation of the membrane glycoproteins of human blood platelets by lectin affinity chromatography. Biochim. Biophys. Acta 464, 493–508.

Coburn, C.T., Knapp, F.F., Febbraio, M., Beets, A.L., Silverstein, R.L., Abumrad, N.A., 2000. Defective uptake and utilization of long chain fatty acids in muscle and adipose tissues of CD36 knockout mice. J. Biol. Chem. 275, 32523–32529.

Cohen, A.W., Park, D.S., Woodman, S.E., Williams, T.M., Chandra, M., Shirani, J., Pereira de Souza, A., Kitsis, R.N., Russell, R.G., Weiss, L.M., Tang, B., Jelicks, L.A., Factor, S.M., Shtutin, V., Tanowitz, H.B., Lisanti, M.P., 2003. Caveolin-1 null mice develop cardiac hypertrophy with hyperactivation of p42/44 MAP kinase in cardiac fibroblasts. Am. J. Physiol. Cell Physiol. 284, C457-474.

Colasante, C., Chen, J., Ahlemeyer, B., Baumgart-Vogt, E., 2015. Peroxisomes in cardiomyocytes and the peroxisome/peroxisome proliferator-activated receptor-loop. Thromb. Haemost. 113, 452–463.

Comunian, C., Rusconi, F., De Palma, A., Brunetti, P., Catalucci, D., Mauri, P.L., 2011. A comparative MudPIT analysis identifies different expression profiles in heart compartments. Proteomics 11, 2320–2328.

Conrad, C.H., Brooks, W.W., Hayes, J.A., Sen, S., Robinson, K.G., Bing, O.H., 1995. Myocardial fibrosis and stiffness with hypertrophy and heart failure in the spontaneously hypertensive rat. Circulation 91, 161–170.

Cooper, C.D., Lampe, P.D., 2002. Casein kinase 1 regulates connexin-43 gap junction assembly. J. Biol. Chem. 277, 44962–44968.

Coort, S.L.M., Luiken, J.J.F.P., van der Vusse, G.J., Bonen, A., Glatz, J.F.C., 2004. Increased FAT (fatty acid translocase)/CD36-mediated long-chain fatty acid uptake in cardiac myocytes from obese Zucker rats. Biochem. Soc. Trans. 32, 83–85.

Cox, J., Hein, M.Y., Luber, C.A., Paron, I., Nagaraj, N., Mann, M., 2014. Accurate Proteome-wide Label-free Quantification by Delayed Normalization and Maximal Peptide Ratio Extraction, Termed MaxLFQ. Mol. Cell. Proteomics MCP 13, 2513–2526.

Daftuar, L., Zhu, Y., Jacq, X., Prives, C., 2013. Ribosomal proteins RPL37, RPS15 and RPS20 regulate the Mdm2-p53-MdmX network. PloS One 8, e68667.

Deng, S., Zhou, H., Xiong, R., Lu, Y., Yan, D., Xing, T., Dong, L., Tang, E., Yang, H., 2007. Over-expression of genes and proteins of ubiquitin specific peptidases (USPs) and proteasome subunits (PSs) in breast cancer tissue observed by the methods of RFDD-PCR and proteomics. Breast Cancer Res. Treat. 104, 21–30.

Di Salvo, T.G., Mathier, M., Semigran, M.J., Dec, G.W., 1995. Preserved right ventricular ejection fraction predicts exercise capacity and survival in advanced heart failure. J. Am. Coll. Cardiol. 25, 1143–1153.

Doggrell, S.A., Brown, L., 1998. Rat models of hypertension, cardiac hypertrophy and failure. Cardiovasc. Res. 39, 89–105.

Dong, S., Kang, S., Gu, T.-L., Kardar, S., Fu, H., Lonial, S., Khoury, H.J., Khuri, F., Chen, J., 2007. 14–3-3 integrates prosurvival signals mediated by the AKT and MAPK pathways in ZNF198-FGFR1–transformed hematopoietic cells. Blood 110, 360–369.

Dror, R.O., Arlow, D.H., Maragakis, P., Mildorf, T.J., Pan, A.C., Xu, H., Borhani, D.W., Shaw, D.E., 2011. Activation mechanism of the β2-adrenergic receptor. Proc. Natl. Acad. Sci. 108, 18684–18689.

Drover, V.A., Abumrad, N.A., 2005. CD36-dependent fatty acid uptake regulates expression of peroxisome proliferator activated receptors. Biochem. Soc. Trans. 33, 311–315.

Ebata, H., Natsume, T., Mitsuhashi, T., Yaginuma, T., 1991. Reduced calcium sensitivity of dihydropyridine binding to calcium channels in spontaneously hypertensive rats. Hypertens. Dallas Tex 1979 17, 234–241.

Ehehalt, R., Sparla, R., Kulaksiz, H., Herrmann, T., Füllekrug, J., Stremmel, W., 2008. Uptake of long chain fatty acids is regulated by dynamic interaction of FAT/CD36 with cholesterol/sphingolipid enriched microdomains (lipid rafts). BMC Cell Biol. 9, 45.

Ehret, G.B., Ferreira, T., Chasman, D.I., Jackson, A.U., Schmidt, E.M., Johnson, T., Thorleifsson, G., Luan, J., Donnelly, L.A., Kanoni, S., Petersen, A.-K., Pihur, V., Strawbridge, R.J., Shungin, D., Hughes, M.F., Meirelles, O., Kaakinen, M., Bouatia-Naji, N., Kristiansson, K., Shah, S., Kleber, M.E., Guo, X., Lyytikäinen, L.-P., Fava, C., Eriksson, N., Nolte, I.M., Magnusson, P.K., Salfati, E.L., Rallidis, L.S., Theusch, E., Smith, A.J.P., Folkersen, L., Witkowska, K., Pers, T.H., Joehanes, R., Kim, S.K., Lataniotis, L., Jansen, R., Johnson, A.D., Warren, H., Kim, Y.J., Zhao, W., Wu, Y., Tayo, B.O., Bochud, M., CHARGE-EchoGen consortium, CHARGE-HF consortium, Wellcome Trust Case Control Consortium, Absher, D., Adair, L.S., Amin, N., Arking, D.E., Axelsson, T., Baldassarre, D., Balkau, B., Bandinelli, S., Barnes, M.R., Barroso, I., Bevan, S.,

Bis, J.C., Bjornsdottir, G., Boehnke, M., Boerwinkle, E., Bonnycastle, L.L., Boomsma, D.I., Bornstein, S.R., Brown, M.J., Burnier, M., Cabrera, C.P., Chambers, J.C., Chang, I.-S., Cheng, C.-Y., Chines, P.S., Chung, R.-H., Collins, F.S., Connell, J.M., Döring, A., Dallongeville, J., Danesh, J., de Faire, U., Delgado, G., Dominiczak, A.F., Doney, A.S.F., Drenos, F., Edkins, S., Eicher, J.D., Elosua, R., Enroth, S., Erdmann, J., Eriksson, P., Esko, T., Evangelou, E., Evans, A., Fall, T., Farrall, M., Felix, J.F., Ferrières, J., Ferrucci, L., Fornage, M., Forrester, T., Franceschini, N., Duran, O.H.F., Franco-Cereceda, A., Fraser, R.M., Ganesh, S.K., Gao, H., Gertow, K., Gianfagna, F., Gigante, B., Giulianini, F., Goel, A., Goodall, A.H., Goodarzi, M.O., Gorski, M., Gräßler, J., Groves, C., Gudnason, V., Gyllensten, U., Hallmans, G., Hartikainen, A.-L., Hassinen, M., Havulinna, A.S., Hayward, C., Hercberg, S., Herzig, K.-H., Hicks, A.A., Hingorani, A.D., Hirschhorn, J.N., Hofman, A., Holmen, J., Holmen, O.L., Hottenga, J.-J., Howard, P., Hsiung, C.A., Hunt, S.C., Ikram, M.A., Illig, T., Iribarren, C., Jensen, R.A., Kähönen, M., Kang, H., Kathiresan, S., Keating, B.J., Khaw, K.-T., Kim, Y.K., Kim, E., Kivimaki, M., Klopp, N., Kolovou, G., Komulainen, P., Kooner, J.S., Kosova, G., Krauss, R.M., Kuh, D., Kutalik, Z., Kuusisto, J., Kvaløy, K., Lakka, T.A., Lee, N.R., Lee, I.-T., Lee, W.-J., Levy, D., Li, X., Liang, K.-W., Lin, H., Lin, L., Lindström, J., Lobbens, S., Männistö, S., Müller, G., Müller-Nurasyid, M., Mach, F., Markus, H.S., Marouli, E., McCarthy, M.I., McKenzie, C.A., Meneton, P., Menni, C., Metspalu, A., Mijatovic, V., Moilanen, L., Montasser, M.E., Morris, A.D., Morrison, A.C., Mulas, A., Nagaraja, R., Narisu, N., Nikus, K., O'Donnell, C.J., O'Reilly, P.F., Ong, K.K., Paccaud, F., Palmer, C.D., Parsa, A., Pedersen, N.L., Penninx, B.W., Perola, M., Peters, A., Poulter, N., Pramstaller, P.P., Psaty, B.M., Quertermous, T., Rao, D.C., Rasheed, A., Rayner, N.W.N.W.R., Renström, F., Rettig, R., Rice, K.M., Roberts, R., Rose, L.M., Rossouw, J., Samani, N.J., Sanna, S., Saramies, J., Schunkert, H., Sebert, S., Sheu, W.H.-H., Shin, Y.-A., Sim, X., Smit, J.H., Smith, A.V., Sosa, M.X., Spector, T.D., Stančáková, A., Stanton, A., Stirrups, K.E., Stringham, H.M., Sundstrom, J., Swift, A.J., Syvänen, A.-C., Tai, E.-S., Tanaka, T., Tarasov, K.V., Teumer, A., Thorsteinsdottir, U., Tobin, M.D., Tremoli, E., Uitterlinden, A.G., Uusitupa, M., Vaez, A., Vaidya, D., van Duijn, C.M., van Iperen, E.P.A., Vasan, R.S., Verwoert, G.C., Virtamo, J., Vitart, V.,

Voight, B.F., Vollenweider, P., Wagner, A., Wain, L.V., Wareham, N.J., Watkins, H., Weder, A.B., Westra, H.-J., Wilks, R., Wilsgaard, T., Wilson, J.F., Wong, T.Y., Yang, T.-P., Yao, J., Yengo, L., Zhang, W., Zhao, J.H., Zhu, X., Bovet, P., Cooper, R.S., Mohlke, K.L., Saleheen, D., Lee, J.-Y., Elliott, P., Gierman, H.J., Willer, C.J., Franke, L., Hovingh, G.K., Taylor, K.D., Dedoussis, G., Sever, P., Wong, A., Lind, L., Assimes, T.L., Njølstad, I., Schwarz, P.E., Langenberg, C., Snieder, H., Caulfield, M.J., Melander, O., Laakso, M., Saltevo, J., Rauramaa, R., Tuomilehto, J., Ingelsson, E., Lehtimäki, T., Hveem, K., Palmas, W., März, W., Kumari, M., Salomaa, V., Chen, Y.-D.I., Rotter, J.I., Froguel, P., Jarvelin, M.-R., Lakatta, E.G., Kuulasmaa, K., Franks, P.W., Hamsten, A., Wichmann, H.-E., Palmer, C.N.A., Stefansson, K., Ridker, P.M., Loos, R.J.F., Chakravarti, A., Deloukas, P., Morris, A.P., Newton-Cheh, C., Munroe, P.B., 2016. The genetics of blood pressure regulation and its target organs from association studies in 342,415 individuals. Nat. Genet. 48, 1171–1184.

Emanuele, M.J., Elia, A.E.H., Xu, Q., Thoma, C.R., Izhar, L., Leng, Y., Guo, A., Chen, Y.-N., Rush, J., Hsu, P.W.-C., Yen, H.-C.S., Elledge, S.J., 2011. Global Identification of Modular Cullin-RING Ligase Substrates. Cell 147, 459–474.

Endemann, G., Stanton, L.W., Madden, K.S., Bryant, C.M., White, R.T., Protter, A.A., 1993. CD36 is a receptor for oxidized low density lipoprotein. J. Biol. Chem. 268, 11811–11816.

Enserink, J.M., Christensen, A.E., Rooij, J. de, Triest, M. van, Schwede, F., Genieser, H.G., Døskeland, S.O., Blank, J.L., Bos, J.L., 2002. A novel Epac-specific cAMP analogue demonstrates independent regulation of Rap1 and ERK. Nat. Cell Biol. 4, 901–906.

Esseltine, J.L., Laird, D.W., 2016. Next-Generation Connexin and Pannexin Cell Biology. Trends Cell Biol. 26, 944–955.

Eyre, N.S., Cleland, L.G., Tandon, N.N., Mayrhofer, G., 2007. Importance of the carboxyl terminus of FAT/CD36 for plasma membrane localization and function in long-chain fatty acid uptake. J. Lipid Res. 48, 528–542.

Failli, P., Ruocco, C., Fazzini, A., Giotti, A., 1997. Calcium waves in unstimulated left ventricular cardiomyocytes isolated from aged spontaneously hypertensive and normotensive rats. Biochem. Biophys. Res. Commun. 237, 103–106.

Febbraio, M., Abumrad, N.A., Hajjar, D.P., Sharma, K., Cheng, W., Pearce, S.F., Silverstein, R.L., 1999. A null mutation in murine CD36 reveals an important role in fatty acid and lipoprotein metabolism. J. Biol. Chem. 274, 19055–19062.

Frank, K., Kranias, E.G., 2000. Phospholamban and cardiac contractility. Ann. Med. 32, 572–578.

Franklin, W.A., Hogg, N., Mason, D.Y., 1987. Human leukocyte differentiation antigens: review of the Third International Workshop. Mol. Cell. Probes 1, 55–60.

Freis, E.D., Ragan, D., 1975. Effect of treatment on longevity in spontaneously hypertensive rats. Proc. Soc. Exp. Biol. Med. Soc. Exp. Biol. Med. N. Y. N 150, 422–424.

Frishman, W.H., 2016. Beta-Adrenergic Receptor Blockers in Hypertension: Alive and Well. Prog. Cardiovasc. Dis. 59, 247–252.

Fujita, T., Toya, Y., Iwatsubo, K., Onda, T., Kimura, K., Umemura, S., Ishikawa, Y., 2001. Accumulation of molecules involved in alpha1-adrenergic signal within caveolae: caveolin expression and the development of cardiac hypertrophy. Cardiovasc. Res. 51, 709–716.

Fukuchi, K., Nozaki, S., Yoshizumi, T., Hasegawa, S., Uehara, T., Nakagawa, T., Kobayashi, T., Tomiyama, Y., Yamashita, S., Matsuzawa, Y., Nishimura, T., 1999. Enhanced myocardial glucose use in patients with a deficiency in long-chain fatty acid transport (CD36 deficiency). J. Nucl. Med. Off. Publ. Soc. Nucl. Med. 40, 239–243.

Fukui, S., Fukumoto, Y., Suzuki, J., Saji, K., Nawata, J., Tawara, S., Shinozaki, T., Kagaya, Y., Shimokawa, H., 2008. Long-term inhibition of Rho-kinase ameliorates diastolic heart failure in hypertensive rats. J. Cardiovasc. Pharmacol. 51, 317–326.

Galbiati, F., Engelman, J.A., Volonte, D., Zhang, X.L., Minetti, C., Li, M., Hou, H., Kneitz, B., Edelmann, W., Lisanti, M.P., 2001. Caveolin-3 null mice show a loss of caveolae, changes in the microdomain distribution of the dystrophin-glycoprotein complex, and t-tubule abnormalities. J. Biol. Chem. 276, 21425–21433.

Galletti, F., Rutledge, A., Krogh, V., Triggle, D.J., 1991. Age related changes in Ca2+ channels in spontaneously hypertensive rats. Gen. Pharmacol. Vasc. Syst. 22, 173–176.

García-Rúa, V., Otero, M.F., Lear, P.V., Rodríguez-Penas, D., Feijóo-Bandín, S., Noguera-Moreno, T., Calaza, M., Álvarez-Barredo, M., Mosquera-Leal, A., Parrington, J., Brugada, J., Portolés, M., Rivera, M., González-Juanatey, J.R., Lago, F., 2012. Increased Expression of Fatty-Acid and Calcium Metabolism Genes in Failing Human Heart. PLOS ONE 7, e37505.

Gervásio, O.L., Phillips, W.D., Cole, L., Allen, D.G., 2011. Caveolae respond to cell stretch and contribute to stretch-induced signaling. J Cell Sci 124, 3581–3590.

Giannocco, G., Oliveira, K.C., Crajoinas, R.O., Venturini, G., Salles, T.A., Fonseca-Alaniz, M.H., MacIel, R.M.B., Girardi, A.C.C., 2013. Dipeptidyl peptidase IV inhibition upregulates GLUT4 translocation and expression in heart and skeletal muscle of spontaneously hypertensive rats. Eur. J. Pharmacol. 698, 74–86.

Gimeno, R.E., Ortegon, A.M., Patel, S., Punreddy, S., Ge, P., Sun, Y., Lodish, H.F., Stahl, A., 2003. Characterization of a heart-specific fatty acid transport protein. J. Biol. Chem. 278, 16039–16044.

Gise, A. von, Lorenz, P., Wellbrock, C., Hemmings, B., Berberich-Siebelt, F., Rapp, U.R., Troppmair, J., 2001. Apoptosis Suppression by Raf-1 and MEK1 Requires MEK- and Phosphatidylinositol 3-Kinase-Dependent Signals. Mol. Cell. Biol. 21, 2324–2336.

Githaka, J.M., Vega, A.R., Baird, M.A., Davidson, M.W., Jaqaman, K., Touret, N., 2016. Ligand-induced growth and compaction of CD36 nanoclusters enriched in Fyn induces Fyn signaling. J. Cell Sci. 129, 4175–4189.

Glatz, J.F.C., Luiken, J., 2017. From fat to FAT (CD36/SR-B2): Understanding the regulation of cellular fatty acid uptake. Biochimie, “Pleiotropic physiological roles of PPARs and Fatty Acids” a tribute to Paul Grimaldi’ 136, 21–26.

Glatz, J.F.C., Schaap, F.G., Binas, B., Bonen, A., van der Vusse, G.J., Luiken, J.J.F.P., 2003. Cytoplasmic fatty acid-binding protein facilitates fatty acid utilization by skeletal muscle. Acta Physiol. Scand. 178, 367–371.

Gnaiger, E., Kuznetsov, a V, Schneeberger, S., Seiler, R., Brandacher, G., Steurer, W., Margreiter, R., 2000. Mitochondria in the cold. In: Life in the Cold. Springer, Berlin, Heidelberg, pp. 431–442.

González, A., López, B., Ravassa, S., Querejeta, R., Larman, M., Díez, J., Fortuño, M.A., 2002. Stimulation of cardiac apoptosis in essential hypertension potential role of angiotensin II. Hypertension 39, 75–80.

Gotoda, T., Iizuka, Y., Kato, N., Osuga, J.I., Bihoreau, M.T., Murakami, T., Yamori, Y., Shimano, H., Ishibashi, S., Yamada, N., 1999. Absence of Cd36 mutation in the original spontaneously hypertensive rats with insulin resistance. Nat. Genet. 22, 226–228.

Grandoch, M., Roscioni, S.S., Schmidt, M., 2010. The role of Epac proteins, novel cAMP mediators, in the regulation of immune, lung and neuronal function. Br. J. Pharmacol. 159, 265–284.

Grisanti, L.A., Schumacher, S.M., Tilley, D.G., Koch, W.J., 2018. Designer Approaches for G Protein–Coupled Receptor Modulation for Cardiovascular Disease. JACC Basic Transl. Sci. 3, 550–562.

Grundmanová, M., Jarkovská, D., Süß, A., Tůma, Z., Marková, M., Grundman, Z., El-Kadi, A., Čedíková, M., Štengl, M., Kuncová, J., 2016. Propofol-induced mitochondrial and contractile dysfunction of the rat ventricular myocardium. Physiol. Res. 65, S601–S609.

Guthmann, F., Maehl, P., Preiss, J., Kolleck, I., Rüstow, B., 2002. Ectoprotein kinase-mediated phosphorylation of FAT/CD36 regulates palmitate uptake by human platelets. Cell. Mol. Life Sci. CMLS 59, 1999–2003.

Guzy, R.D., Sharma, B., Bell, E., Chandel, N.S., Schumacker, P.T., 2008. Loss of the SdhB, but Not the SdhA, Subunit of Complex II Triggers Reactive Oxygen Species-Dependent Hypoxia-Inducible Factor Activation and Tumorigenesis. Mol. Cell. Biol. 28, 718–731.

Gygi, S.P., Corthals, G.L., Zhang, Y., Rochon, Y., Aebersold, R., 2000. Evaluation of two-dimensional gel electrophoresis-based proteome analysis technology. Proc. Natl. Acad. Sci. U. S. A. 97, 9390–9395.

Hajri, T., Han, X.X., Bonen, A., Abumrad, N.A., 2002. Defective fatty acid uptake modulates insulin responsiveness and metabolic responses to diet in CD36-null mice. J. Clin. Invest. 109, 1381–1389.

Hajri, T., Ibrahimi, A., Coburn, C.T., Knapp, F.F., Kurtz, T., Pravenec, M., Abumrad, N.A., 2001. Defective Fatty Acid Uptake in the Spontaneously Hypertensive Rat

Is a Primary Determinant of Altered Glucose Metabolism, Hyperinsulinemia, and Myocardial Hypertrophy. J. Biol. Chem. 276, 23661–23666.

Hames, K.C., Vella, A., Kemp, B.J., Jensen, M.D., 2014. Free fatty acid uptake in humans with CD36 deficiency. Diabetes 63, 3606–3614.

Hanai, N., Nagata, K., Kawajiri, A., Shiromizu, T., Saitoh, N., Hasegawa, Y., Murakami, S., Inagaki, M., 2004. Biochemical and cell biological characterization of a mammalian septin, Sept11. FEBS Lett. 568, 83–88.

Hanse, E.A., Ruan, C., Kachman, M., Wang, D., Lowman, X.H., Kelekar, A., 2017. Cytosolic malate dehydrogenase activity helps support glycolysis in actively proliferating cells and cancer. Oncogene 36, 3915–3924.

Hardie, D.G., Ross, F.A., Hawley, S.A., 2012. AMPK - a nutrient and energy sensor that maintains energy homeostasis. Nat. Rev. Mol. Cell Biol. 13, 251–262.

Harmon, C.M., Luce, P., Beth, A.H., Abumrad, N.A., 1991. Labeling of adipocyte membranes by sulfo-N-succinimidyl derivatives of long-chain fatty acids: inhibition of fatty acid transport. J. Membr. Biol. 121, 261–268.

Head, B.P., Patel, H.H., Insel, P.A., 2014. Interaction of membrane/lipid rafts with the cytoskeleton: impact on signaling and function. Biochim. Biophys. Acta 1838.

Head, B.P., Patel, H.H., Roth, D.M., Lai, N.C., Niesman, I.R., Farquhar, M.G., Insel, P.A., 2005. G-protein-coupled receptor signaling components localize in both sarcolemmal and intracellular caveolin-3-associated microdomains in adult cardiac myocytes. J. Biol. Chem. 280, 31036–31044.

Head, B.P., Patel, H.H., Roth, D.M., Murray, F., Swaney, J.S., Niesman, I.R., Farquhar, M.G., Insel, P.A., 2006. Microtubules and actin microfilaments regulate lipid raft/caveolae localization of adenylyl cyclase signaling components. J. Biol. Chem. 281, 26391–26399.

Heinzel, F.R., Hohendanner, F., Jin, G., Sedej, S., Edelmann, F., 2015. Myocardial Hypertrophy and Its Role in Heart Failure with Preserved Ejection Fraction. J. Appl. Physiol. Bethesda Md 1985 119, 1233–1242.

Hirschey, M.D., Shimazu, T., Goetzman, E., Jing, E., Schwer, B., Lombard, D.B., Grueter, C.A., Harris, C., Biddinger, S., Ilkayeva, O.R., Stevens, R.D., Li, Y., Saha, A.K., Ruderman, N.B., Bain, J.R., Newgard, C.B., Farese, R.V., Alt, F.W., Kahn, C.R., Verdin, E., 2010. SIRT3 regulates mitochondrial fatty-acid oxidation by reversible enzyme deacetylation. Nature 464, 121–125.

Hoosdally, S.J., Andress, E.J., Wooding, C., Martin, C.A., Linton, K.J., 2009. The Human Scavenger Receptor CD36: glycosylation status and its role in trafficking and function. J. Biol. Chem. 284, 16277–16288.

Horton, J.L., Martin, O.J., Lai, L., Riley, N.M., Richards, A.L., Vega, R.B., Leone, T.C., Pagliarini, D.J., Muoio, D.M., Bedi, K.C., Margulies, K.B., Coon, J.J., Kelly, D.P., 2016. Mitochondrial protein hyperacetylation in the failing heart. JCI Insight 2.

Hsieh, F.-L., Turner, L., Bolla, J.R., Robinson, C.V., Lavstsen, T., Higgins, M.K., 2016. The structural basis for CD36 binding by the malaria parasite. Nat. Commun. 7, 12837.

Huang, M.M., Bolen, J.B., Barnwell, J.W., Shattil, S.J., Brugge, J.S., 1991. Membrane glycoprotein IV (CD36) is physically associated with the Fyn, Lyn, and Yes protein-tyrosine kinases in human platelets. Proc. Natl. Acad. Sci. U. S. A. 88, 7844–7848.

Huangfu, P., Pikhart, H., Peasey, A., 2014. Healthy diet indicator score and metabolic syndrome in the Czech Republic, Russia, and Poland: Cross-sectional findings from the HAPIEE study. J. Epidemiol. Community Health 68, A49–A50.

Iemitsu, M., Miyauchi, T., Maeda, S., Sakai, S., Fujii, N., Miyazaki, H., Kakinuma, Y., Matsuda, M., Yamaguchi, I., 2003. Cardiac hypertrophy by hypertension and exercise training exhibits different gene expression of enzymes in energy metabolism. Hypertens. Res. Off. J. Jpn. Soc. Hypertens. 26, 829–837.

Iemitsu, M., Shimojo, N., Maeda, S., Irukayama-Tomobe, Y., Sakai, S., Ohkubo, T., Tanaka, Y., Miyauchi, T., 2008. The benefit of medium-chain triglyceride therapy on the cardiac function of SHRs is associated with a reversal of metabolic and signaling alterations. Am. J. Physiol. Heart Circ. Physiol. 295, H136-144.

Ikonen, E., 2001. Roles of lipid rafts in membrane transport. Curr. Opin. Cell Biol. 13, 470–477.

Ikonen, E., Fiedler, K., Parton, R.G., Simons, K., 1995. Prohibitin, an antiproliferative protein, is localized to mitochondria. FEBS Lett. 358, 273–277.

Imanaka, T., Aihara, K., Takano, T., Yamashita, A., Sato, R., Suzuki, Y., Yokota, S., Osumi, T., 1999. Characterization of the 70-kDa peroxisomal membrane protein, an ATP binding cassette transporter. J. Biol. Chem. 274, 11968–11976.

Iritani, N., Fukuda, E., Nara, Y., Yamori, Y., 1977. Lipid metabolism in spontaneously hypertensive rats (SHR). Atherosclerosis 28, 217–222.

Isomaa, B., Almgren, P., Tuomi, T., Forsén, B., Lahti, K., Nissén, M., Taskinen, M.R., Groop, L., 2001. Cardiovascular morbidity and mortality associated with the metabolic syndrome. Diabetes Care 24, 683–689.

Jain, S.S., Chabowski, A., Snook, L.A., Schwenk, R.W., Glatz, J.F.C., Luiken, J.J.F.P., Bonen, A., 2009. Additive effects of insulin and muscle contraction on fatty acid transport and fatty acid transporters, FAT/CD36, FABPpm, FATP1, 4 and 6. FEBS Lett. 583, 2294–2300.

Jain, S.S., Luiken, J.J.F.P., Snook, L.A., Han, X.X., Holloway, G.P., Glatz, J.F.C., Bonen, A., 2015. Fatty acid transport and transporters in muscle are critically regulated by Akt2. FEBS Lett. 589, 2769–2775.

Jansen, J.A., van Veen, T.A.B., de Bakker, J.M.T., van Rijen, H.V.M., 2010. Cardiac connexins and impulse propagation. J. Mol. Cell. Cardiol. 48, 76–82.

Jay, A.G., Hamilton, J.A., 2016. The enigmatic membrane fatty acid transporter CD36: New insights into fatty acid binding and their effects on uptake of oxidized LDL. Prostaglandins Leukot. Essent. Fatty Acids.

Jensen, B.C., O'Connell, T.D., Simpson, P.C., 2014. Alpha-1-Adrenergic Receptors in Heart Failure: The Adaptive Arm of the Cardiac Response to Chronic Catecholamine Stimulation. J. Cardiovasc. Pharmacol. 63, 291–301.

Jochen, A., Hays, J., 1993. Purification of the major substrate for palmitoylation in rat adipocytes: N-terminal homology with CD36 and evidence for cell surface acylation. J. Lipid Res. 34, 1783–1792.

Juhan-Vague, I., Alessi, M.C., 1997. PAI-1, obesity, insulin resistance and risk of cardiovascular events. Thromb. Haemost. 78, 656–660.

Jüllig, M., Hickey, A.J.R., Chai, C.C., Skea, G.L., Middleditch, M.J., Costa, S., Choong, S.Y., Philips, A.R.J., Cooper, G.J.S., 2008. Is the failing heart out of fuel or a worn engine running rich? A study of mitochondria in old spontaneously hypertensive rats. PROTEOMICS 8, 2556–2572.

Kaakinen, M., Kaisto, T., Rahkila, P., Metsikkö, K., 2012. Caveolin 3, flotillin 1 and influenza virus hemagglutinin reside in distinct domains on the sarcolemma of skeletal myofibers. Biochem. Res. Int. 2012, 497572.

Kako, K., Takehara, A., Arai, H., Onodera, T., Takahashi, Y., Hanagata, H., Ogra, Y., Takagi, H., Kodama, H., Suzuki, K.T., Munekata, E., Fukamizu, A., 2004. A selective requirement for copper-dependent activation of cytochrome c oxidase by Cox17p. Biochem. Biophys. Res. Commun. 324, 1379–1385.

Kalinowska, A., Górski, J., Harasim, E., Harasiuk, D., Bonen, A., Chabowski, A., 2009. Differential effects of chronic, in vivo, PPAR's stimulation on the myocardial subcellular redistribution of FAT/CD36 and FABPpm. FEBS Lett. 583, 2527–2534.

Kawabe, J., Okumura, S., Nathanson, M.A., Hasebe, N., Ishikawa, Y., 2006. Caveolin regulates microtubule polymerization in the vascular smooth muscle cells. Biochem. Biophys. Res. Commun. 342, 164–169.

Keller, E., Bond, M., Moravec, C.S., 1997. Progression of left ventricular hypertrophy does not change the sarcoplasmic reticulum calcium store in the spontaneously hypertensive rat heart. J. Mol. Cell. Cardiol. 29, 461–469.

Khan, S., Kowluru, A., 2018. CD36 mediates lipid accumulation in pancreatic beta cells under the duress of glucolipotoxic conditions: Novel roles of lysine deacetylases. Biochem. Biophys. Res. Commun. 495, 2221–2226.

Kimelberg, H.K., 1975. Alterations in phospholipid-dependent (Na++K+)-ATPase activity due to lipid fluidity: Effects of cholesterol and Mg2+. Biochim. Biophys. Acta BBA - Biomembr. 413, 143–156.

King, K.L., Stanley, W.C., Rosca, M., Kerner, J., Hoppel, C.L., Febbraio, M., 2007. Fatty acid oxidation in cardiac and skeletal muscle mitochondria is unaffected by deletion of CD36. Arch. Biochem. Biophys. 467, 234–238.

King, N., Hittinger, C.T., Carroll, S.B., 2003. Evolution of key cell signaling and adhesion protein families predates animal origins. Science 301, 361–363.

Klevstig, M., Manakov, D., Kasparova, D., Brabcova, I., Papousek, F., Zurmanova, J., Zidek, V., Silhavy, J., Neckar, J., Pravenec, M., Kolar, F., Novakova, O., Novotny, J., 2013. Transgenic rescue of defective Cd36 enhances myocardial adenylyl cyclase signaling in spontaneously hypertensive rats. Pflugers Arch. 465, 1477–1486.

Koonen, D.P.Y., Febbraio, M., Bonnet, S., Nagendran, J., Young, M.E., Michelakis, E.D., Dyck, J.R.B., 2007. CD36 expression contributes to age-induced cardiomyopathy in mice. Circulation 116, 2139–2147.

Kuda, O., Pietka, T.A., Demianova, Z., Kudova, E., Cvacka, J., Kopecky, J., Abumrad, N.A., 2013. Sulfo-N-succinimidyl oleate (SSO) inhibits fatty acid uptake and signaling for intracellular calcium via binding CD36 lysine 164: SSO also inhibits oxidized low density lipoprotein uptake by macrophages. J. Biol. Chem. 288, 15547–15555.

Kuo, W.-W., Chu, C.-Y., Wu, C.-H., Lin, J.A., Liu, J.-Y., Ying, T.-H., Lee, S.-D., Hsieh, Y.-H., Chu, C.-H., Lin, D.-Y., Hsu, H.-H., Huang, C.-Y., 2005. The profile of cardiac cytochrome c oxidase (COX) expression in an accelerated cardiac-hypertrophy model. J. Biomed. Sci. 12, 601–610.

Kupper, N., Ge, D., Treiber, F.A., Snieder, H., 2006. Emergence of novel genetic effects on blood pressure and hemodynamics in adolescence: the Georgia Cardiovascular Twin Study. Hypertens. Dallas Tex 1979 47, 948–954.

Kusaka, Y., Tanaka, T., Okamoto, F., Terasaki, F., Matsunaga, Y., Miyazaki, H., Kawamura, K., 1995. Effect of sulfo-N-succinimidyl palmitate on the rat heart: myocardial long-chain fatty acid uptake and cardiac hypertrophy. J. Mol. Cell. Cardiol. 27, 1605–1612.

Lamichane, S., Dahal Lamichane, B., Kwon, S.-M., 2018. Pivotal Roles of Peroxisome Proliferator-Activated Receptors (PPARs) and Their Signal Cascade for Cellular and Whole-Body Energy Homeostasis. Int. J. Mol. Sci. 19.

Lang, P., Gesbert, F., Delespine-Carmagnat, M., Stancou, R., Pouchelet, M., Bertoglio, J., 1996. Protein kinase A phosphorylation of RhoA mediates the morphological and functional effects of cyclic AMP in cytotoxic lymphocytes. EMBO J. 15, 510–519.

Laugerette, F., Passilly-Degrace, P., Patris, B., Niot, I., Febbraio, M., Montmayeur, J.-P., Besnard, P., 2005. CD36 involvement in orosensory detection of dietary lipids, spontaneous fat preference, and digestive secretions. J. Clin. Invest. 115, 3177–3184.

Lauzier, B., Merlen, C., Vaillant, F., McDuff, J., Bouchard, B., Beguin, P.C., Dolinsky, V.W., Foisy, S., Villeneuve, L.R., Labarthe, F., Dyck, J.R.B., Allen, B.G., Charron, G., Des Rosiers, C., 2011. Post-translational modifications, a key process in CD36 function: Lessons from the spontaneously hypertensive rat heart. J. Mol. Cell. Cardiol. 51, 99–108.

Lecine, P., Italiano, J.E., Kim, S.W., Villeval, J.L., Shivdasani, R.A., 2000. Hematopoietic-specific beta 1 tubulin participates in a pathway of platelet biogenesis dependent on the transcription factor NF-E2. Blood 96, 1366–1373.

Lee, M.A., Böhm, M., Paul, M., Bader, M., Ganten, U., Ganten, D., 1996. Physiological characterization of the hypertensive transgenic rat TGR(mREN2)27. Am. J. Physiol. 270, E919-929.

Lee, S.M., Kim, J.H., Cho, E.J., Youn, H.D., 2009. A nucleocytoplasmic malate dehydrogenase regulates p53 transcriptional activity in response to metabolic stress. Cell Death Differ. 16, 738–748.

Leong, X.-F., Ng, C.-Y., Jaarin, K., 2015. Animal Models in Cardiovascular Research: Hypertension and Atherosclerosis. BioMed Res. Int. 2015, 528757.

Leri, A., Fiordaliso, F., Setoguchi, M., Limana, F., Bishopric, N.H., Kajstura, J., Webster, K., Anversa, P., 2000. Inhibition of p53 function prevents renin-angiotensin system activation and stretch-mediated myocyte apoptosis. Am. J. Pathol. 157, 843–857.

Li, Z., Bing, O.H., Long, X., Robinson, K.G., Lakatta, E.G., 1997. Increased cardiomyocyte apoptosis during the transition to heart failure in the spontaneously hypertensive rat. Am. J. Physiol. 272, H2313-2319.

Li, Z., Yue, Y., Hu, F., Zhang, C., Ma, X., Li, N., Qiu, L., Fu, M., Chen, L., Yao, Z., Bilan, P.J., Klip, A., Niu, W., 2018. Electrical pulse stimulation induces GLUT4 translocation in C2C12 myotubes that depends on Rab8A, Rab13, and Rab14. Am. J. Physiol. Endocrinol. Metab. 314, E478–E493.

Lin, D., Zhou, J., Zelenka, P.S., Takemoto, D.J., 2003. Protein kinase Cgamma regulation of gap junction activity through caveolin-1-containing lipid rafts. Invest. Ophthalmol. Vis. Sci. 44, 5259–5268.

Lingwood, D., Simons, K., 2010. Lipid rafts as a membrane-organizing principle. Science 327, 46–50.

Lips, D.J., Bueno, O.F., Wilkins, B.J., Purcell, N.H., Kaiser, R.A., Lorenz, J.N., Voisin, L., Saba-El-Leil, M.K., Meloche, S., Pouysségur, J., Pagès, G., De Windt, L.J., Doevendans, P.A., Molkentin, J.D., 2004. MEK1-ERK2 signaling pathway protects myocardium from ischemic injury in vivo. Circulation 109, 1938–1941.

Lisanti, M.P., Scherer, P.E., Tang, Z., Sargiacomo, M., 1994. Caveolae, caveolin and caveolin-rich membrane domains: a signalling hypothesis. Trends Cell Biol. 4, 231–235.

Liu, X.-J., Yang, C., Gupta, N., Zuo, J., Chang, Y.-S., Fang, F.-D., 2007. Protein kinase C-zeta regulation of GLUT4 translocation through actin remodeling in CHO cells. J. Mol. Med. Berl. Ger. 85, 851–861.

Lloyd, T., 1984. Food restriction increases life span of hypertensive animals. Life Sci. 34, 401–407.

Luiken, J.J., Schaap, F.G., van Nieuwenhoven, F.A., van der Vusse, G.J., Bonen, A., Glatz, J.F., 1999. Cellular fatty acid transport in heart and skeletal muscle as facilitated by proteins. Lipids 34 Suppl, S169-175.

Luiken, J.J., van Nieuwenhoven, F.A., America, G., van der Vusse, G.J., Glatz, J.F., 1997. Uptake and metabolism of palmitate by isolated cardiac myocytes from adult rats: involvement of sarcolemmal proteins. J. Lipid Res. 38, 745–758.

Luiken, J.J.F.P., Momken, I., Habets, D.D.J., El Hasnaoui, M., Coumans, W.A., Koonen, D.P.Y., Glatz, J.F.C., Bonen, A., 2006. Arsenite modulates cardiac substrate preference by translocation of GLUT4, but not CD36, independent of mitogen-activated protein kinase signaling. Endocrinology 147, 5205–5216.

Luiken, J.J.F.P., Ouwens, D.M., Habets, D.D.J., van der Zon, G.C.M., Coumans, W.A., Schwenk, R.W., Bonen, A., Glatz, J.F.C., 2009. Permissive action of protein kinase C-zeta in insulin-induced CD36- and GLUT4 translocation in cardiac myocytes. J. Endocrinol. 201, 199–209.

Lundby, A., Lage, K., Weinert, B.T., Bekker-Jensen, D.B., Secher, A., Skovgaard, T., Kelstrup, C.D., Dmytriyev, A., Choudhary, C., Lundby, C., Olsen, J.V., 2012. Proteomic analysis of lysine acetylation sites in rat tissues reveals organ specificity and subcellular patterns. Cell Rep. 2, 419–431.

Macdonald, J.L., Pike, L.J., 2005. A simplified method for the preparation of detergent-free lipid rafts. J. Lipid Res. 46, 1061–1067.

Macdonald, S.G., Crews, C.M., Wu, L., Driller, J., Clark, R., Erikson, R.L., McCormick, F., 1993. Reconstitution of the Raf-1-MEK-ERK signal transduction pathway in vitro. Mol. Cell. Biol. 13, 6615–6620.

Matasova, L.V., Popova, T.N., 2008. Aconitate hydratase of mammals under oxidative stress. Biochem. Biokhimiia 73, 957–964.

Matta, C., Zhang, X., Liddell, S., Smith, J.R., Mobasheri, A., 2015. Label-free proteomic analysis of the hydrophobic membrane protein complement in articular chondrocytes: a technique for identification of membrane biomarkers. Biomarkers 20, 572–589.

McCarron, D.A., Yung, N.N., Ugoretz, B.A., Krutzik, S., 1981. Disturbances of calcium metabolism in the spontaneously hypertensive rat. Hypertension 3, I162-7.

McDermott-Roe, C., Ye, J., Ahmed, R., Sun, X.-M., Serafín, A., Ware, J., Bottolo, L., Muckett, P., Cañas, X., Zhang, J., Rowe, G.C., Buchan, R., Lu, H., Braithwaite, A., Mancini, M., Hauton, D., Martí, R., García-Arumí, E., Hubner, N., Jacob, H., Serikawa, T., Zidek, V., Papousek, F., Kolar, F., Cardona, M., Ruiz-Meana, M., García-Dorado, D., Comella, J.X., Felkin, L.E., Barton, P.J.R., Arany, Z., Pravenec, M., Petretto, E., Sanchis, D., Cook, S.A., 2011. Endonuclease G is a novel determinant of cardiac hypertrophy and mitochondrial function. Nature 478, 114–118.

Means, T.K., Mylonakis, E., Tampakakis, E., Colvin, R.A., Seung, E., Puckett, L., Tai, M.F., Stewart, C.R., Pukkila-Worley, R., Hickman, S.E., Moore, K.J., Calderwood, S.B., Hacohen, N., Luster, A.D., El Khoury, J., 2009. Evolutionarily conserved recognition and innate immunity to fungal pathogens by the scavenger receptors SCARF1 and CD36. J. Exp. Med. 206, 637–653.

Miao, B., Skidan, I., Yang, J., Lugovskoy, A., Reibarkh, M., Long, K., Brazell, T., Durugkar, K.A., Maki, J., Ramana, C.V., Schaffhausen, B., Wagner, G., Torchilin, V., Yuan, J., Degterev, A., 2010. Small molecule inhibition of phosphatidylinositol-3,4,5-triphosphate (PIP3) binding to pleckstrin homology domains. Proc. Natl. Acad. Sci. U. S. A. 107, 20126–20131.

Miesel, A., Müller, H., Thermann, M., Heidbreder, M., Dominiak, P., Raasch, W., 2010. Overfeeding-induced obesity in spontaneously hypertensive rats: an animal model of the human metabolic syndrome. Ann. Nutr. Metab. 56, 127–142.

Mills, K.T., Bundy, J.D., Kelly, T.N., Reed, J.E., Kearney, P.M., Reynolds, K., Chen, J., He, J., 2016. Global disparities of hypertension prevalence and control. Circulation 134, 441–450.

Minetti, C., Bado, M., Broda, P., Sotgia, F., Bruno, C., Galbiati, F., Volonte, D., Lucania, G., Pavan, A., Bonilla, E., Lisanti, M.P., Cordone, G., 2002.

Impairment of caveolae formation and T-system disorganization in human muscular dystrophy with caveolin-3 deficiency. Am. J. Pathol. 160, 265–270.

Minetti, C., Beltrame, F., Marcenaro, G., Bonilla, E., 1992. Dystrophin at the plasma membrane of human muscle fibers shows a costameric localization. Neuromuscul. Disord. NMD 2, 99–109.

Mitchell, G.F., Pfeffer, J.M., Pfeffer, M.A., 1997. The Transition to Failure in the Spontaneously Hypertensive Rat. Am. J. Hypertens. 10, 120S-126S.

Monhart, V., 2013. Hypertension and chronic kidney diseases. Cor Vasa, Heart Failure 55, e397–e402.

Moore, K.J., El Khoury, J., Medeiros, L.A., Terada, K., Geula, C., Luster, A.D., Freeman, M.W., 2002. A CD36-initiated signaling cascade mediates inflammatory effects of beta-amyloid. J. Biol. Chem. 277, 47373–47379.

Mootha, V.K., Arai, A.E., Balaban, R.S., 1997. Maximum oxidative phosphorylation capacity of the mammalian heart. Am. J. Physiol. 272, H769-775.

Morrow, I.C., Parton, R.G., 2005. Flotillins and the PHB domain protein family: rafts, worms and anaesthetics. Traffic Cph. Den. 6, 725–740.

Müller, H., Deckers, K., Eckel, J., 2002. The fatty acid translocase (FAT)/CD36 and the glucose transporter GLUT4 are localized in different cellular compartments in rat cardiac muscle. Biochem. Biophys. Res. Commun. 293, 665–669.

Murray, J., Taylor, S.W., Zhang, B., Ghosh, S.S., Capaldi, R.A., 2003. Oxidative damage to mitochondrial complex I due to peroxynitrite: identification of reactive tyrosines by mass spectrometry. J. Biol. Chem. 278, 37223–37230.

Nakatani, K., Watabe, T., Masuda, D., Imaizumi, M., Shimosegawa, E., Kobayashi, T., Sairyo, M., Zhu, Y., Okada, T., Kawase, R., Nakaoka, H., Naito, A., Ohama, T., Koseki, M., Oka, T., Akazawa, H., Nishida, M., Komuro, I., Sakata, Y., Hatazawa, J., Yamashita, S., 2015. Myocardial energy provision is preserved by increased utilization of glucose and ketone bodies in CD36 knockout mice. Metabolism. 64, 1165–1174.

Narishige, T., Blade, K.L., Ishibashi, Y., Nagai, T., Hamawaki, M., Menick, D.R., Kuppuswamy, D., Cooper, G., 1999. Cardiac Hypertrophic and Developmental Regulation of the β-Tubulin Multigene Family. J. Biol. Chem. 274, 9692–9697.

Nassir, F., Wilson, B., Han, X., Gross, R.W., Abumrad, N.A., 2007. CD36 is important for fatty acid and cholesterol uptake by the proximal but not distal intestine. J. Biol. Chem. 282, 19493–19501.

Neckář, J., Šilhavy, J., Zídek, V., Landa, V., Mlejnek, P., Šimáková, M., Seidman, J.G., Seidman, C., Kazdová, L., Klevstig, M., Novák, F., Vecka, M., Papoušek, F., Houštěk, J., Drahota, Z., Kurtz, T.W., Kolář, F., Pravenec, M., 2012. CD36 overexpression predisposes to arrhythmias but reduces infarct size in spontaneously hypertensive rats: gene expression profile analysis. Physiol. Genomics 44, 173–182.

Nielsen, T.T., Støttrup, N.B., Løfgren, B., Bøtker, H.E., 2011. Metabolic fingerprint of ischaemic cardioprotection: Importance of the malateaspartate shuttle. Cardiovasc. Res. 91, 382–391.

Nikolaev, V.O., Moshkov, A., Lyon, A.R., Miragoli, M., Novak, P., Paur, H., Lohse, M.J., Korchev, Y.E., Harding, S.E., Gorelik, J., 2010. Beta2-adrenergic receptor redistribution in heart failure changes cAMP compartmentation. Science 327, 1653–1657.

Oh, P., Schnitzer, J.E., 2001. Segregation of Heterotrimeric G Proteins in Cell Surface Microdomains. Mol. Biol. Cell 12, 685–698.

Okamoto, K., Aoki, K., 1963. Development of a Strain of Spontaneously Hypertensive Rats. Jpn. Circ. J. 27, 282–293.

Okere, I.C., Young, M.E., McElfresh, T.A., Chess, D.J., Sharov, V.G., Sabbah, H.N., Hoit, B.D., Ernsberger, P., Chandler, M.P., Stanley, W.C., 2006. Low carbohydrate/high-fat diet attenuates cardiac hypertrophy, remodeling, and altered gene expression in hypertension. Hypertens. Dallas Tex 1979 48, 1116–1123.

Olsen, S., Uhler, M.D., 1991. Inhibition of Protein Kinase-A by Overexpression of the Cloned Human Protein Kinase Inhibitor. Mol. Endocrinol. 5, 1246–1256.

Oquendo, P., Hundt, E., Lawler, J., Seed, B., 1989. CD36 directly mediates cytoadherence of Plasmodium falciparum parasitized erythrocytes. Cell 58, 95–101.

Ostrom, R.S., Insel, P.A., 2004. The evolving role of lipid rafts and caveolae in G protein-coupled receptor signaling: implications for molecular pharmacology. Br. J. Pharmacol. 143, 235–245.

Palacios-Ortega, S., Varela-Guruceaga, M., Algarabel, M., Ignacio Milagro, F., Alfredo Martínez, J., de Miguel, C., 2015. Effect of TNF-Alpha on Caveolin-1 Expression and Insulin Signaling During Adipocyte Differentiation and in Mature Adipocytes. Cell. Physiol. Biochem. Int. J. Exp. Cell. Physiol. Biochem. Pharmacol. 36, 1499–1516.

Parton, R.G., Collins, B.M., 2016. Unraveling the architecture of caveolae. Proc. Natl. Acad. Sci. U. S. A. 113, 14170–14172.

Parton, R.G., Way, M., Zorzi, N., Stang, E., 1997. Caveolin-3 associates with developing T-tubules during muscle differentiation. J. Cell Biol. 136, 137–154.

Patel, H.H., Tsutsumi, Y.M., Head, B.P., Niesman, I.R., Jennings, M., Horikawa, Y., Huang, D., Moreno, A.L., Patel, P.M., Insel, P.A., Roth, D.M., 2007. Mechanisms of cardiac protection from ischemia/reperfusion injury: a role for caveolae and caveolin-1. FASEB J. 21, 1565–1574.

Paternostro, G., Clarke, K., Heath, J., Anne-Marie, L.S., Seymour, L., Radda, G.K., 1995. Decreased GLUT-4 mRNA content and insulin-sensitive deoxyglucose uptake show insulin resistance in the hypertensive rat heart. Cardiovasc. Res. 30, 205–211.

Paulson, A.F., Lampe, P.D., Meyer, R.A., TenBroek, E., Atkinson, M.M., Walseth, T.F., Johnson, R.G., 2000. Cyclic AMP and LDL trigger a rapid enhancement in gap junction assembly through a stimulation of connexin trafficking. J. Cell Sci. 113 (Pt 17), 3037–3049.

Peluso, J.J., Pappalardo, A., Fernandez, G., Wu, C.A., 2004. Involvement of an Unnamed Protein, RDA288, in the Mechanism through which Progesterone Mediates Its Antiapoptotic Action in Spontaneously Immortalized Granulosa Cells. Endocrinology 145, 3014–3022.

Pepino, M.Y., Kuda, O., Samovski, D., Abumrad, N.A., 2014. Structure-Function of CD36 and Importance of Fatty Acid Signal Transduction in Fat Metabolism. Annu. Rev. Nutr. 34, 281–303.

Petretto, E., Sarwar, R., Grieve, I., Lu, H., Kumaran, M.K., Muckett, P.J., Mangion, J., Schroen, B., Benson, M., Punjabi, P.P., Prasad, S.K., Pennell, D.J., Kiesewetter, C., Tasheva, E.S., Corpuz, L.M., Webb, M.D., Conrad, G.W., Kurtz, T.W., Kren, V., Fischer, J., Hubner, N., Pinto, Y.M., Pravenec, M., Aitman, T.J.,

Cook, S.A., 2008. Integrated genomic approaches implicate osteoglycin (Ogn) in the regulation of left ventricular mass. Nat. Genet. 40, 546–552.

Pitcher, J.A., Inglese, J., Higgins, J.B., Arriza, J.L., Casey, P.J., Kim, C., Benovic, J.L., Kwatra, M.M., Caron, M.G., Lefkowitz, R.J., 1992. Role of beta gamma subunits of G proteins in targeting the beta-adrenergic receptor kinase to membrane-bound receptors. Science 257, 1264–1267.

Plowman, S.J., Muncke, C., Parton, R.G., Hancock, J.F., 2005. H-ras, K-ras, and inner plasma membrane raft proteins operate in nanoclusters with differential dependence on the actin cytoskeleton. Proc. Natl. Acad. Sci. 102, 15500–15505.

Pohl, J., Ring, A., Korkmaz, U., Ehehalt, R., Stremmel, W., 2005. FAT/CD36-mediated long-chain fatty acid uptake in adipocytes requires plasma membrane rafts. Mol. Biol. Cell 16, 24–31.

Poliseno, L., Salmena, L., Zhang, J., Carver, B., Haveman, W.J., Pandolfi, P.P., 2010. A coding-independent function of gene and pseudogene mRNAs regulates tumour biology. Nature 465, 1033–1038.

Pontier, S.M., Percherancier, Y., Galandrin, S., Breit, A., Galés, C., Bouvier, M., 2008. Cholesterol-dependent Separation of the β2-Adrenergic Receptor from Its Partners Determines Signaling Efficacy INSIGHT INTO NANOSCALE ORGANIZATION OF SIGNAL TRANSDUCTION. J. Biol. Chem. 283, 24659–24672.

Poston, C.N., Duong, E., Cao, Y., Bazemore-Walker, C.R., 2011. Proteomic Analysis of Lipid Raft-enriched Membranes Isolated from Internal Organelles. Biochem. Biophys. Res. Commun. 415, 355–360.

Powell, S.R., Herrmann, J., Lerman, A., Patterson, C., Wang, X., 2012. The Ubiquitin–Proteasome System and Cardiovascular Disease. Prog. Mol. Biol. Transl. Sci. 109, 295–346.

PrabhuDas, M.R., Baldwin, C.L., Bollyky, P.L., Bowdish, D.M.E., Drickamer, K., Febbraio, M., Herz, J., Kobzik, L., Krieger, M., Loike, J., McVicker, B., Means, T.K., Moestrup, S.K., Post, S.R., Sawamura, T., Silverstein, S., Speth, R.C., Telfer, J.C., Thiele, G.M., Wang, X.-Y., Wright, S.D., El Khoury, J., 2017. A Consensus Definitive Classification of Scavenger Receptors and Their Roles in Health and Disease. J. Immunol. Baltim. Md 1950 198, 3775–3789.

Pravenec, M., Churchill, P.C., Churchill, M.C., Viklicky, O., Kazdova, L., Aitman, T.J., Petretto, E., Hubner, N., Wallace, C.A., Zimdahl, H., Zidek, V., Landa, V., Dunbar, J., Bidani, A., Griffin, K., Qi, N., Maxova, M., Kren, V., Mlejnek, P., Wang, J., Kurtz, T.W., 2008. Identification of renal Cd36 as a determinant of blood pressure and risk for hypertension. Nat. Genet. 40, 952–954.

Pravenec, M., Landa, V., Zídek, V., Musilová, A., Kazdová, L., Qi, N., Wang, J., St Lezin, E., Kurtz, T.W., 2003. Transgenic expression of CD36 in the spontaneously hypertensive rat is associated with amelioration of metabolic disturbances but has no effect on hypertension. Physiol. Res. 52, 681–688.

Pravenec, M., Landa, V., Zidek, V., Musilova, A., Kren, V., Kazdova, L., Aitman, T.J., Glazier, A.M., Ibrahimi, A., Abumrad, N.A., Qi, N., Wang, J.M., St. Lezin, E.M., Kurtz, T.W., 2001. Transgenic rescue of defective Cd36 ameliorates insulin resistance in spontaneously hypertensive rats. Nat. Genet. 27, 156–158.

Pravenec, M., Zidek, V., Simakova, M., Kren, V., Krenova, D., Horky, K., Jachymova, M., Mikova, B., Kazdova, L., Aitman, T.J., Churchill, P.C., Webb, R.C., Hingarh, N.H., Yang, Y., Wang, J.M., Lezin, E.M., Kurtz, T.W., 1999. Genetics of Cd36 and the clustering of multiple cardiovascular risk factors in spontaneous hypertension. J. Clin. Invest. 103, 1651–1657.

Prieto-Godino, L.L., Rytz, R., Bargeton, B., Abuin, L., Arguello, J.R., Peraro, M.D., Benton, R., 2016. Olfactory receptor pseudo-pseudogenes. Nature 539, 93–97.

Pundir, S., Martin, M.J., O'Donovan, C., UniProt Consortium, 2016. UniProt Tools. Curr. Protoc. Bioinforma. 53, 1.29.1-15.

Qiao, L., Zou, C., Shao, P., Schaack, J., Johnson, P.F., Shao, J., 2008. Transcriptional Regulation of Fatty Acid Translocase/CD36 Expression by CCAAT/Enhancer-binding Protein α. J. Biol. Chem. 283, 8788–8795.

Rabilloud, T., Lescuyer, P., 2014. The proteomic to biology inference, a frequently overlooked concern in the interpretation of proteomic data: A plea for functional validation. Proteomics 14, 157–161.

Raizada, V., Pathak, D., Avery, G., Woodfin, B., 1993. Accelerated glycolysis in early hypertensive left ventricular hypertrophy. Cardiology 83, 160–164.

Ralston, E., Ploug, T., 1999. Caveolin-3 is associated with the T-tubules of mature skeletal muscle fibers. Exp. Cell Res. 246, 510–515.

Rao, R.H., 1993. Insulin resistance in spontaneously hypertensive rats: Difference in interpretation based on insulin infusion rate or on plasma insulin in glucose clamp studies. Diabetes 42, 1364–1371.

Rao, V., Cheng, Y., Lindert, S., Wang, D., Oxenford, L., McCulloch, A.D., McCammon, J.A., Regnier, M., 2014. PKA Phosphorylation of Cardiac Troponin I Modulates Activation and Relaxation Kinetics of Ventricular Myofibrils. Biophys. J. 107, 1196–1204.

Rasmussen, J.T., Berglund, L., Rasmussen, M.S., Petersen, T.E., 1998. Assignment of disulfide bridges in bovine CD36. Eur. J. Biochem. 257, 488–494.

Rasmussen, S.G.F., DeVree, B.T., Zou, Y., Kruse, A.C., Chung, K.Y., Kobilka, T.S., Thian, F.S., Chae, P.S., Pardon, E., Calinski, D., Mathiesen, J.M., Shah, S.T.A., Lyons, J.A., Caffrey, M., Gellman, S.H., Steyaert, J., Skiniotis, G., Weis, W.I., Sunahara, R.K., Kobilka, B.K., 2011. Crystal structure of the β2 adrenergic receptor-Gs protein complex. Nature 477, 549–555.

Razani, B., Lisanti, M.P., 2001. Caveolin-deficient mice: insights into caveolar function human disease. J. Clin. Invest. 108, 1553–1561.

Razani, B., Woodman, S.E., Lisanti, M.P., 2002. Caveolae: From Cell Biology to Animal Physiology. Pharmacol. Rev. 54, 431–467.

Reaven, G.M., Chang, H., Hoffman, B.B., Azhar, S., 1989. Resistance to insulin-stimulated glucose uptake in adipocytes isolated from spontaneously hypertensive rats. Diabetes 38, 1155–1160.

Redout, E.M., Wagner, M.J., Zuidwijk, M.J., Boer, C., Musters, R.J.P., van Hardeveld, C., Paulus, W.J., Simonides, W.S., 2007. Right-ventricular failure is associated with increased mitochondrial complex II activity and production of reactive oxygen species. Cardiovasc. Res. 75, 770–781.

Resh, M.D., 1999. Fatty acylation of proteins: new insights into membrane targeting of myristoylated and palmitoylated proteins. Biochim. Biophys. Acta 1451, 1–16.

Ring, A., Le Lay, S., Pohl, J., Verkade, P., Stremmel, W., 2006. Caveolin-1 is required for fatty acid translocase (FAT/CD36) localization and function at the plasma membrane of mouse embryonic fibroblasts. Biochim. Biophys. Acta 1761, 416–423.

Rolli-Derkinderen, M., Sauzeau, V., Boyer, L., Lemichez, E., Baron, C., Henrion, D., Loirand, G., Pacaud, P., 2005. Phosphorylation of serine 188 protects RhoA

from ubiquitin/proteasome-mediated degradation in vascular smooth muscle cells. Circ. Res. 96, 1152–1160.

Rubin, D., Ismail-Beigi, F., 2003. Distribution of Glut1 in detergent-resistant membranes (DRMs) and non-DRM domains: effect of treatment with azide. Am. J. Physiol. Cell Physiol. 285, C377–C383.

Ruis-González, M.D., Cañete, M.D., Gómez-Chaparro, J.L., Abril, N., Cañete, R., López-Barea, J., 2015. Alterations of protein expression in serum of infants with intrauterine growth restriction and different gestational ages. J. Proteomics 119, 169–182.

Rybin, V.O., Pak, E., Alcott, S., Steinberg, S.F., 2003. Developmental changes in beta2-adrenergic receptor signaling in ventricular myocytes: the role of Gi proteins and caveolae microdomains. Mol. Pharmacol. 63, 1338–1348.

Rybin, V.O., Xu, X., Lisanti, M.P., Steinberg, S.F., 2000. Differential targeting of beta -adrenergic receptor subtypes and adenylyl cyclase to cardiomyocyte caveolae. A mechanism to functionally regulate the cAMP signaling pathway. J. Biol. Chem. 275, 41447–41457.

Saifudeen, I., Subhadra, L., Konnottil, R., Nair, R.R., 2017. Metabolic Modulation by Medium-Chain Triglycerides Reduces Oxidative Stress and Ameliorates CD36-Mediated Cardiac Remodeling in Spontaneously Hypertensive Rat in the Initial and Established Stages of Hypertrophy. J. Card. Fail. 23, 240–251.

Salminen, A., Kaarniranta, K., Kauppinen, A., 2013. Crosstalk between Oxidative Stress and SIRT1: Impact on the Aging Process. Int. J. Mol. Sci. 14, 3834–3859.

Samovski, D., Su, X., Xu, Y., Abumrad, N.A., Stahl, P.D., 2012. Insulin and AMPK regulate FA translocase/CD36 plasma membrane recruitment in cardiomyocytes via Rab GAP AS160 and Rab8a Rab GTPase. J. Lipid Res. 53, 709–717.

Samovski, D., Sun, J., Pietka, T., Gross, R.W., Eckel, R.H., Su, X., Stahl, P.D., Abumrad, N.A., 2015. Regulation of AMPK Activation by CD36 Links Fatty Acid Uptake to β-Oxidation. Diabetes 64, 353–359.

Sandin, M., Chawade, A., Levander, F., 2015. Is label-free LC-MS/MS ready for biomarker discovery? Proteomics Clin. Appl. 9, 289–294.

Santamaria, M.H., Chen, A.Y., Chow, J., Muñoz, D.C., Schmid-Schönbein, G.W., 2014. Cleavage and reduced CD36 ectodomain density on heart and spleen

macrophages in the Spontaneously Hypertensive Rat. Microvasc. Res. 95, 131–142.

Sawada, N., Itoh, H., Yamashita, J., Doi, K., Inoue, M., Masatsugu, K., Fukunaga, Y., Sakaguchi, S., Sone, M., Yamahara, K., Yurugi, T., Nakao, K., 2001. cGMP-dependent protein kinase phosphorylates and inactivates RhoA. Biochem. Biophys. Res. Commun. 280, 798–805.

Schindelin, J., Arganda-Carreras, I., Frise, E., Kaynig, V., Longair, M., Pietzsch, T., Preibisch, S., Rueden, C., Saalfeld, S., Schmid, B., Tinevez, J.Y., White, D.J., Hartenstein, V., Eliceiri, K., Tomancak, P., Cardona, A., 2012. Fiji: An open-source platform for biological-image analysis. Nat. Methods 9, 676–682.

Schubert, A.-L., Schubert, W., Spray, D.C., Lisanti, M.P., 2002. Connexin family members target to lipid raft domains and interact with caveolin-1. Biochemistry 41, 5754–5764.

Schwencke, C., Okumura, S., Yamamoto, M., Geng, Y.J., Ishikawa, Y., 1999. Colocalization of beta-adrenergic receptors and caveolin within the plasma membrane. J. Cell. Biochem. 75, 64–72.

Sen, S., Tarazi, R.C., Khairallah, P.A., Bumpus, F.M., 1974. Cardiac hypertrophy in spontaneously hypertensive rats. Circ. Res. 35, 775–781.

Sethi, R., Manchanda, S., Perepu, R.S.P., Kumar, A., Garcia, C., Kennedy, R.H., Palakurthi, S., Dostal, D., 2012. Differential expression of caveolin-1 and caveolin-3: Potential marker for cardiac toxicity subsequent to chronic ozone inhalation. Mol. Cell. Biochem. 369, 9–15.

Shah, A., Chen, D., Boda, A.R., Foster, L.J., Davis, M.J., Hill, M.M., 2015. RaftProt: mammalian lipid raft proteome database. Nucleic Acids Res. 43, D335–D338.

Shaw, R.J., Kosmatka, M., Bardeesy, N., Hurley, R.L., Witters, L.A., DePinho, R.A., Cantley, L.C., 2004. The tumor suppressor LKB1 kinase directly activates AMP-activated kinase and regulates apoptosis in response to energy stress. Proc. Natl. Acad. Sci. U. S. A. 101, 3329–3335.

Shaywitz, A.J., Greenberg, M.E., 1999. CREB: a stimulus-induced transcription factor activated by a diverse array of extracellular signals. Annu. Rev. Biochem. 68, 821–861.

Shimamoto, N., Goto, N., Tanabe, M., Imamoto, T., Fujiwara, S., Hirata, M., 1982. Myocardial energy metabolism in the hypertrophied hearts of spontaneously hypertensive rats. Basic Res. Cardiol. 77, 359–371.

Shimokawa, H., Sunamura, S., Satoh, K., 2016. RhoA/Rho-Kinase in the Cardiovascular System. Circ. Res. 118, 352–366.

Shimoyama, M., De Pons, J., Hayman, G.T., Laulederkind, S.J.F., Liu, W., Nigam, R., Petri, V., Smith, J.R., Tutaj, M., Wang, S.-J., Worthey, E., Dwinell, M., Jacob, H., 2015. The Rat Genome Database 2015: genomic, phenotypic and environmental variations and disease. Nucleic Acids Res. 43, D743-750.

Silverstein, R.L., Li, W., Park, Y.M., Rahaman, S.O., 2010. Mechanisms of cell signaling by the scavenger receptor CD36: implications in atherosclerosis and thrombosis. Trans. Am. Clin. Climatol. Assoc. 121, 206–220.

Smart, E.J., Ying, Y.S., Mineo, C., Anderson, R.G., 1995. A detergent-free method for purifying caveolae membrane from tissue culture cells. Proc. Natl. Acad. Sci. U. S. A. 92, 10104–10108.

Smith, J., Su, X., El-Maghrabi, R., Stahl, P.D., Abumrad, N.A., 2008. Opposite regulation of CD36 ubiquitination by fatty acids and insulin: effects on fatty acid uptake. J. Biol. Chem. 283, 13578–13585.

Smith, P.K., Krohn, R.I., Hermanson, G.T., Mallia, A.K., Gartner, F.H., Provenzano, M.D., Fujimoto, E.K., Goeke, N.M., Olson, B.J., Klenk, D.C., 1985. Measurement of protein using bicinchoninic acid. Anal. Biochem. 150, 76–85.

Solomon, S., Masilamani, M., Rajendran, L., Bastmeyer, M., Stuermer, C.A.O., Illges, H., 2002. The lipid raft microdomain-associated protein reggie-1/flotillin-2 is expressed in human B cells and localized at the plasma membrane and centrosome in PBMCs. Immunobiology 205, 108–119.

Somekawa, S., Fukuhara, S., Nakaoka, Y., Fujita, H., Saito, Y., Mochizuki, N., 2005. Enhanced functional gap junction neoformation by protein kinase A-dependent and Epac-dependent signals downstream of cAMP in cardiac myocytes. Circ. Res. 97, 655–662.

Song, K.S., Li, S., Okamoto, T., Quilliam, L.A., Sargiacomo, M., Lisanti, M.P., 1996a. Co-purification and Direct Interaction of Ras with Caveolin, an Integral Membrane Protein of Caveolae Microdomains DETERGENT-FREE

PURIFICATION OF CAVEOLAE MEMBRANES. J. Biol. Chem. 271, 9690–9697.

Song, K.S., Scherer, P.E., Tang, Z., Okamoto, T., Li, S., Chafel, M., Chu, C., Kohtz, D.S., Lisanti, M.P., 1996b. Expression of Caveolin-3 in Skeletal, Cardiac, and Smooth Muscle Cells CAVEOLIN-3 IS A COMPONENT OF THE SARCOLEMMA AND CO-FRACTIONATES WITH DYSTROPHIN AND DYSTROPHIN-ASSOCIATED GLYCOPROTEINS. J. Biol. Chem. 271, 15160–15165.

Sonnino, S., Prinetti, A., 2013. Membrane domains and the "lipid raft" concept. Curr. Med. Chem. 20, 4–21.

Sotgia, F., Lee, J.K., Das, K., Bedford, M., Petrucci, T.C., Macioce, P., Sargiacomo, M., Bricarelli, F.D., Minetti, C., Sudol, M., Lisanti, M.P., 2000. Caveolin-3 directly interacts with the C-terminal tail of beta -dystroglycan. Identification of a central WW-like domain within caveolin family members. J. Biol. Chem. 275, 38048–38058.

Souto, R.P., Vallega, G., Wharton, J., Vinten, J., Tranum-Jensen, J., Pilch, P.F., 2003. Immunopurification and characterization of rat adipocyte caveolae suggest their dissociation from insulin signaling. J. Biol. Chem. 278, 18321–18329.

Srere, P.A., 1969. [1] Citrate synthase: [EC 4.1.3.7. Citrate oxaloacetate-lyase (CoA-acetylating)]. In: Enzymology, B.-M. in (Ed.), Citric Acid Cycle, Citric Acid Cycle. Academic Press, pp. 3–11.

Stewart, C.R., Stuart, L.M., Wilkinson, K., van Gils, J.M., Deng, J., Halle, A., Rayner, K.J., Boyer, L., Zhong, R., Frazier, W.A., Lacy-Hulbert, A., El Khoury, J., Golenbock, D.T., Moore, K.J., 2010. CD36 ligands promote sterile inflammation through assembly of a Toll-like receptor 4 and 6 heterodimer. Nat. Immunol. 11, 155–161.

Stolba, P., Dobesová, Z., Husek, P., Opltová, H., Zicha, J., Vrána, A., Kunes, J., 1992. The hypertriglyceridemic rat as a genetic model of hypertension and diabetes. Life Sci. 51, 733–740.

Stüven, E., Porat, A., Shimron, F., Fass, E., Kaloyanova, D., Brügger, B., Wieland, F.T., Elazar, Z., Helms, J.B., 2003. Intra-Golgi Protein Transport Depends on a Cholesterol Balance in the Lipid Membrane. J. Biol. Chem. 278, 53112–53122.

Sun, L., Yu, J., Qi, S., Hao, Y., Liu, Y., Li, Z., 2014. Bone morphogenetic protein-10 induces cardiomyocyte proliferation and improves cardiac function after myocardial infarction. J. Cell. Biochem. 115, 1868–1876.

Sung, M.M., Byrne, N.J., Kim, T.T., Levasseur, J., Masson, G., Boisvenue, J.J., Febbraio, M., Dyck, J.R.B., 2017. Cardiomyocyte-specific ablation of CD36 accelerates the progression from compensated cardiac hypertrophy to heart failure. Am. J. Physiol. Heart Circ. Physiol. 312, H552–H560.

Sutherland, E., Dixon, B.S., Leffert, H.L., Skally, H., Zaccaro, L., Simon, F.R., 1988. Biochemical localization of hepatic surface-membrane Na+,K+-ATPase activity depends on membrane lipid fluidity. Proc. Natl. Acad. Sci. 85, 8673–8677.

Tadic, M., Pieske-Kraigher, E., Cuspidi, C., Morris, D.A., Burkhardt, F., Baudisch, A., Haßfeld, S., Tschöpe, C., Pieske, B., 2017. Right ventricular strain in heart failure: Clinical perspective. Arch. Cardiovasc. Dis. 110, 562–571.

Talan, M.I., Ahmet, I., Xiao, R.-P., Lakatta, E.G., 2011. β2 AR Agonists in Treatment of Chronic Heart Failure: Long Path to Translation. J. Mol. Cell. Cardiol. 51, 529–533.

Talle, M.A., Rao, P.E., Westberg, E., Allegar, N., Makowski, M., Mittler, R.S., Goldstein, G., 1983. Patterns of antigenic expression on human monocytes as defined by monoclonal antibodies. Cell. Immunol. 78, 83–99.

Tandon, N.N., Kralisz, U., Jamieson, G.A., 1989. Identification of glycoprotein IV (CD36) as a primary receptor for platelet-collagen adhesion. J. Biol. Chem. 264, 7576–7583.

Tang, W.J., Gilman, A.G., 1991. Type-specific regulation of adenylyl cyclase by G protein beta gamma subunits. Science 254, 1500–1503.

Tang, Y., Mi, C., Liu, J., Gao, F., Long, J., 2014. Compromised mitochondrial remodeling in compensatory hypertrophied myocardium of spontaneously hypertensive rat. Cardiovasc. Pathol. Off. J. Soc. Cardiovasc. Pathol. 23, 101–106.

Tarze, A., Deniaud, A., Le Bras, M., Maillier, E., Molle, D., Larochette, N., Zamzami, N., Jan, G., Kroemer, G., Brenner, C., 2007. GAPDH, a novel regulator of the pro-apoptotic mitochondrial membrane permeabilization. Oncogene 26, 2606–2620.

Taylor, C.W., 1990. The role of G proteins in transmembrane signalling. Biochem. J. 272, 1–13.

Taylor, E.B., An, D., Kramer, H.F., Yu, H., Fujii, N.L., Roeckl, K.S.C., Bowles, N., Hirshman, M.F., Xie, J., Feener, E.P., Goodyear, L.J., 2008. Discovery of TBC1D1 as an insulin-, AICAR-, and contraction-stimulated signaling nexus in mouse skeletal muscle. J. Biol. Chem. 283, 9787–9796.

Teiger, E., Than, V.D., Richard, L., Wisnewsky, C., Tea, B.S., Gaboury, L., Tremblay, J., Schwartz, K., Hamet, P., 1996. Apoptosis in pressure overload-induced heart hypertrophy in the rat. J. Clin. Invest. 97, 2891–2897.

TenBroek, E.M., Lampe, P.D., Solan, J.L., Reynhout, J.K., Johnson, R.G., 2001. Ser364 of connexin43 and the upregulation of gap junction assembly by cAMP. J. Cell Biol. 155, 1307–1318.

Thandapilly, S.J., Wojciechowski, P., Behbahani, J., Louis, X.L., Yu, L., Juric, D., Kopilas, M.A., Anderson, H.D., Netticadan, T., 2010. Resveratrol prevents the development of pathological cardiac hypertrophy and contractile dysfunction in the SHR without lowering blood pressure. Am. J. Hypertens. 23, 192–196.

Thompson, S., Loftus, L., Ashley, M., Meller, R., 2008. Ubiquitin-Proteasome System as a Modulator of Cell Fate. Curr. Opin. Pharmacol. 8, 90–95.

Torrealba, N., Aranguiz, P., Alonso, C., Rothermel, B.A., Lavandero, S., 2017. Mitochondria in Structural and Functional Cardiac Remodeling. Adv. Exp. Med. Biol. 982, 277–306.

Trzaskowski, B., Latek, D., Yuan, S., Ghoshdastider, U., Debinski, A., Filipek, S., 2012. Action of molecular switches in GPCRs--theoretical and experimental studies. Curr. Med. Chem. 19, 1090–1109.

Tsutsumi, Y.M., Kawaraguchi, Y., Horikawa, Y.T., Niesman, I.R., Kidd, M.W., Chin-Lee, B., Head, B.P., Patel, P.M., Roth, D.M., Patel, H.H., 2010. Role for Caveolin-3 and Glucose Transporter 4 in Isoflurane-induced Delayed Cardiac Protection. Anesthesiology 112, 1136–1145.

Umbarawan, Y., Syamsunarno, M.R.A.A., Koitabashi, N., Obinata, H., Yamaguchi, A., Hanaoka, H., Hishiki, T., Hayakawa, N., Sano, M., Sunaga, H., Matsui, H., Tsushima, Y., Suematsu, M., Kurabayashi, M., Iso, T., 2018. Myocardial fatty acid uptake through CD36 is indispensable for sufficient bioenergetic

metabolism to prevent progression of pressure overload-induced heart failure. Sci. Rep. 8, 12035.

Valentine, C.D., Haggie, P.M., 2011. Confinement of β(1)- and β(2)-adrenergic receptors in the plasma membrane of cardiomyocyte-like H9c2 cells is mediated by selective interactions with PDZ domain and A-kinase anchoring proteins but not caveolae. Mol. Biol. Cell 22, 2970–2982.

Van Eyk, J.E., 2011. The maturing of proteomics in cardiovascular research. Circ. Res. 108, 490–498.

Van Nieuwenhoven, F.A., Luiken, J.J., De Jong, Y.F., Grimaldi, P.A., Van der Vusse, G.J., Glatz, J.F., 1998. Stable transfection of fatty acid translocase (CD36) in a rat heart muscle cell line (H9c2). J. Lipid Res. 39, 2039–2047.

van Oort, M.M., Drost, R., Janβen, L., Van Doorn, J.M., Kerver, J., Van der Horst, D.J., Luiken, J.J.F.P., Rodenburg, K.C.W., 2014. Each of the four intracellular cysteines of CD36 is essential for insulin- or AMP-activated protein kinase-induced CD36 translocation. Arch. Physiol. Biochem. 120, 40–49.

van Oort, M.M., van Doorn, J.M., Bonen, A., Glatz, J.F.C., van der Horst, D.J., Rodenburg, K.W., Luiken, J.J.F.P., 2008. Insulin-induced translocation of CD36 to the plasma membrane is reversible and shows similarity to that of GLUT4. Biochim. Biophys. Acta 1781, 61–71.

van Vliet-Ostaptchouk, J. V, Nuotio, M.-L., Slagter, S.N., Doiron, D., Fischer, K., Foco, L., Gaye, A., Gögele, M., Heier, M., Hiekkalinna, T., Joensuu, A., Newby, C., Pang, C., Partinen, E., Reischl, E., Schwienbacher, C., Tammesoo, M.-L., Swertz, M.A., Burton, P., Ferretti, V., Fortier, I., Giepmans, L., Harris, J.R., Hillege, H.L., Holmen, J., Jula, A., Kootstra-Ros, J.E., Kvaløy, K., Holmen, T.L., Männistö, S., Metspalu, A., Midthjell, K., Murtagh, M.J., Peters, A., Pramstaller, P.P., Saaristo, T., Salomaa, V., Stolk, R.P., Uusitupa, M., van der Harst, P., van der Klauw, M.M., Waldenberger, M., Perola, M., Wolffenbuttel, B.H., 2014. The prevalence of metabolic syndrome and metabolically healthy obesity in Europe: a collaborative analysis of ten large cohort studies. BMC Endocr. Disord. 14, 9.

Vanhaesebroeck, B., Alessi, D.R., 2000. The PI3K-PDK1 connection: more than just a road to PKB. Biochem. J. 346 Pt 3, 561–576.

Vařecha, M., Potěšilová, M., Matula, P., Kozubek, M., 2012. Endonuclease G interacts with histone H2B and DNA topoisomerase II alpha during apoptosis. Mol. Cell. Biochem. 363, 301–307.

Volonte, D., McTiernan, C.F., Drab, M., Kasper, M., Galbiati, F., 2008. Caveolin-1 and caveolin-3 form heterooligomeric complexes in atrial cardiac myocytes that are required for doxorubicin-induced apoptosis. Am. J. Physiol. - Heart Circ. Physiol. 294, H392–H401.

Wakana, Y., Koyama, S., Nakajima, K., Hatsuzawa, K., Nagahama, M., Tani, K., Hauri, H.-P., Melançon, P., Tagaya, M., 2005. Reticulon 3 is involved in membrane trafficking between the endoplasmic reticulum and Golgi. Biochem. Biophys. Res. Commun. 334, 1198–1205.

Wan, Q., Kuang, E., Dong, W., Zhou, S., Xu, H., Qi, Y., Liu, Y., 2007. Reticulon 3 mediates Bcl-2 accumulation in mitochondria in response to endoplasmic reticulum stress. Apoptosis Int. J. Program. Cell Death 12, 319–328.

Wang, D., Villasante, A., Lewis, S.A., Cowan, N.J., 1986. The mammalian beta-tubulin repertoire: hematopoietic expression of a novel, heterologous beta-tubulin isotype. J. Cell Biol. 103, 1903–1910.

Wang, Y., Zhou, X.O., Zhang, Y., Gao, P.J., Zhu, D.L., 2012. Association of the CD36 gene with impaired glucose tolerance, impaired fasting glucose, type-2 diabetes, and lipid metabolism in essential hypertensive patients. Genet. Mol. Res. GMR 11, 2163–2170.

Waskova-Arnostova, P., Kasparova, D., Elsnicova, B., Novotny, J., Neckar, J., Kolar, F., Zurmanova, J., 2014. Chronic Hypoxia Enhances Expression and Activity of Mitochondrial Creatine Kinase and Hexokinase in the Rat Ventricular Myocardium. Cell. Physiol. Biochem. 33, 310–320.

Watanabe, Y., Yoshida, M., Yamanishi, K., Yamamoto, H., Okuzaki, D., Nojima, H., Yasunaga, T., Okamura, H., Matsunaga, H., Yamanishi, H., 2015. Genetic analysis of genes causing hypertension and stroke in spontaneously hypertensive rats: Gene expression profiles in the kidneys. Int. J. Mol. Med. 36, 712–724.

WHO, 2013. A Global Brief on Hypertension. WHO.

Wiehe, R.S., Gole, B., Chatre, L., Walther, P., Calzia, E., Ricchetti, M., Wiesmüller, L., 2018. Endonuclease G promotes mitochondrial genome cleavage and replication. Oncotarget 9, 18309–18326.

Williams, T.M., Lisanti, M.P., 2004. The caveolin proteins. Genome Biol. 5, 214.

Woo, A.Y.-H., Song, Y., Xiao, R.-P., Zhu, W., 2015. Biased β2-adrenoceptor signalling in heart failure: pathophysiology and drug discovery. Br. J. Pharmacol. 172, 5444–5456.

Woodman, S.E., Park, D.S., Cohen, A.W., Cheung, M.W.-C., Chandra, M., Shirani, J., Tang, B., Jelicks, L.A., Kitsis, R.N., Christ, G.J., Factor, S.M., Tanowitz, H.B., Lisanti, M.P., 2002. Caveolin-3 knock-out mice develop a progressive cardiomyopathy and show hyperactivation of the p42/44 MAPK cascade. J. Biol. Chem. 277, 38988–38997.

Wool, I.G., Chan, Y.L., Glück, A., 1995. Structure and evolution of mammalian ribosomal proteins. Biochem. Cell Biol. Biochim. Biol. Cell. 73, 933–947.

Wright, P.T., Bhogal, N.K., Diakonov, I., Pannell, L.M.K., Perera, R.K., Bork, N.I., Schobesberger, S., Lucarelli, C., Faggian, G., Alvarez-Laviada, A., Zaccolo, M., Kamp, T.J., Balijepalli, R.C., Lyon, A.R., Harding, S.E., Nikolaev, V.O., Gorelik, J., 2018. Cardiomyocyte Membrane Structure and cAMP Compartmentation Produce Anatomical Variation in β2AR-cAMP Responsiveness in Murine Hearts. Cell Rep. 23, 459–469.

Wright, P.T., Nikolaev, V.O., O'Hara, T., Diakonov, I., Bhargava, A., Tokar, S., Schobesberger, S., Shevchuk, A.I., Sikkel, M.B., Wilkinson, R., Trayanova, N.A., Lyon, A.R., Harding, S.E., Gorelik, J., 2014. Caveolin-3 regulates compartmentation of cardiomyocyte beta2-adrenergic receptor-mediated cAMP signaling. J. Mol. Cell. Cardiol. 67, 38–48.

Yang, X., Okamura, D.M., Lu, X., Chen, Y., Moorhead, J., Varghese, Z., Ruan, X.Z., 2017. CD36 in chronic kidney disease: novel insights and therapeutic opportunities. Nat. Rev. Nephrol. 13, 769–781.

Ye, L., Kynaston, H., Jiang, W.G., 2009. Bone morphogenetic protein-10 suppresses the growth and aggressiveness of prostate cancer cells through a Smad independent pathway. J. Urol. 181, 2749–2759.

Yipp, B.G., Robbins, S.M., Resek, M.E., Baruch, D.I., Looareesuwan, S., Ho, M., 2003. Src-family kinase signaling modulates the adhesion of Plasmodium falciparum on human microvascular endothelium under flow. Blood 101, 2850–2857.

You, M., Fischer, M., Cho, W.K., Crabb, D., 2002. Transcriptional control of the human aldehyde dehydrogenase 2 promoter by hepatocyte nuclear factor 4: inhibition

by cyclic AMP and COUP transcription factors. Arch. Biochem. Biophys. 398, 79–86.

Yuasa, T., Uchiyama, K., Ogura, Y., Kimura, M., Teshigawara, K., Hosaka, T., Tanaka, Y., Obata, T., Sano, H., Kishi, K., Ebina, Y., 2009. The Rab GTPase-activating protein AS160 as a common regulator of insulin- and Galphaq-mediated intracellular GLUT4 vesicle distribution. Endocr. J. 56, 345–359.

Zaini, M.A., Müller, C., de Jong, T.V., Ackermann, T., Hartleben, G., Kortman, G., Gührs, K.-H., Fusetti, F., Krämer, O.H., Guryev, V., Calkhoven, C.F., 2018. A p300 and SIRT1 Regulated Acetylation Switch of C/EBPα Controls Mitochondrial Function. Cell Rep. 22, 497–511.

Zamorano-León, J.J., Modrego, J., Mateos-Cáceres, P.J., Macaya, C., Martín-Fernández, B., Miana, M., de las Heras, N., Cachofeiro, V., Lahera, V., López-Farré, A.J., 2010. A proteomic approach to determine changes in proteins involved in the myocardial metabolism in left ventricles of spontaneously hypertensive rats. Cell. Physiol. Biochem. Int. J. Exp. Cell. Physiol. Biochem. Pharmacol. 25, 347–358.

Zecchin, H.G., Bezerra, R.M.N., Carvalheira, J.B.C., Carvalho-Filho, M.A., Metze, K., Franchini, K.G., Saad, M.J.A., 2003. Insulin signalling pathways in aorta and muscle from two animal models of insulin resistance—the obese middle-aged and the spontaneously hypertensive rats. Diabetologia 46, 479–491.

Zeng, Y., Tao, N., Chung, K.-N., Heuser, J.E., Lublin, D.M., 2003. Endocytosis of Oxidized Low Density Lipoprotein through Scavenger Receptor CD36 Utilizes a Lipid Raft Pathway That Does Not Require Caveolin-1. J. Biol. Chem. 278, 45931–45936.

Zhang, H., Li, J., Li, R., Zhang, Q., Ma, H., Ji, Q., Guo, W., Wang, H., Lopez, B.L., Christopher, T.A., Ma, X., Gao, F., 2008. Reduced cardiotropic response to insulin in spontaneously hypertensive rats: role of peroxisome proliferator-activated receptor-gamma-initiated signaling. J. Hypertens. 26, 560–569.

Zheng, Y.Z., Berg, K.B., Foster, L.J., 2009. Mitochondria do not contain lipid rafts, and lipid rafts do not contain mitochondrial proteins. J. Lipid Res. 50, 988–998.

Zhou, S.-G., Zhou, S.-F., Huang, H.-Q., Chen, J.-W., Huang, M., Liu, P.-Q., 2006. Proteomic analysis of hypertrophied myocardial protein patterns in

renovascularly hypertensive and spontaneously hypertensive rats. J. Proteome Res. 5, 2901–2908.

Zingg, J.-M., Hasan, S.T., Nakagawa, K., Canepa, E., Ricciarelli, R., Villacorta, L., Azzi, A., Meydani, M., 2017. Modulation of cAMP levels by high-fat diet and curcumin and regulatory effects on CD36/FAT scavenger receptor/fatty acids transporter gene expression. BioFactors Oxf. Engl. 43, 42–53.

Zou, Z., DiRusso, C.C., Ctrnacta, V., Black, P.N., 2002. Fatty acid transport in Saccharomyces cerevisiae. Directed mutagenesis of FAT1 distinguishes the biochemical activities associated with Fat1p. J. Biol. Chem. 277, 31062–31071.

LIST OF PUBLICATIONS RELATED TO THIS THESIS

Statement about the extent of participation

1. **Manakov, D.**, Ujcikova, H., Pravenec, M. and Novotny, J. (2016) Alterations in the cardiac proteome of the spontaneously hypertensive rat induced by transgenic expression of CD36. *Journal of Proteomics* 145:177-86 (IF = 3.722).

   My contribution: I performed sample preparations, assisted with 2D electrophoresis experiments, analyzed the proteomic data and contributed significantly to the writing of the manuscript.

2. **Manakov, D.**, Kolar, D., Zurmanova, J., Pravenec, M., and Novotny, J. (2018). Changes in the activity of some metabolic enzymes in the heart of SHR rat incurred by transgenic expression of CD36. *Journal of Physiology and Biochemistry* [*In press*] (IF = 2.444).

   My contribution: I performed sample preparations, respirometric measurements and assisted in conduction of enzymatic assays. I also performed Western blotting experiments, analyzed the data and drafted a substantial portion of the manuscript.

I confirm, on behalf of all co-authors, that the above stated information about contribution of Dmitry Manakov to both articles is correct.

Doc. RNDr. Jiří Novotný, DSc.